



Michigan Technological University
Create the Future Digital Commons @ Michigan Tech

Dissertations, Master's Theses and Master's
Reports - Open

Dissertations, Master's Theses and Master's
Reports

2012

Quantum modeling of bioconjugated nanomaterials

Saikat Mukhopadhyay
Michigan Technological University

Follow this and additional works at: <https://digitalcommons.mtu.edu/etds>


 Part of the [Physics Commons](#)

Copyright 2012 Saikat Mukhopadhyay

Recommended Citation

Mukhopadhyay, Saikat, "Quantum modeling of bioconjugated nanomaterials", Dissertation, Michigan Technological University, 2012.
<https://doi.org/10.37099/mtu.dc.etds/113>

Follow this and additional works at: <https://digitalcommons.mtu.edu/etds>

 Part of the [Physics Commons](#)

QUANTUM MODELING OF BIOCONJUGATED NANOMATERIALS

By

Saikat Mukhopadhyay

A DISSERTATION

Submitted in partial fulfillment of the requirements for the degree of

DOCTOR OF PHILOSOPHY

(Physics)

MICHIGAN TECHNOLOGICAL UNIVERSITY

2012

© 2012 Saikat Mukhopadhyay

This dissertation, “Quantum Modeling of Bioconjugated Nanomaterials”, is hereby approved in partial fulfillment of the requirements for the Degree of DOCTOR OF PHILOSOPHY IN PHYSICS.

Department of Physics

Signatures:

Dissertation Co-Advisor

Ravindra Pandey

Dissertation Co-Advisor

Shashi P. Karna

Department Chair

Ravindra Pandey

Date

To my uncle, Late Tarun Banerjee

Contents

Table of Contents

List of Figures	vii
List of Tables.....	xiii
Acknowledgements.....	xiv
Acronyms	xvi
Abstract	xviii
Introduction	1
1.1. Bioconjugated Nanomaterials.....	1
1.2.1. Boron Nitride Nanotube	4
1.2.2. Boron Nitride Nanotubes in Biology.....	6
1.3.1. Molecular electronics	9
1.3.2. Molecular Electronics in Biology.....	14
Theoretical Methods	16
2.1. Electronic Structure from First Principles	16
2.1.1. Born-Oppenheimer Approximation.....	18
2.1.2. Hartree-Fock Approximation	20
2.2. Density Functional Theory	23
2.2.1. Thomas-Fermi Theory.....	24
2.2.2. Hohenberg-Kohn theorem	25
2.2.3. Kohn-Sham Theorem	26
2.2.4. Exchange and Correlation Functional Forms	29
2.2.5. Local Density Approximation	30
2.2.6. Generalized-Gradient Approximation	31
2.2.7. Exchange and Correlation Functional Forms	32
2.3. Molecular Orbital Theory	33
2.4. Basis Sets.....	34
2.4.1. Gaussian-Type Basis Sets.....	35
2.4.2. Plane Wave Basis Set	37
2.4.3. Numerical Basis Set.....	39

2.5. Pseudopotentials	40
2.6. Quantum Transport.....	43
2.6.1 Green's Functions and Quantum Transport.....	45
2.6.2. Landauer Formalism.....	49
2.6.3. Büttiker Equation.....	52
2.6.4. Non-Equilibrium Green's Function.....	54
Theoretical Study of Physisorption of Nucleobases on Boron Nitride Nanotubes: A New Class of Hybrid Nano-Bio Materials.....	56
3.1. Introduction	56
3.2. Simulation Model and Computational Details	59
3.3. Results and Discussions.....	63
3.4. Summary.....	72
Sensitivity of Boron Nitride Nanotubes toward Biomolecules of Different Polarities	73
4.1. Introduction	73
4.2. Simulation Model and Computational Details	77
4.3. Results and Discussions.....	80
4.4. Summary.....	90
Controlling the performance of a three-terminal molecular transistor: Conformational versus Conventional gating.....	91
5.1. Introduction	91
5.2. Simulation Model and Computational Details	95
5.3. Results and Discussions.....	101
5.3. A. Conformational gating.....	102
5.3. B. Voltage gating.....	107
5.3. C. Conformational and Voltage gating.....	108
5.4. Summary.....	112
Effect of Molecular Adsorption on the Transport Properties of Boron Nitride Nanotubes and Carbon Nanotubes:Applicability of BNNTSs and CNTs as Biosensors.....	114
6.1. Introduction	114
6.2. Simulation Model and Computational Details	116
6.3. Results and Discussions.....	119
6.4. Summary.....	126
Summary and Future Perspectives.....	128
7.1. Summary.....	128
7.2. Future Perspectives.....	132

References	136
Appendix A	155
Computational Resources	155
Appendix B.....	156
List of Related Publications.....	156
Appendix C	159
Copyrights	159
Appendix D	160
Copyrights	160
Appendix E.....	161
Copyrights	161

List of Figures

- Figure 1.1:** A schematic representation of boron nitride nanotube formed by rolling of boron nitride-sheet. The naming-scheme, similar to that of carbon nanotube with alternating boron and nitrogen atoms on a rolled hexagonal lattice, is also included. **5**
- Figure 2.1:** Schematic of molecular coordinate system adapted from the book “Modern Quantum Chemistry: Introduction to Advanced Electronic Structure Theory” where ‘i’ and ‘j’ stands for electronic and ‘A’ and ‘B’ represents nuclear coordinates, respectively. **18**
- Figure 2.2:** A schematic representation of the self-consistent field approach for solving the Kohn-Sham equations in electronic structure calculations, adapted from the book “Electronic Structure; Basic Theory and Practical Methods”. **29**
- Figure 2.3:** A schematic representation of molecular scale device. Adapted from the book “Electronic Transport in Mesoscopic Systems” by Supriyo Datta. **44**
- Figure 2.4:** A schematic representation of mechanism of electron flow through a one-level channel in molecular scale devices. Adapted from the book “Electronic Transport in Mesoscopic Systems” by Supriyo Datta. **46**
- Figure 3.1:** Potential energy surface plot (eV) for guanine scanning the surface of the BNNT. The energy barrier between the two adjacent local minima is 0.15eV. **61**

Figure 3.2: Equilibrium geometry of nucleobases adsorbed on the surface of the BNNT: (a) guanine, (b) adenine, (c) cytosine, (d) thymine and (e) uracil. 64

Figure 3.3: The distance between the nucleobase atoms and the tubular surface atoms in the equilibrium configurations of BNNT conjugates. 65

Figure 3.4: The potential energy variation of the nucleobases interacting with the BNNT as a function of the distance. The distance represents the separation between the center of the mass of the tubular surface and that of the base. A, G, C, T and U are represented by black, red, blue, green and pink lines, respectively. The zero of the energy is aligned to the non-interacting regime of the surface. 66

Figure 3.5: Total charge density of (a) guanine- (b) thymine- conjugated BNNTs. The iso-surface levels were set at $0.08 e/\text{bohr}^3$. 67

Figure 3.6: Density of states of a pristine BNNT, guanine- and thymine- conjugated BNNTs. The zero of the energy is aligned to the top of the valence band. 70

Figure 3.7: Partial charge density of the valence band of (left) guanine and (right) thymine- conjugated BNNTs. The iso-surface levels were set at $0.0002 e^-/\text{bohr}^3$. 71

Figure 4.1: Chemical formulas of the studied amino acid molecules: (a) Arg [$\text{C}_6\text{H}_{14}\text{N}_4\text{O}_2$], (b) Asp [$\text{C}_4\text{H}_7\text{NO}_4$] and (c) Trp [$\text{C}_{11}\text{H}_{12}\text{N}_2\text{O}_2$]. 76

Figure 4.2: The calculated potential energy surface of the arginine scanning tubular surface of BNNT. The energy barrier between two adjacent local minima is 1.5 eV. 79

Figure 4.3: Equilibrium geometries of (a) Arg, (b) Asp and (c) Trp on the surface of BNNTs. Boron and nitrogen atoms are represented with pink and blue, respectively, where as green, red and white colors stand for carbon, oxygen and hydrogen atoms, respectively. **80**

Figure 4.4: The distance between the atoms of the amino acid molecules and the tubular surface atoms in the equilibrium configurations of BNNT conjugates. **82**

Figure 4.5: The potential energy variation of the amino acid molecules interacting with the BNNT as a function of the distance. Zero of the energy is aligned to the non-interacting regime of the surface. Zero of displacement represents the equilibrium configuration of the conjugated system. **83**

Figure 4.6: Projected density of states of pristine BNNT and amino acid conjugated BNNT. The black lines represent contributions from BNNT atoms and the red lines refer to contribution from atoms of the amino acid molecules. **87**

Figure 4.7: Total charge density of amino acid conjugated BNNT. The isosurface levels were set at $0.02 e^-/\text{bohr}^3$ for all the cases. **89**

Figure 5.1: Schematic diagram of the setup of a unimolecular transistor-like device ABD-IC-DBA. C, N, H and Au atoms are depicted by green, blue, white and yellow spheres, respectively. A positive bias is applied at the source (S) and a gate field ' \vec{E} ' is applied in the direction as shown. **96**

Figure 5.2: The effect of the conformational changes of the gate molecule on the total energy of the system. The zero of energy is aligned to the ground state energy of the system. 'O' corresponds to the ground state configuration and 'A' and 'B' represent the cases when IC_2 is rotated w. r. t. IC_1 by 30° , anti-clockwise and

clockwise, respectively. 101

Figure 5.3: The effect of the conformational gating at the gate arm on the I_d-V_{ds} curves. The ‘O’ corresponds to the ground state and ‘A’ and ‘B’ corresponds to 30° anti-clockwise and clockwise rotation of IC_2 relative to the ground state configuration of the device, respectively. 103

Figure 5.4: The effect of the conformational gating at the gate arm on the transmission functions responsible for the I_d-V_{ds} curves for (a) $V_g=0V$ and (b) $V_g=3V$. 104

Figure 5.5: Evolution of molecular orbital under (a) conformational gating and (b) both the conformational and voltage gating. Zero of the energy represents the Fermi energy of the system. A square indicates the significant rearrangement. 105

Figure 5.6: Evolution of HOMO for (a) conformational gating (i.e. “A”, “O” and “B” configurations) and (b) both conformational and voltage gating. An isovalue of $0.002 \text{ e/bohr}^{-3}$ ($1/10^{\text{th}}$ of the default) is used. 106

Figure 5.7: $I_d - V_{ds}$ curves for the ground state of the device under various applied gate voltages. 107

Figure 5.8: Effects of conformational and voltage gating; I_d-V_{ds} curves for all three-conformations at: (a) $V_g=1V$, (b) $V_g=2V$, (c) $V_g=3V$. 110

Figure 5.9: Transfer curve representing variation of I_d as a function of applied V_g at $V_{ds}=2V$. The ground state of the device is “O”. The current corresponding to the configuration ‘A’ and ‘B’ varies with the applied V_g with a phase factor of $\pi/2$. 111

Figure 6.1: A schematic view of G+BNNT coupled with [001] gold electrodes. Symbols: Au in yellow, B in green, N in dark blue, H in light blue, C in grey and O in pink. The optimum distance between BNNT and gold as adopted is 1.8Å in each side from single-point calculations. The average distance between Guanine and BNNT is about 3.5 Å. **120**

Figure 6.2: I-V characteristics of pristine BNNT and CNT in the small bias regime. **121**

Figure 6.3: Characteristic transmission function of pristine BNNT and CNT at zero external bias explaining the I-V characteristics in Figure 6.2. **123**

Figure 6.4: Effect of molecular adsorption on the transport properties of CNT and BNNT: I-V characteristics of (a) CNT and (b) BNNT with the nucleobases adsorbed on it. Note: I-V characteristics for other CNT-conjugates [CNT+A/C/T/U] are not shown here as they superimpose with that of CNT. **124**

Figure 6.5: Effect of molecular adsorption on the Transmission functions corresponding the I-V characteristics in Figure 4: (a) Transmission function of CNT and CNT+G and (b) Transmission function of BNNT, BNNT+G and BNNT+U at zero external bias. **125**

Figure 7.1: The self-assembly of a fragment of ss-DNA on the top of BNNT. **134**

Figure C.1: Copyright permission from IOPScience for using the content, partially or completely, published by S. Mukhopadhyay *et al.* The results and related discussion has been used in Chapter 3. **159**

Figure D.1: Copyright permission from American Chemical Society (ACS) for using the content, partially or completely, published by S. Mukhopadhyay *et al.* The results and related discussion has been used in Chapter 4. **160**

Figure E.1: Copyright permission from American Chemical Society (ACS) for using the content, partially or completely, published by S. Mukhopadhyay *et al.* The results and related discussion has been used in Chapter 5.

161

List of Tables

- Table 3.1:** Binding energy (E_b), band gap, and nearest-neighbor distance ($R_{\text{base-BNNT}}$) of nucleobase conjugated BNNT. The calculated LDA band gap of the pristine (5, 0) BNNT is 2.2 eV. **69**
- Table 4.1:** Nearest-neighbor distance ($R_{\text{amino-BNNT}}$), binding energy, and band gap of amino acid conjugated BNNT. **84**
- Table A.1:** A typical CPU-time required for the major optimization steps in Chapters 3 and 4. **155**

Acknowledgements

This dissertation in its current form would not have been possible without the continuous support from the Department of Physics, Michigan Technological University, Houghton. I would like to take this opportunity to thank *‘our department’* for providing me with all the resources and facilities, whenever needed, and for maintaining a friendly environment, which never let me feel *‘away from home’*.

I would probably run out of words in expressing my thankfulness to Prof. Ravindra Pandey, my advisor. Throughout my graduate studies, he taught me how to appreciate physics and the philosophy of life, more importantly, with a smiling face! I cannot help but express my deepest gratitude to him for the tremendous patience and tireless guidance.

I am indebted to Dr. Shashi P. Karna and Dr. Ralph H. Scheicher for implanting the ideas and setting the level of aspiration, which essentially helped me shaping this dissertation. I would like to thank Dr. Ranjit Pati, specially, for all his time teaching me molecular electronics from the scratch and letting me attend his group discussions, occasionally, which were really helpful for me in understanding the basic aspects of quantum transport.

I am truly thankful to Dr. Maximilian Seel, Dr. Donald Beck and Dr. Loredana Valenzano, my advisory committee members, for critically reviewing my work and giving me valuable suggestions.

I would also like to thank our collaborators Dr. Ishan Boustani, Dr. Aurora Costales, Dr. Gavind Mallick, Dr. Radhakrishnan Balu and my mentors during summer internship (2011) at Los Alamos National Laboratory, Dr. Enrique Batista, Dr. Richard Martin and collaborator, Dr. Xiaodong Wen, for their continuous support.

Working with the past group members Dr. Haiying He and Dr. Shankara Gowtham was very helpful in knowing and understanding the tools in computational materials science. I also acknowledge my colleagues Wil Slough, Xiaoliang, Chunhui, Jiajie and the visitors in our group Vasundhara, Prachi, Dr. Rodrigo Amorim and Dr. Mrinalini Deshpande for many fruitful discussions.

I am lucky to have friends like Arya, Sundar, Arnab, to name just a few, who have been very supportive and motivating, in all possible ways, from my college days. I am also thankful to my friends in Houghton such as Partha, a true guide, Subhasish, Colina, Niraj, Abhay, Bibhu, and the list go on.

Last, but not the least, I am immensely thankful to my parents, sisters and brothers-in-law. It is because of their inspirations and encouragements, I am, where I am right now. I am really blessed to have my wife, Rima. Her patience, support and continuous support have helped me to overcome all the barriers I faced during the last year. I also thank my entire extended family for their care and love.

Acronyms

CNT	Carbon nanotube
MWCNT	Multiwalled CNT
BNNT	Boron nitride nanotube
MWBNNT	Multiwalled BNNT
DNA	Deoxyribonucleic acid
ss-DNA	Single-stranded DNA
RNA	Ribonucleic acid
HF	Hartree-Fock
DFT	Density functional theory
LDA	Local density approximation
GGA	Generalized gradient approximation
KS	Kohn-Sham
LCAO	Linear combination of atomic orbitals
HOMO	Highest occupied molecular orbital

LUMO	Lowest unoccupied molecular orbital
NEGF	Non-equilibrium Green's function
NDR	Negative differential resistance
FET	Field effect transistor
SCF	Self-consistent field
VASP	Vienna Ab initio Simulation Package
SMEAGOL	Spin and Molecular Electronics in an Atomically Generated Orbital Landscape program
MD	Molecular dynamics
DOS	Density of states
PDOS	Partial DOS
vdW	van der Waals
Arg	Arginine
Asp	Aspartic acid
Trp	Tryptophan

Abstract

In recent years, the bio-conjugated nanostructured materials have emerged as a new class of materials for the bio-sensing and medical diagnostics applications. In spite of their multi-directional applications, interfacing nanomaterials with bio-molecules has been a challenge due to somewhat limited knowledge about the underlying physics and chemistry behind these interactions and also for the complexity of biomolecules.

The main objective of this dissertation is to provide such a detailed knowledge on bioconjugated nanomaterials toward their applications in designing the next generation of sensing devices. Specifically, we investigate the changes in the electronic properties of a boron nitride nanotube (BNNT) due to the adsorption of different bio-molecules, ranging from neutral (DNA/RNA nucleobases) to polar (amino acid molecules).

BNNT is a typical member of III-V compounds semiconductors with morphology similar to that of carbon nanotubes (CNTs) but with its own distinct properties. More specifically, the natural affinity of BNNTs toward living cells with no apparent toxicity instigates the applications of BNNTs in drug delivery and cell therapy.

Our results predict that the adsorption of DNA/RNA nucleobases on BNNTs amounts to different degrees of modulation in the band gap of BNNTs, which can be exploited for distinguishing these nucleobases from each other. Interestingly, for the polar amino acid molecules, the nature of interaction appeared to vary ranging from Coulombic, van der Waals and covalent depending on the polarity of the individual

molecules, each with a different binding strength and amount of charge transfer involved in the interaction.

The strong binding of amino acid molecules on the BNNTs explains the observed protein wrapping onto BNNTs without any linkers, unlike carbon nanotubes (CNTs). Additionally, the widely varying binding energies corresponding to different amino acid molecules toward BNNTs indicate to the suitability of BNNTs for the biosensing applications, as compared to the metallic CNTs.

The calculated I-V characteristics in these bioconjugated nanotubes predict notable changes in the conductivity of BNNTs due to the physisorption of DNA/RNA nucleobases. This is not the case with metallic CNTs whose transport properties remained unaltered in their conjugated systems with the nucleobases. Collectively, the bioconjugated BNNTs are found to be an excellent system for the next generation sensing devices.

CHAPTER 1

Introduction

1.1. Bioconjugated Nanomaterials

Recent trends to shrink the dimensionality of materials are instigated by the desire to access the unique material properties and their applications in novel fields ranging from device applications to biomedical applications. Interfacing the biomolecules, typically called ‘soft’ molecules, with the generally ‘hard’ nanostructured materials requires control of both the nature and spatial distribution of the molecular interactions that take place between the two to ensure that the former retain their remarkable properties. When the biomolecules are deoxyribonucleic Acid (DNA) or protein/peptide, the task is particularly challenging because of the heterogeneous chemical nature of nucleotide/peptide surface.

In recent years, there has been a keen interest in understanding the interaction between biomolecules and nanostructured materials ¹⁻⁹ due to potential applications of the unique signature of the latter in probing the structural and conformational changes ^{10,11} of the former resulting in a new detection mechanism ¹² and medical diagnostic tools. Very

recently, bioconjugated nanostructured materials including nanotubes^{13,14}, nanowires¹⁵, fullerenes¹⁶, and nanoparticles^{17,18} have emerged as a new class of materials for biosensing and medical diagnostics applications. Combining nanomaterials with the biological systems has a two-fold advantage. For example, DNA-decorated carbon nanotubes were shown to be effective for chemical sensing of various odors¹⁹. On the other hand, probing of conformational changes in DNA in vivo triggered by a change in the surrounding ionic concentration showed a great possibility for a new detection mechanism¹². Conversely, the structure-specific binding property of biomolecules has been used to sort carbon nanotubes of different kinds⁹. It has been already reported that molecular adsorption on inert-surfaces, such as graphene, offers an excellent model for tracking single molecules and intermolecular interaction via sophisticated surface analysis techniques⁸. Moreover, manipulating single molecules by scanning tunneling microscopy techniques is found to address the role of hydrogen bonds between the nucleobases in DNA-replication explaining the origin of life. It is a general conviction that the self-assemblies of biological macromolecules (*e.g.* DNA/RNA) on the template surface, such as graphene, has to do with the emergence of life under pre-biotic conditions⁸.

Nonetheless, the most appealing and impacting application of nanostructured materials in recent days is their use in medical diagnostics applications. Nanoparticles such as gold²⁰, titania²¹, mesoporous silica²² have been in the frontier of diagnostics tool for a long time. However, when it comes to functionalization of nanoparticles, it becomes critically important to quantify the amount of functional groups residing at the surface of

these nanoparticles and their availability to perform the desired activity. For example, carbon nanotubes (CNTs) are shown to be very effective in various biomedical applications such as imaging, photoluminescence and photo-acoustic labels, and sensing and drug delivery²³. Although, in some cases CNTs were made biocompatible after an appropriate functionalization, their toxicity along with electronic properties might vary with the tube helicity, concentric layers and so forth²⁴.

Therefore, a detailed assessment of the factors that influence biocompatibility and/or toxicity of nanoparticles to design safe and sustainable development of emerging nanotechnologies demands unification of chemistry, biology and microelectronics constrained by the physical laws at the nanometer length-scale. In spite of rapid progresses in technologies, it is yet to fully realize the advancements in detection, diagnosis, and treatment. It has been a challenging task to achieve, so far, due to the limited knowledge about the underlying physics and chemistry behind the interactions between nanomaterial and biomolecules and also the complexity of biomolecules. In order to fully capitalize on the novel properties of nano-bioconjugates, a detailed understanding of the nature, physical and chemical mechanisms, structure, and spatial distribution of conjugating molecules and nanomaterials is critically important.

The objective of this dissertation is to address some of the issues mentioned above. In Chapters 3 and 4, we shall discuss some of the features of conjugating biomolecules with the nanomaterials and their criticality in deciding the strength of interaction. Specifically, we considered boron nitride nanotube (BNNT) as a substrate on

which the biomolecules are adsorbed to lead us to different types of interaction depending on their nature and polarities.

1.2.1. Boron Nitride Nanotube

The nano-revolution has swept the world over the last couples of decades, and continues to rule the recent research work at the nanoscale regime because of its extraordinarily peculiar electronic, mechanical, optical and magnetic properties. The quantum confinement in 2D- and 1D- nanostructures offers interesting materials properties compared with their bulk counterparts, which enable us to embrace nanoscience, nanotechnology and nano-biotechnology. This new era governed by the nanostructured materials was started with the discovery of carbon nanotube (CNT) in 1991²⁵ and continues with a number of dimensionally reduced nanostructured materials such as 1D- tubes, wires, ribbons, fibers and rods which were synthesized and applied in multidirectional applications. The carbon based nanostructured materials, however, have emerged themselves as a class apart, which consists of graphene^{26,27}, CNTs^{2,28} and fullerenes^{16,29,30}.

The existence of boron nitride nanotubes was first predicted in 1994³¹, immediately after the discovery of CNT. In the seminal paper by Cohen *et al.*, the authors proposed the possibility of microscopic tubular structures form the hexagonal graphitic structure made of III-V compounds such as boron and nitrogen with both sp^2 - and sp^3 -bonded structures, similar to the C-C bonding in a carbon nanotube. The formation of a

BNNT from a BN-sheet may be seen in Fig. 1.1, exactly similar to how CNTs are formed by rolling graphene along a particular direction.

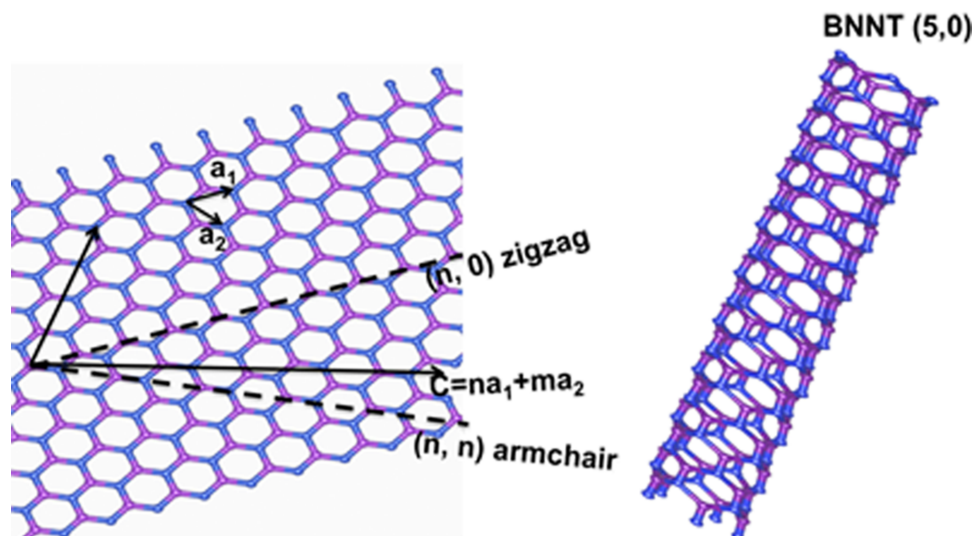


Figure 1.1: A schematic representation of boron nitride nanotube formed by rolling of boron nitride-sheet. The naming-scheme, similar to that of carbon nanotube with alternating boron and nitrogen atoms on a rolled hexagonal lattice, is also included.

Amongst all the non-carbon nanostructured materials, boron nitride nanotubes have become equally important during the last decade because of their possible technological applications that CNTs cannot provide. As far as the chemistry is involved, B-N pairs are isoelectronic substitute for the C-C pairs in CNTs but BNNTs exhibit pyroelectric, piezoelectric behaviors and photo-galvanic properties unlike CNTs. Chemical inertness and uniform electronic properties of BNNTs are the key advantages

over CNTs for their usages in nano-electronic devices⁵. In addition to these fascinating properties and applications, the reason behind the popularity of BNNTs is the uniformity in their electronic properties, which is independent of their structural parameters, chirality or helicity. For example, CNTs are reported to be metallic³², semiconductor³³ or insulator³⁴ depending on their structural parameters and therefore, synthesis of CNTs of a desired kind has been a challenge. BNNTs, on the other hand, are semiconductors with a band gap of 5.5 eV²⁴, irrespective of their structural parameters and can be tuned in a number of ways³⁻¹⁰ including molecular adsorption³⁵ and chemical functionalization,³⁶ and thereby might be used as the active component in nano-devices.

1.2.2. Boron Nitride Nanotubes in Biology

Realizing ultrasensitive single-molecule detection has been a prime goal of the scientific communities, as it involves varieties of societal areas ranging from clinical diagnostics to environmental protection. Even though mass spectroscopic techniques using amplified signal from functionalized nanomaterials have adequate sensitivity, they suffer from lack of cost-efficiency and time-consuming derivatization³⁷. Biosensing with a desired level of sensitivity and selectivity requires functionalization of nanomaterials with biomolecules with specific recognition and signal enhancing elements. Nanomaterials can be functionalized with the biomolecules mediated by electrostatic^{38,39}, covalent^{36,40,41} or van der Waals forces^{3,4,42}. However, the non-covalent functionalization^{13,43,44} of nanomaterials was reported to be more efficient as it does not completely destroy the characteristic features of the nanomaterials. Covalent approaches of

functionalizing the nanomaterials, on the other hand, are promising in terms of stability and reproducibility of the surface functionalization ³⁷. It indicates the criticality of appropriateness of how nanomaterials are to be functionalized to derive the desired materials properties.

As far as biomedical applications of nanomaterials are concerned, the first and foremost criterion that the nanomaterials has to qualify for is their biocompatibility or cytotoxicity. Although the unique signature of the nanomaterials on biological entities appeared to be very promising, only some of them have been approved for clinical use and many others are at different preclinical development. For example, performance of CNTs in drug delivery, imaging, transporter and protein stabilization is well explored and is reported to be very promising. However, the cytotoxicity of CNTs is not beyond question. Boron nitride nanotubes were recently found to be inherently noncytotoxic ⁴⁵ upon culturing the Human Embryonic Kidney (HEK)-293 cells with multi-walled (MW) BNNTs. For comparison, the HEK-293 cells were treated with the MWCNTs for a long time (4 days). The number of living cells in the solution of MWBNNT was found to be indistinguishable compared to the untreated controls, unlike the case with the MWCNTs where cell count appeared to decrease significantly. It may therefore be claimed that BNNTs are non-toxic and do not inhibit HEK-293 cell proliferation. To reconfirm this finding, similar investigations were performed on the Chinese Hamster Ovary (CHO)-cells and a similar signature was found⁴⁵. These findings call for immediate interdisciplinary efforts to verify and reconfirm the possibilities of applying BNNTs instead of CNTs and also to explore the materials properties observed with the CNTs.

With this objective, numerous efforts have been devoted to investigate the appropriateness of BNNTs for biomedical applications both from theoretical and experimental point of view. Functionalized BNNTs, similar to functionalized CNTs, were reported to bind to the proteins via ligand-receptor interactions with a targeted chemoselectivity. More importantly, no apparent toxicity was found even when BNNTs were attached to the cell surface directly ⁴⁵. BNNTs with a dimension comparable to that of CNTs, were also found to serve as molecular transporter, the most exciting application of CNTs, to deliver DNA or proteins into the cells ⁴⁵. Ciofani *et al.* investigated the cell viability of BNNTs against human neuroblastoma cells and the assessment, based on cell morphology, growth and metabolism, led to the conclusion that the cells maintain a good viability even after 3-days of the treatment ^{46,47}. BNNTs and their derivatives with quantum dots have been already shown to be promising for cellular tracking-studies by fluorescence microscopy and laser scanning techniques ⁴⁸.

Furthermore, for all biomedical applications, the nanomaterials are required to be dispersed in aqueous solution first which neither CNTs nor BNNTs qualify for. In order to overcome the poor solubility of these nanotubes, different approaches were explored via surface modification using various surfactants or polymers. BNNTs were made to disperse in the organic solvents upon wrapping them with the proteins ⁴⁹ where as Ikuno *et al.* used functionalization of BNNTs with amine-group for an efficient way of dissolving BNNTs in chloroform ⁵⁰. It is worth mentioning that these functional groups often affect the properties of the nanotube and act like impurities unless appropriate measures are taken to remove them. An efficient way of functionalizing BNNTs for their

dispersion in the solution is to choose the functional group with no apparent toxicity. Polyethyleneimine (PEI), for example, is known to have an acceptable cytocompatibility and is used widely for drug delivery. Yu *et al.* used PEI to coat the BNNTs for their dispersion in aqueous solution. Another advantage in choosing PEI as a surfactant is that it can be easily washed away by water⁵¹.

Due to the above-mentioned advantages and lack of a detailed and accurate knowledge about the biomolecular interaction of BNNTs, we shall investigate the interaction of BNNTs with biomolecules of different polarities in Chapters 3 and 4 along with the transport properties in the hybrid-systems in Chapter 6. From a theoretical point of view, we shall illustrate the nature of interaction as a function of the molecular-polarities and compare them with the previously reported results on biomolecular interaction of CNTs, whenever possible.

1.3.1. Molecular electronics

Owing to the fundamental physical limit on further downscaling of the solid-state device components, molecular-scale electronics has been a subject of intense experimental^{52,53} and theoretical studies^{54,55}, soon after Aviram-Ratner predicted the possibility of electrical rectification by a single molecule⁵⁶. Various characteristic functions representing active elements of electronic devices ranging from wires⁵⁷, switches⁵⁸, diodes^{56,59}, transistors^{54,60-64} and memories⁶⁵ have been illustrated by single molecules. The challenging part in electron transport at mesoscopic length-scale is to

understand the coupling of molecular structure to the macroscopic electrodes under non-equilibrium conditions. There were two types of transport junctions at the initial stage of molecular electronics: (a) a single molecule attached to the metal electrodes via thiol-linkers, and (b) a self assembled monolayer on a metallic surface where the current was measured using scanning probe tip. In the latter approach, the measured current was always found to be under-estimated, as the scanning probe was not chemically bound to the molecule, in contrast to the former one. As far as the theoretical investigations are concerned, aligning the Fermi-energy of the molecules to that of the electrodes was one of the difficult issues. Assuming the molecular Fermi-energy to lie within that of the junctions, was a very common practice, which is, in general, not true for most of the cases. Generally, the highest occupied orbital of a single molecule is roughly at -9 eV whereas the Fermi energy of a noble metal electrode is at around -5 eV⁶⁶. This issue with matching the Fermi-energy of the electrode to that of the molecule, however, has been resolved in the non-equilibrium Green's function approach⁶⁶.

The breakthroughs in molecular electronics, in earlier days, involve the observation of unimolecular electrical rectification in hexadecylquinolinium tricyanoquinodimethanide⁶⁷, which confirms the theoretical prediction by Aviram-Ratner. In the same year (1997), the electrical conductance of a single molecule (benzene-1,4-dithiol) sandwiched in between two electrodes was measured by Mark Reed and co-workers⁶⁸. These are amongst those pioneering experiments providing the direct evidences of the predicted electronic conduction at molecular scale, from the theoretical perspective. It would be injustice not to mention the measurement of

‘conductance quantum’ by Frank *et al.*⁶⁹ in this context. In this experiment, the conductance of MWCNTs was measured replacing the scanning probe microscope with a nanotube fiber and thereby, establishing a gentle electrical contact with the nanotube at the tip of the fiber. The findings from this experiment are of significant importance as this was the first-ever measurement of the fundamental constant ‘quantum conductance’ ($G_0 = 2e^2/h = 12.9 \text{ K}\Omega^{-1}$) implying that the electrons in MWCNTs are strongly decoupled from the lattice.

The electronic conduction through metal-molecule junctions involves many interesting phenomenon such as Coulomb blockage, Kondo effect and negative differential resistance, which deserved mentioning here. Coulomb blockade was observed for fullerene (C_{60})⁶⁴, p-phenylenevinylene (PPV) oligomers⁷⁰, with five benzene rings connected via C-C double bonds. In the experiment, the single C_{60} -transistor architecture was formed by depositing the dilute toluene solution of C_{60} in the gap of the electrodes which were formed by electro-migration⁶⁴. The current-voltage characteristics observed for the device was found to exhibit strongly suppressed conductance near zero bias voltage with a subsequent jumps at higher voltages, an evident signature of Coulomb blockade due to the coupling between the quantized electronic and mechanical degrees of freedom of the molecule with that of the electrode. As shown by Park and co-authors, the charging energy of the C_{60} molecule can exceed 150 meV , which appears to be larger than in semiconductor quantum dots^{64,71}. Furthermore, Kubatkin *et al.*⁷⁰ reported eight successive charge states for PPV-oligomer suggesting that the transport experiment had access to many different charge or redox

states. Although the inherent HOMO–LUMO of the oligomer is approximately 2.5 eV, it reduces significantly (0.2 eV) in the presence of the metallic contacts due to the image charges generated in the source and drain electrodes by the charges on the molecule.

The Kondo effect^{70,72,73}, essentially the scattering of conduction electrons in a metal due to magnetic impurities, was also illustrated experimentally in a molecule incorporating transition-metal atoms due to the single-electron charging and energy-level quantization. With the increasing coupling to the electrodes at higher bias, higher-order tunneling and correlated electronic-motion is concluded to give rise to interesting phenomena such as the Kondo resonance.

Negative differential resistance (NDR) was found in Fe-terpyridine linker molecule⁷⁴ due to the broken symmetry of the wavefunction of the molecule as a result of increasing applied bias due to the mixing of occupied and unoccupied molecular orbitals. As a consequence, a nonlinear change in the coupling between the molecule and the lead results in a non-linear current, which leads to the reduction of current with increasing bias.⁷⁴

However, demonstration of three-terminal devices^{54,75}, where the current through a molecular architecture under biased condition can be modulated by a second gate field, analogous to the field-effect transistors (FETs), has not so far been realized experimentally. Inability to controllably assemble molecules in desired architectures and techniques to measure single-molecule current (I)-voltage (V) characteristics and appropriate physical principles to synthesize collective response of molecules into individual elements similar to a solid state “voltage gated” three-terminal device, have

been the major bottleneck against a rapid advancement in molecular electronics. Despite all the challenges and difficulties, the first break through experiment to observe direct evidence of orbital gating at molecular scale was reported by Song *et al.* in 1, 8-octanedithiol (ODT) and 1,4-benzenedithiol (BDT) molecules⁷⁶ sandwiched between two gold electrodes. The gate-field dependent I-V characteristics was found to be originated because of the relative movement of the molecular orbitals with respect to Fermi-energy (E_f), as a result of gating, and thereby, an enhanced orbital coupling at the metal-molecule junctions.

Electric field gating of organic molecular current under bias can be assumed as a natural extension of field effect transistor (FET) in microelectronics. It has been beyond the reach of experimental efforts because of the technical challenges associated in assembling the organic molecular system with a desired orientation in the presence of another electrode (gate-electrode). Observation of transistor effect is therefore very tricky and sometimes misleading too, since the transport properties through the molecular structure greatly depends upon the molecular orientation. The transistor effect can also be realized by introducing conformational changes in the molecules without introducing the third electrode. Organic molecular architectures, specifically, offer the possibilities of chemical/structural gating in which the change in the structure due to molecular rotation, conformational change or coupling of vibrational modes with electronic modes is known to modulate the current across the molecule under biased condition⁶³.

1.3.2. Molecular Electronics in Biology

Although the development of molecular electronics was to substitute the silicon by molecular architecture as an active element in solid state devices in order to overcome the limitation on further miniaturization of the solid state components, it has fascinating applications in biology. In fact, molecular electronics was first introduced by Albert Szent-Györgyi (1967), a biochemist, to relate the electronic mobility and charge transfer. Very recently, molecular electronics was used to explain the role of chemical gating in naturally occurring processes such as photosynthetic reaction center and enzyme specificity where the geometrical changes in the enzymes turns the active site to inert to substrate and vice versa ⁶³. Apart from that, molecular electronics has ample scope in explaining a number of biological processes, which particularly involve electronic transport. This explains the recent craze to bridge quantum transport with biology.

The application of this idea promises benefits in two ways: use of mesoscopic transport in biology and use of biomolecules in mesoscopic transport. The former is important to resolve the controversial experimental observations to assess the transport properties in DNA. The conclusions from experiments vary from insulator to semiconductor and conductor. However, the actual mechanism of the charge transport through DNA has been illusive so far. This is partly because of the numerous parameters to be controlled in experiments and also due to the complexity of the structure to deal with in the presence of electrodes. Additionally, in order to design genome-based medicine we need faster and cheaper schemes for DNA-sequencing. To tackle the problem, one needs to have the flexibility to measure time-dependent current as a

function of relative orientation of the nucleobases both in the presence and absence of the transverse electric field. Using biomolecules for molecular electronics is already discussed in the previous section.

In Chapter 5, we shall consider a model three terminal transistor to illustrate how the performance of the transistor can be controlled via voltage gating as well as conformational gating. We shall also connect our findings from the conformational gating to the role of chemical gating in the naturally occurring phenomenon such as photosynthetic reaction center and enzyme specificity. In Chapter 6, on the other hand, we shall use quantum transport to generate signals in bioconjugated BNNTs and CNTs for their applicability as biosensors.

CHAPTER 2

Theoretical Methods

Throughout in this dissertation we shall use theoretical approaches to model the systems of interests and investigate their properties to serve our objectives. In order to do that, we employed electronic structure calculation and mesoscopic transport phenomenon. In this Chapter, we shall focus on describing the essential concepts belonging to the above-mentioned categories. Since the number of approaches and approximations related to these categories is fairly large, we shall highlight only those used in this dissertation.

2.1. Electronic Structure from First Principles

For a single electron, the time-independent Schrödinger equation can be expressed as:

$$H\psi(\mathbf{r}) = \varepsilon\psi(\mathbf{r}) \quad (2.1)$$

with $\psi(\mathbf{r})$ being the electronic wavefunction at \mathbf{r} , and ε being the eigenenergies of the Hamiltonian:

$$H = -\frac{\hbar^2}{2m}\nabla^2 + V(\mathbf{r}) \quad (2.2)$$

where $V(\mathbf{r})$ is the potential energy of the electron at \mathbf{r} . Solving the one electronic Schrödinger equation to obtain a complete set of energy eigenfunctions is trivial. However, to investigate the materials properties, it is essential to solve the many-body Schrödinger equation taking the perturbations of all kinds into account. For example, for a typical molecular coordinate system with two representative nuclei and two electrons, as shown in Fig. 2.1, the Hamiltonian, in the atomic units, can be represented as ⁷⁷:

$$\begin{aligned} H = & -\sum_{i=1}^N \frac{1}{2} \nabla_i^2 - \sum_{A=1}^M \frac{1}{2M_A} \nabla_A^2 - \sum_{i=1}^N \sum_{A=1}^M \frac{Z_A}{(\mathbf{r}_i - \mathbf{R}_A)} \\ & + \sum_{i=1}^N \sum_{j>i}^N \frac{1}{(\mathbf{r}_i - \mathbf{r}_j)} + \sum_{A=1}^M \sum_{B>A}^M \frac{Z_A Z_B}{(\mathbf{R}_A - \mathbf{R}_B)} \end{aligned} \quad (2.3)$$

Eq. 2.3 is a generic equation of Hamiltonian of a typical system with N-electrons and M-nuclei with M_A being the ratio of mass of the nucleus A to the electronic mass and Z_A (Z_B) is the atomic number of the nucleus A (B). For the coordinate system in Fig. 2.1, M=N=2. The first and second term in Eq. 2.3 is the kinetic energy operator of the electrons and nuclei, respectively; the third term stands for the Coulombic attraction between the electrons and nuclei; the fourth and fifth term represents the repulsion between the electrons and nuclei, respectively. Despite all the advances and improvements in the modern quantum chemistry, it is not possible to obtain the exact

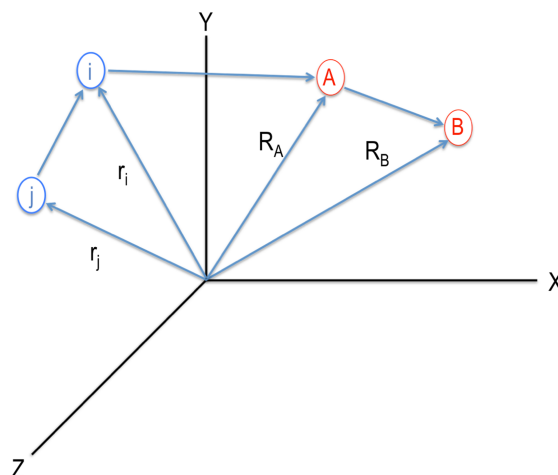


Figure 2.1: Schematic representation of molecular coordinate system adapted from the book “Modern Quantum Chemistry: Introduction to Advanced Electronic Structure Theory”⁷⁷ where ‘*i*’ and ‘*j*’ stands for electronic and ‘A’ and ‘B’ represents nuclear coordinates, respectively.

solutions for the Hamiltonian in Eq. 2.3, except for the simplest cases. Rationale approximations, however, enables us to find its approximated solutions.

2.1.1. Born-Oppenheimer Approximation

The Born-Oppenheimer approximation⁷⁸ is one of the central approximations in quantum chemistry. It is based on the fact that the nuclei are much heavier than the electrons and they move much slowly in comparison with the electrons. Hence, the electrons in a molecule can be approximated to move in the field of the fixed nuclei. As a consequence, the second term in Eq. 2.3, the kinetic energy of the nuclei, vanishes for

smallness. Additionally, the last term, the repulsion between the nuclei, becomes a mere constant. Since a constant added to an operator merely shifts its eigenvalues without changing its eigenfunctions ⁷⁷, the electronic Hamiltonian under the influence of M-point charges may be rewritten as:

$$H = -\sum_{i=1}^N \frac{1}{2} \nabla_i^2 - \sum_{i=1}^N \sum_{A=1}^M \frac{Z_A}{(\mathbf{r}_i - \mathbf{R}_A)} + \sum_{i=1}^N \sum_{j>i}^N \frac{1}{(\mathbf{r}_i - \mathbf{r}_j)} \quad (2.4)$$

with the electronic wavefunction in the Schrödinger equation as:

$$\Phi_{elec} = \Phi_{elec}(\{\mathbf{r}_i\}; \{\mathbf{R}_A\}) \quad (2.5)$$

Eq. 2.5 describes the motion of electrons and explicitly depends on the electronic coordinates with a parametric dependence on the nuclear coordinates. It implies that for different rearrangements of the nuclei coordinates Φ_{elec} will be a function of different electronic coordinates. Born-Oppenheimer approximation makes it easier and affordable to solve the many-body Schrödinger equation without affecting the accuracy of the results.

2.1.2. Hartree-Fock Approximation

Even within the Born-Oppenheimer approximation, which makes the many-body Hamiltonian much simpler, finding solutions to the many-body Schrödinger equation beyond the simplest cases like H_2^+ , has been a major preoccupation of the quantum chemist-community. In 1927, Hartree proposed the first step towards further simplification to this problem. The Hartree approximation considers the electrons as distinguishable particles. This simplifies the summations and reduces the number of variables the summations need to be carried over in Eq. 2.3; however, electrons, being indistinguishable spin-1/2 particles, follow the Pauli's exclusion principle, which essentially demands that no two fermions can have same quantum states. This unique and fundamental principle requires the wavefunction to be antisymmetric and therefore, to flip sign under particle exchange. The Hartree-approximation lacks this antisymmetric behavior of the electronic wavefunction.

The Hartree-Fock [HF] approximation⁷⁷ was the next step towards the immediate improvement over what was proposed previously by Hartree. In this approximation, the antisymmetric nature of the electronic wavefunction was incorporated introducing the spatial and spin component of the electrons into the electronic wavefunction and expressing them in terms of Slater determinant as follows:

$$\Phi_{HF}(x_1, x_2, \dots, x_N) = \frac{1}{\sqrt{N!}} \begin{vmatrix} \varphi_1(1) & \varphi_2(1) & \dots & \varphi_N(1) \\ \varphi_1(2) & \varphi_2(2) & \dots & \varphi_N(2) \\ \vdots & \vdots & \dots & \vdots \\ \varphi_1(N) & \varphi_2(N) & \dots & \varphi_N(N) \end{vmatrix}$$

$$= SD\{\varphi_1(1)\varphi_2(2)\varphi_3(3) \dots \dots \dots, \varphi_N(N)\} \quad (2.6)$$

where N represents the total number of electrons in the system and $\varphi_i(j)$ stands for the i^{th} electron spin-orbital, which changes its sign when the spatial and spin component of the j^{th} electron is exchanged with it. Even though it is not a completely general description, yet this treatment introduces the particle-exchange exactly. With this postulation, the Hartree-Fock energy can be written as:

$$E_{HF} = \sum_{i=1}^N E_{ii} + \frac{1}{2} \sum_{i=1}^N \sum_{j=1}^N (J_{ij} - K_{ij}) + V_{nn} \quad (2.7)$$

with

$$\sum_{i=1}^N E_{ii} = \int \varphi_i^* h_1(1) \varphi_i dx_1. \quad (2.8)$$

In Eq. 2.7, E_{ii} represents the one-electron contribution to the total energy with ' h_1 ' as one-electron Hamiltonian operator given in Eq. 2.3 and V_{nn} stands for the inter-nuclei interaction energy. The second term in Eq. 2.7 is the two-electron terms to the energy^{77,79}.

In the Slater-determinant representation the two electronic interactions can be expressed as:

$$E_{ijklmn}^{(2)} = \iint \varphi_1^*(i) \varphi_2^*(j) \frac{1}{|\mathbf{r}_k - \mathbf{r}_l|} \varphi_1(m) \varphi_2(n) d\mathbf{x}_1 d\mathbf{x}_2 \quad (2.9)$$

with $i \neq j$, $k \neq l$ and $m \neq n$. Two kinds of situation may arise for the two electronic contributions in Eq. 2.9, depending upon the values of the indexes. For example, when $i = k = m$ and $j = l = n$, the two-electronic contribution is simply the Coulomb integrals in the Hartree method and can be represented as:

$$J_{ij} = E_{iijj}^{(2)} = \iint \varphi_1^*(i) \varphi_2^*(j) \frac{1}{|\mathbf{r}_i - \mathbf{r}_j|} \varphi_1(i) \varphi_2(j) d\mathbf{x}_i d\mathbf{x}_j. \quad (2.10)$$

The other class belongs to the case when $i = k = n$ and $j = l = m$ and is called exchange integrals:

$$K_{ij} = E_{ijji}^{(2)} = \iint \varphi_1^*(i) \varphi_2^*(j) \frac{1}{|\mathbf{r}_i - \mathbf{r}_j|} \varphi_1(j) \varphi_2(i) d\mathbf{x}_i d\mathbf{x}_j \quad (2.11)$$

It is worth mentioning here that the exchange integrals do not have any counterpart from a classical standpoint. They correspond to the extra-stability of the electronic systems due to the antisymmetric nature of the wavefunction. The pre-factor, $\frac{1}{2}$, in Eq. 2.7 compensates for the double counting in the double sum (ij and ji) following the classical two-body potentials⁷⁹.

The main difference between the Hartree-Fock equations from that in the Hartree approximation is the presence of exchange integrals, which take into account the coupling between the two independent one-particle states in the Hartree approximation. This non-local term makes the position of each of the electrons to depend on the surrounding electrons, which basically ensures the electrons from being independent-one-particle to fermions obeying the Pauli's exclusion principle. The proposition in Hartree-Fock theory, therefore, has an immense impact on the modern quantum chemistry. However, it is not complete, as it does not include the correlation between the electrons. Additionally, since it is based on the electronic wavefunction, it is prohibitively expensive for large systems; the cost goes up to N^5 with N being the number of electrons in the system⁸⁰. The role of correlation energy in the many-body interaction has duly been taken care of in Density Functional Theory, discussed in the following section.

2.2. Density Functional Theory

In the previous section, we discussed the electron-electron interactions from perturbative approaches. This method is affordable either for non-interacting electrons under the effect of external potential or interacting electrons not perturbed by the external potential. Nevertheless, in the real case scenario, the electrons undergo interactions of both the kinds. This makes the size of the Hilbert space and the Hamiltonian matrix to be diagonalized, grow factorially with the number of electrons in the system. Practically, it is formidable to deal with, although the imposition of symmetry is expected to reduce the size of the Hamiltonian by a factor of ten^{81} . This called for an urgent need of some

alternative way to include the electron-electron interaction correctly and systematically but at the same time at an affordable computation cost. Realistically, the only way to do so is what was proposed in Density Functional Theory (DFT).

2.2.1. Thomas-Fermi Theory

The origin of DFT takes us back in 1927 when Thomas and Fermi (1928) independently proposed a scheme to calculate the energy of an electronic system in terms of electronic density⁸². The idea was to express the total electronic energy in such a way that the kinetic, exchange and correlation energies were derived from the homogeneous electron gas with known approximations as:

$$E_{TF}[n] = C_1 \int d^3r \rho(\mathbf{r})^{5/3} + \int d^3r V_{ext}(\mathbf{r})\rho(\mathbf{r}) + C_2 \int d^3r \rho(\mathbf{r})^{4/3} + \frac{1}{2} \int d^3r \int d^3r' \frac{\rho(\mathbf{r})\rho(\mathbf{r}')}{|\mathbf{r} - \mathbf{r}'|} \quad (2.12)$$

with $C_1 = 2.871$ and $C_2 = 0.289$ in atomic units. As can be seen in Eq. 2.12, the energies and density has a functional dependency on the electronic density $\rho(\mathbf{r})$ where $\int d^3r \rho(\mathbf{r}) = N$; total number of electrons⁸¹. The assumption of taking inhomogeneous system as an ensemble of locally homogeneous systems for kinetic energy-term might be sensible for condensed phases such as metals but for atomic and molecular systems it is too severe of an approximation. This results in density profiles, which diverge at the nucleus and does not decay exponentially at long distance. Improvement over these shortcomings requires a better kinetic energy functional; however, this may be taken as

the first ever attempt to express electronic energy in terms of a locally homogenous electronic density, essentially the backbone of local density approximation (LDA) in modern DFT.

2.2.2. Hohenberg-Kohn theorem

The Thomas-Fermi theory was based on the assumption that the electronic energies may be expressed in terms of electronic density, exclusively. The concept was innovative but based on intuition. The mathematical formulation of the theorem and its proof was given by Hohenberg and Kohn (1964), based on a concept similar to that of Thomas-Fermi theory. This is known as the Hohenberg-Kohn theorem⁸³. It essentially states that mapping from external potential energy to the ground state electron density of the system is invertible. Explicitly, if we have a system with N-electrons and ground state electronic density $\rho(\mathbf{r})$; then the Hamiltonian of the system and thereby the eigenstates and expectation value of any other operators can be determined uniquely. In other words,

$$\varepsilon[\rho] \equiv \langle \Psi_0[\rho] | T + V_{ext} + V | \Psi_0[\rho] \rangle \quad (2.13)$$

Here, V_{ext} is the external potential of a particular system with ground state density $\rho(r)$ and ground state energy ε_0 . It implies that knowing the ground state density of a N-electronic system allows determining ‘*everything*’ of the system. In principle ‘*everything*’ includes excited states, excitation energies, transport properties and so forth. The reason

behind the popularity of DFT in computational physics and chemistry is the reduction of the number of parameters to optimize, which shrinks the computational cost significantly. The accuracy of the results, however, immensely depends on the ‘exactness’ of the ground state density, which by no means one can guarantee.

2.2.3. Kohn-Sham Theorem

The Kohn-Sham approach leads us to very useful approximations, which are now the basis of most of the calculations attempting to make ‘first-principles’ predictions for material properties in both solids and molecules. The Kohn–Sham (KS)⁸⁴ approach to deal with the many-body interacting systems is to replace them by an auxiliary non-equilibrium system whose independent-particle equations can be exactly soluble numerically. The many-body terms in the actual Hamiltonian of the interacting system is then incorporated by introducing an exchange–correlation functional of the density. This approach is based on two assumptions:

- I. It is possible to represent the exact ground state of any system by the ground state density of an auxiliary system of non-interacting electrons, namely ‘non-interacting-V-representability’.
- II. The auxiliary Hamiltonian can be divided into the usual kinetic operator and an effective local potential $V_{\text{eff}}(\mathbf{r})$ acting on electrons at \mathbf{r} :

$$H_{aux} = \frac{1}{2} \nabla^2 + V_{eff}(\mathbf{r}) . \quad (2.14)$$

Here, we used the Hartree atomic units with $m_e = e = 4\pi/\epsilon_0 = \hbar/2\pi = 1$. The actual calculations are then performed using this Hamiltonian with the ground state electronic density of the auxiliary system, constructed from the electronic wavefunction, $\psi(\mathbf{r})$:

$$\rho(\mathbf{r}) = \sum \rho(\mathbf{r}) = \sum_{i=1}^N |\psi_i(\mathbf{r})|^2 . \quad (2.15)$$

The kinetic energy of the non-interacting electrons is expressed as:

$$T_s = -\frac{1}{2} \sum_{i=1}^N \int |\nabla \psi_i(\mathbf{r})|^2 d\mathbf{r}^3 . \quad (2.16)$$

The full interacting many-body problem reduces now to rewrite the Hohenberg-Kohn equation for the ground state energy functional as:

$$E_{KS} = T_s[\rho] + \int d\mathbf{r} V_{eff}(\mathbf{r})\rho(\mathbf{r}) + E_{Hartree}[\rho] + E_{nu} + E_{xc}[\rho] . \quad (2.17)$$

Here, $V_{eff}(\mathbf{r})$ is the potential due to the nuclei and any additional external field present, $E_{Hartree}$ stands for the Hartree energy having functional dependency of the ground state electronic density and E_{nu} is the interaction between the nuclei. It is important to note

that the Kohn-Sham approach is also applicable for the spin-polarized systems where the ground state density is assumed to depend on the electronic spin (σ)^{79,85}.

The introduction of the non-interacting auxiliary system in the Kohn-Sham scheme allows us to account for the most important part of the kinetic energy exactly but at the cost of expensive numerical tasks. A good description of the kinetic energy forces us to solve the equations for N -lowest eigenstates rather than solving a single equation of the ground state density under the influence of an external potential. Nonetheless, the Kohn-Sham approach leads us to a practical and reasonable accurate way to investigate ground state properties by mapping the many-body problem onto a self-consistent one-electron problem. The task that remains at this stage is to design reliable and practical approximations for the exchange-correlation functional. A schematic representation of the self-consistent-field approach for solving the Kohn-Sham equations in a electron structure calculation is shown in Fig. 2.2.

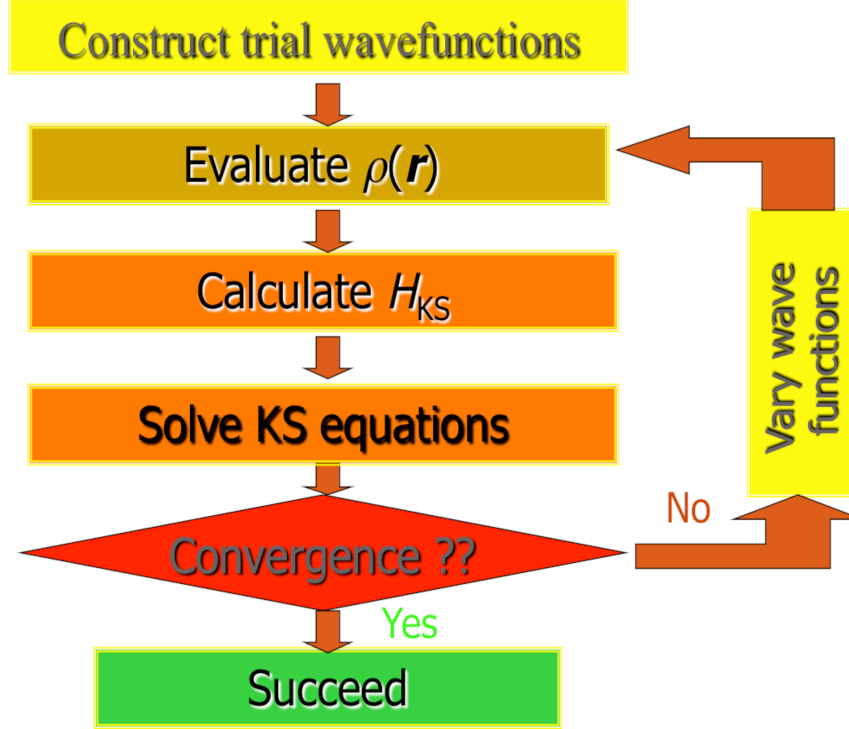


Figure 2.2: A schematic representation of the self-consistent field approach for solving the Kohn-Sham equations in electronic structure calculations, adapted from the book “Electronic Structure; Basic Theory and Practical Methods”⁸¹.

2.2.4. Exchange and Correlation Functional Forms

The ingenuity of the Kohn-Sham approach is to tackle the many-body electronic system by splitting the independent-particle kinetic energy and the long-range Hartree terms. The remaining exchange-correlation functional $E_{xc}[\rho]$ can be approximated in terms of local, if not, nearly local density functional as:

$$E_{xc}[\rho] = \int d\mathbf{r} \rho(\mathbf{r}) \epsilon_{xc}([\rho], \mathbf{r}). \quad (2.18)$$

The exchange-correlation term is, however, a big unknown, which is required to be formulated under consistent approximations. One trivial solution is to describe the auxiliary system by homogeneous electron gas but it essentially limits the application of this approach to the metallic systems of simplest correlated electrons only. The solutions to the problem of inhomogeneous systems, such as molecules, remain elusive.

2.2.5. Local Density Approximation

The local density approximation (LDA) within DFT has been one of the most popular approximations to define the exchange-correlation term in the KS-approach proposed by Kohn and Sham (1965)⁸⁴. It has been widely used and reasonably accurate description since then; however, the philosophy behind it was already presented in the Thomas-Fermi-Dirac theory. The main idea is to consider the inhomogeneous systems as locally homogeneous and then treat the exchange correlation hole corresponding to the locally homogeneous electron gas, which is known to an excellent accuracy. Practically, the energy terms, which are local in the density, are calculated by integrating over the volume that the electronic system assumes at every point \mathbf{r} :

$$E_{XC}^{LDA}[\rho] = \int d^3\mathbf{r} \rho(\mathbf{r}) \varepsilon_{xc}^h[\rho(\mathbf{r})]. \quad (2.19)$$

Here $\varepsilon_{xc}^h[\rho(\mathbf{r})]$ is the exchange–correlation energy density of the electron gas was treated as locally homogeneous. The rationality of LDA is that the range of effects of exchange and correlation is rather short for densities found in the solids, which reduces the

computational cost as well as suits best for the approximation: ‘locally inhomogeneous’. The most important limitation in LDA is the spurious self-interaction, which may be negligible in the homogeneous gas but gets manifested in confined systems, for example, atoms or molecules. However, the extent to what LDA has been successful in predicting the ground state properties of systems is amazingly wide, satisfactorily physical and accurate⁸⁵.

2.2.6. Generalized-Gradient Approximation

To address the shortcomings of LDA and treat the inhomogeneity in the electron density, the exchange-correlation energy is expressed in the generalized-gradient expansion with a correction function, F_{xc} , an enhancement factor that modifies the LDA-description of the electron-density according to the variation of the density in the vicinity of the point (\mathbf{r}) under consideration:

$$E_{xc}[\rho] = \int \rho(\mathbf{r}) \varepsilon_{xc}^h[\rho(\mathbf{r})] F_{xc}[\rho(\mathbf{r}), \nabla \rho(\mathbf{r}), \nabla^2 \rho(\mathbf{r}), \dots] d^3\mathbf{r} . \quad (2.20)$$

The Generalized-Gradient Approximation (GGA) generally improves the accuracy over the LDA by removing some of its shortcomings. Experiences, so far, show that GGA improves binding energies, bond lengths, energetics, properties of semiconductors and so forth over LDA but it has its own limitations in describing the known asymptotic nature far from atomic nuclei^{81,85}.

2.2.7. Exchange and Correlation Functional Forms

It is evident that neither LDA nor GGA works accurately for all systems owing to their own limitations and known drawbacks. One of the main problems in the known exchange correlation is the presence of the self-interaction term, which in general is absent in the Hartree-Fock exchange. This instigates the need of functional forms of third kind, called hybrid functional where the orbital-dependent Hartree-Fock exchange is combined with the explicit density functional. It was Becke⁸⁶ who first proposed to express the exchange-correlation energy as a linear combination of Hartree-Fock and local, and gradient-corrected exchange term as:

$$E_{xc} = \frac{1}{2}(E_x^{HF} + E_{xc}^{DFA}) \quad (2.21)$$

Where DFA stands for LDA or GGA functional. Amongst all the varieties of hybrid exchange-correlation functional such as B3P91⁸⁷, PBE⁸⁸, BLYP^{89,90} and so forth, the most popular and knowingly accurate to work for almost all the systems is B3LYP, which defines the exchange-correlation energy as:

$$E_{xc} = E_{xc}^{LDA} + a_0(E_x^{HF} - E_x^{DFA}) + a_x E_x^{Becke} + a_c E_c \quad (2.22)$$

where the coefficients are empirically adjusted to fit the atomic and molecular data. Since the orbital interpretation in B3LYP^{89,90} is more rigorous, it produces a rationale description of band gap in semiconductors, more often, more accurate than that LDA or GGA⁸¹ leads to.

It is worth mentioning here that DFT with all its approximations does not work and produce results of desired accuracy for all systems. It is therefore instructive to test the functional forms for known systems and check their applicability with respect to the systems under investigation and it is also a good practice to use different exchange-functional forms to validate their suitability for the particular system.

2.3. Molecular Orbital Theory

In the previous section we mainly focused on the many-body Hamiltonian to describe the interactions present in the many electronic and nuclei systems. However, solving the electronic structure problem, either via Hartree-Fock approximation or density functional theory, demands a proper representation of the one-electron orbitals, the building blocks of the many-electron systems. The most prevailing approach towards this is Molecular Orbital (MO) Theory, which represents the molecular orbitals as a linear combination of atomic orbitals (LCAO) as:

$$\psi_k(\mathbf{r}) = \sum_{\mu} a_{\mu k} \phi_{\mu}(\mathbf{r}) \quad (2.23)$$

where $\phi_\mu(\mathbf{r})$ stands for the atomic orbitals and $a_{\mu k}$ represents the corresponding expansion coefficients. The atomic orbitals are then expressed as linear combination of suitable basis functions χ_i and basis function expansion coefficients $c_{i\mu}$ as:

$$\phi_\mu(\mathbf{r}) = \sum_i c_{i\mu} \chi_i(\mathbf{r}). \quad (2.24)$$

It is evident that solving the Schrödinger equation and thereby obtaining the eigenenergies centrally depends upon the appropriateness of the basis functions. Unfortunately, by no means a single basis function qualifies to work for systems ranging from atoms-to-molecules-to-solids. Depending on the nature of the problem to address, there are many basis functions formulated so far. Broadly, they may be categorized into two classes: localized and delocalized basis sets; and two types: analytical and numerical. In this dissertation we have used Gaussian type, numerical and plane wave basis sets to address different problems with different boundary conditions (periodic/finite).

2.4. Basis Sets

As mentioned in Sec. 2.3 the central idea in MO-theory is to represent the molecular orbitals as a linear combination of atomic orbitals. In order to mathematically satisfy the completeness of the expansion of the function, the summation in Eq. 2.3 should in principle run over μ , with infinitely large value. Practically, it blows up the cost of computation immensely, which is probably beyond the scope of the modern quantum

chemistry. Instead, the basis functions are designed keeping two factors in consideration: (a) inclusion of the fewest possible number of basis functions and yet represent the system rationally; (b) ease out the computation of the integrals needed to performed. In the following section we shall introduce three typical basis sets used explicitly in this dissertation.

2.4.1. Gaussian-Type Basis Sets

Perhaps the most popular and useful basis functions used in electronic structure calculations of molecules are Gaussians multiplied by polynomials, namely, the Gaussian-type orbitals (GTO), proposed by Boys (1950). The Gaussians have enormous advantages because all the integrals can be computed analytically. The exponents of the Gaussian functions are variationally optimized to fit the corresponding atomic wavefunctions. Gaussian functions in Cartesian coordinate may be represented as:

$$\phi_{ijk}(\mathbf{r}) = \chi_i(\mathbf{x})\chi_j(\mathbf{y})\chi_k(\mathbf{z}) \quad (2.25)$$

where

$$\chi_i(x) = \left(\frac{2\alpha}{\pi}\right)^{1/4} \sqrt{\frac{(4\alpha)^i}{(2i-1)!}} x^i e^{-\alpha x^2} \quad (2.26)$$

and $\chi_j(\mathbf{y})$ and $\chi_k(\mathbf{x})$ may be obtained similarly. The main advantage of Cartesian GTOs is that molecular integrals factorize into three Cartesian variables. The extremely important property of Gaussian functions is that the product of two Gaussian with

different centers is also a Gaussian with different center and exponent. The main problem with Gaussian functions is their properties at the origin, where the derivative of GTOs becomes zero. To recover the cusp-condition using GTO, a new class of orbitals is constructed as fixed linear combination of primitive Gaussians (PGTOs) as ⁷⁹:

$$G^{CGTO}(\mathbf{r}, \{\alpha_i\}) = \sum_{i=1}^k a_i G^{PGTO}(\mathbf{r}, \alpha_i). \quad (2.27)$$

G^{CGTO} are known as contracted GTOs (CGTOs) and a_i are the contraction coefficients. In this approach, both the coefficients and the exponents in the CGTOs are optimized to reproduce the ground state orbitals at desired level of theory and accuracy. It is important to keep in mind that the most popular basis sets optimized for the HF calculations might not be as desirable for LDA or GGA.

Various types of basis functions are now available in modern quantum chemistry. For example, a minimal or single- ζ basis set assigns a single basis function per atomic orbital, which works fairly well for isolated atoms. In double (triple)- ζ basis set two (three) orbitals are used per atomic orbital. Of course, increasing the size of the basis functions enhances the accuracy of the results but it increases the cost of computations too. It is therefore advisable to choose a basis set, which is affordable yet reasonably accurate. There is another class of basis set, which is known to be more efficient, namely, split valence type where the core shells are represented by a single VGTO and multiple CGTOs are considered for the valence orbitals. The commonly used basis sets 3-21G, 6-31G, and so forth belongs to this category. These basis sets when

supplemented with a single set of 3d polarization primitives are called 3-21G*, 6-31G* and so forth.

Nevertheless, the heavy atoms, such as transition metals, demand extra attention by including relativistic effects, which affect the valence electrons substantially. To address this issue, the chemically inert core electrons are replaced by an effective potential. Treating the molecule with heavy elements becomes a feasible valence-electron problem with the relativistic effect partially taken into account. Basis sets of these kinds are called effective core potential (ECP)-type basis sets^{79,81}. For example, Los Alamos National Laboratory Double-Zeta (LANL2DZ)⁹¹ basis set uses Los Alamos ECP with scalar relativistic effect plus DZ on Na-La, Hf-Bi. In chapter 5, we shall be using LANL2DZ extensively for the gold atoms used as electrodes for the transport calculations.

2.4.2. Plane Wave Basis Set

In the previous section we discussed about different approaches to formulate the basis sets for molecules where the motion of the electrons are influenced by limited number of ions; additionally, the number of electrons were also finite. By no means we can proceed with these approaches to define wavefunctions for the electrons in solids or in general condensed phases. This is because both the number of interacting electrons and the number of ions the electrons move under the effect of becomes infinite in these systems. It implies that the basis set required to define the wavefunctions become

infinitely large and moreover, we need infinitely large number of wavefunctions to define infinite number of electrons extended over the entire space of the system.

To overcome these problems Plane Wave (PW) basis sets were formulated exploiting the periodicity in systems in condensed phases. The central idea behind PW-basis sets is basically the Bloch's theorem on the translational symmetry in solids. According to this theorem the wavefunctions must be composed of a phase factor and a periodic part, which obeys translational symmetry:

$$u_k(\mathbf{r}) = u_k(\mathbf{r} + \mathbf{a}_i) \quad (2.28)$$

with \mathbf{a}_i being the lattice vector. With this periodicity, the problem of defining wavefunctions for an infinite number of electrons now reduces to a finite number of electrons in the unit cell of the crystal structure, which can be expressed as:

$$\psi_j(r) = \sum_{\mathbf{G}} \chi_{j,\mathbf{K}+\mathbf{G}} e^{i(\mathbf{K}+\mathbf{G})\cdot\mathbf{r}} \quad (2.29)$$

where \mathbf{G} , the lattice vectors in the reciprocal space, are constrained to follow the relationship:

$$\mathbf{G} \cdot \mathbf{a}_i = 2n\pi \quad (2.30)$$

with n being an integer, for all $i= 1, 2, 3 \dots$, and \mathbf{K} stands for the wave vector in the first Brillouin zone. In principle, the number of \mathbf{G} vectors required to represent the

wavefunctions with infinite accuracy is infinite. However, the Fourier coefficients $\chi_{j,\mathbf{K}+\mathbf{G}}$ in Eq. 2.29 decrease with increasing $|\mathbf{K}+\mathbf{G}|$. Therefore, in practical implementation, the plane wave expansion is effectively truncated so that the kinetic energy of the system is limited to a cutoff energy.

$$\frac{\hbar^2}{2m} |\mathbf{K} + \mathbf{G}|^2 < E_{cut} \quad (2.31)$$

In Chapters 3 and 4, we shall use Vienna Ab initio simulation code (VASP)^{92,93} exclusively, to investigate the nano-bio interaction with the cutoff energy = 850 eV.

2.4.3. Numerical Basis Set

It is evident from the previous sections of this chapter that the most straightforward and efficient way of constructing the basis set is from AOs that are solutions of the atomic problem at a desired level of theory. This approach is most suitable for atomic problems with spherically symmetric potential where the shape of the AOs is qualitatively known. For problems with many nuclei, such as molecules and solids, they are not very suitable due to their long-range tails, which rule out the possibility to find analytic functional form to describe them accurately enough. The alternative route is to represent the AOs numerically instead of analytically. Basis sets of these kinds are called numerical basis set⁹⁴ or fireball basis set as the AOs where the long-range tails are forced to vanish at centers beyond certain distance. This essentially

enables the kinetic energy-, overlap-, and nuclear attraction matrix elements to vanish after certain distance. The wavefunction in this approach is represented as:

$$\psi_i(\mathbf{r}) = \sum_m \lambda_{im} \chi_m(\mathbf{r} - \mathbf{R}_m) \quad (2.32)$$

where $\chi_m(\mathbf{r} - \mathbf{R}_m)$ are the localized basis functions and \mathbf{R}_m denotes the position of the atom at \mathbf{R}_I on which the orbital is centered⁸¹.

In Chapter 6, we shall use the commonly used *ab-initio* code SIESTA⁹⁵ and SMEAGOL^{96,97} where numerical basis sets are used incorporating pseudopotential approach to further reduce the cost of computation.

2.5. Pseudopotentials

The basic idea behind introducing pseudopotentials in electronic structure calculations is to replace the strong Coulomb potential of the nucleus and its effects on the strongly bound core electrons by an effective ionic potential acting on the valence electrons. The potential originating from the atomic nuclei is rather crumpled and even diverges at the center of the nucleus since the Coulomb potential varies inversely proportional with the distance from the nucleus. Therefore, the inspiration behind this approach is to look for a smooth potential inside the atoms so that the orbitals for the corresponding atoms become smooth. The justification of the pseudopotential approach is the following: (a) the core electrons near to the nucleus of the atom are highly localized and do not contribute to the chemical bonding, (b) the valence electrons and their

corresponding states are extended and therefore participate in chemical bonding, (c) semi-core states are localized but polarizable; however, their contribution to the chemical bonding is slender and insignificant compared with that from the valence electrons. The first attempt was proposed by Herring [1940] via the orthogonalized plane wave (OPW) method where the valence wave functions were constructed as linear combination of plane waves and core wavefunctions. The pseudopotentials are generally generated for each of the atoms and then the properties of the valence electrons are then probed in the molecules or solids consisted of these atoms. The pseudopotential approach affects the calculations in two ways: (a) It removes the core electrons from the calculations and then interaction between the core electrons and the nucleus together with the core electrons is substituted by an effective, screened potential, which depends on the angular momentum of the valence electrons. (b) The ion-electron interactions, which include the orthogonality-condition imposed on the valence states to the core states, are smoothed. Pseudopotentials and their developments include varieties of flavors to make them suitable for widely varied problems. Nonetheless, there are two forms of pseudopotentials, which are seemingly popular in modern quantum chemistry community; *norm conserving pseudopotentials*⁹⁸⁻¹⁰¹ and *ultrasoft pseudopotentials*^{102,103}.

The most important part in constructing the norm conserving pseudopotential was proposed by Hamann, Schlüter and Chiang¹⁰¹ which ensures the eigenvalues of the pseudo-wavefunction to coincide with that from the all-electronic consideration for a specific electronic configuration in atoms. Additionally, the radial part of the pseudo-wavefunction, $R_{pseudo}(\mathbf{r})$, is made to be node-less yet identical to $R_{true}(\mathbf{r})$ of a true

wavefunction outside a cutoff radius r_c keeping the total charge enclosed within the same cutoff radius for both the pseudo- and true- wavefunction:

$$\int_0^{r_c} |\mathbf{r} R_{pseudo}(\mathbf{r})|^2 d\mathbf{r} = \int_0^{r_c} |\mathbf{r} R_{true}(\mathbf{r})|^2 d\mathbf{r} \quad (2.33)$$

Eq. 2.33 is essentially the norm-conserving condition imposed to construct the pseudopotentials. This condition, however, imposes limitation when applied in the plane wave calculation where the valence electrons are expanded in Fourier components. In order to have maximum smoothness, the range in the Fourier space required describing the properties of valence electrons needed to be minimized. The norm-conserving condition takes care of the accuracy but at the cost of smoothness.

This issue with plane wave calculations was resolved by relaxing the norm-conserving condition in *ultrasoft pseudopotentials*. With this relaxed constraint, all the wavefunctions at various reference energies can be pseudized by matching their logarithmic derivatives at the cutoff radius. This implies that the cutoff radius can be chosen large enough, even larger than the radial part of the wavefunction, avoiding the sharp peaks in the pseudo wavefunctions¹⁰³. In Chapters 3 and 4, ultrasoft pseudopotentials has been along with the plane wave basis set employed in VASP whereas, norm-conserving pseudopotentials have been used in Chapter 6 in the SIESTA-SMEAGOL calculations with the numerical basis set.

2.6. Quantum Transport

The current through a macroscopic conductor varies directly proportional to the potential difference across its ends and also inversely proportional to the *resistance*, which is an intrinsic property of the conductor. The origin of the resistance experienced by the electrons while travelling through the conductor can be explained classically in terms of the collisions that the electrons suffer during the course of travelling through the conductor. This is because the dimension of the conductor is larger than the mean free path (λ_e) of the electrons. According to the classical explanation, the electrons should travel through the conductors, with dimension comparable with λ_e , without facing any collisions whatsoever. Physically, this indicates to the zero-resistance or infinite conductivity of the conductors with the above-mentioned dimensionality such as molecules or inorganic structures of finite size. Obviously, this is far from what one should anticipate in practice. This issue can be resolved seeking the help of quantum mechanics, thus, it is given with the name ‘quantum transport’. In this section, we shall discuss some of the major aspects of quantum transport, which will be used in Chapters 5 and 6.

The simplest architecture in quantum transport deals with a molecule sandwiched between two metal electrodes as shown in Fig. 2.3, which can be divided into two parts. The active part consists of the molecule and few layers of atoms in the electrodes, in which the electronic distribution undergoes rearrangements due to the molecular adsorption¹⁰⁴. The second part of the device, however, is assumed to retain their bulk

properties, which serve as *source* and *sink* in the architecture of this kind in the biased condition.

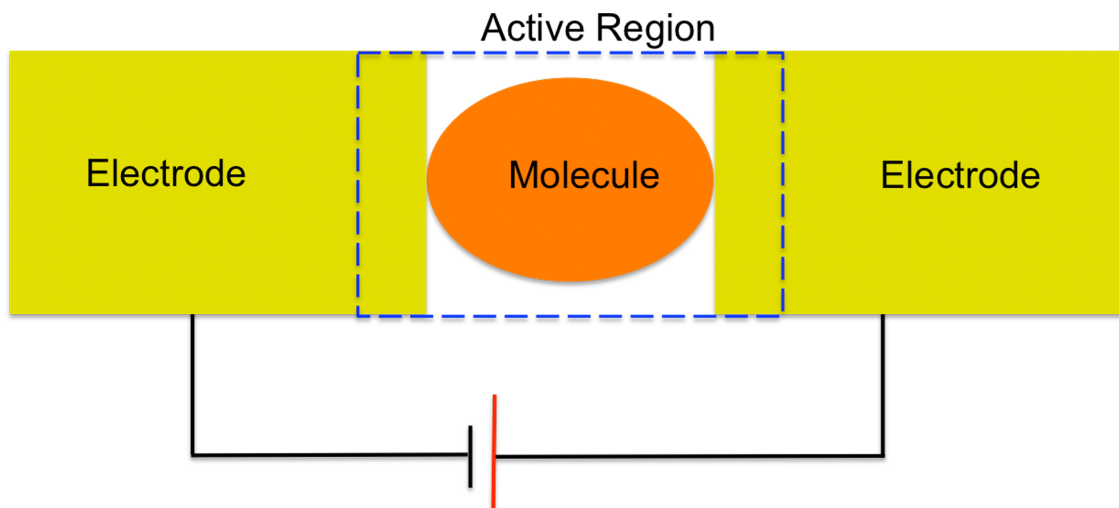


Figure 2.3: A schematic representation of molecular scale device. Adapted from the book “Electronic Transport in Mesoscopic Systems” by Supriyo Datta¹⁰⁵.

When the molecule is placed in between the electrodes, an equilibrium electrochemical potential μ is set by the electrodes. This equilibrium condition gets perturbed in the presence of the external potential provided by external devices (battery), which maintains the two contacts at different electrochemical potentials, μ_1 and μ_2 as shown in Fig. 2.4. In order to regain the equilibrium condition, the electrons start flowing from the higher to lower potential through the molecule. The energy levels of the molecule lying within the energy range $(\mu_1 - \mu_2)$ act as conduction channels for the electrons to flow from the right to the left electrode. Although the metal contacts are considered to be an electron-sea, the flow of electrons, *i.e.*, the conductivity of mesoscopic devices, is limited by the number of conduction channels available within the

specified energy range and the maximum conductance of each of the channels, which is constrained to be the fundamental constant¹⁰⁶ :

$$G_0 = \frac{q^2}{h} = 38.7 \mu S = (25.8 k\Omega)^{-1} . \quad (2.34)$$

Therefore, the conductance per channel measured in practice is less than its maximum value, $2G_0$ (G_0 for spin up and G_0 for spin down electrons). This explains the origin of *resistance* in the devices at mesoscopic length-scale and rules out the existence of a conductor of infinite conductivity. In the following section we shall discuss some of the essential aspects in molecular electronics.

2.6.1 Green's Functions and Quantum Transport

Let us consider a molecule (C) in contact with two electrodes (L and R) as shown in Fig. 2.3. Assuming the molecule is coupled with the left electrode via potential (V_{LC}) and with the right electrode via (V_{CR}), the Hamiltonian for such a system can be partitioned as¹⁰⁷:

$$H_S = H_L + H_R + H_C + V_{LC} + V_{CR} + V_{LC}^\dagger + V_{CR}^\dagger. \quad (2.35)$$

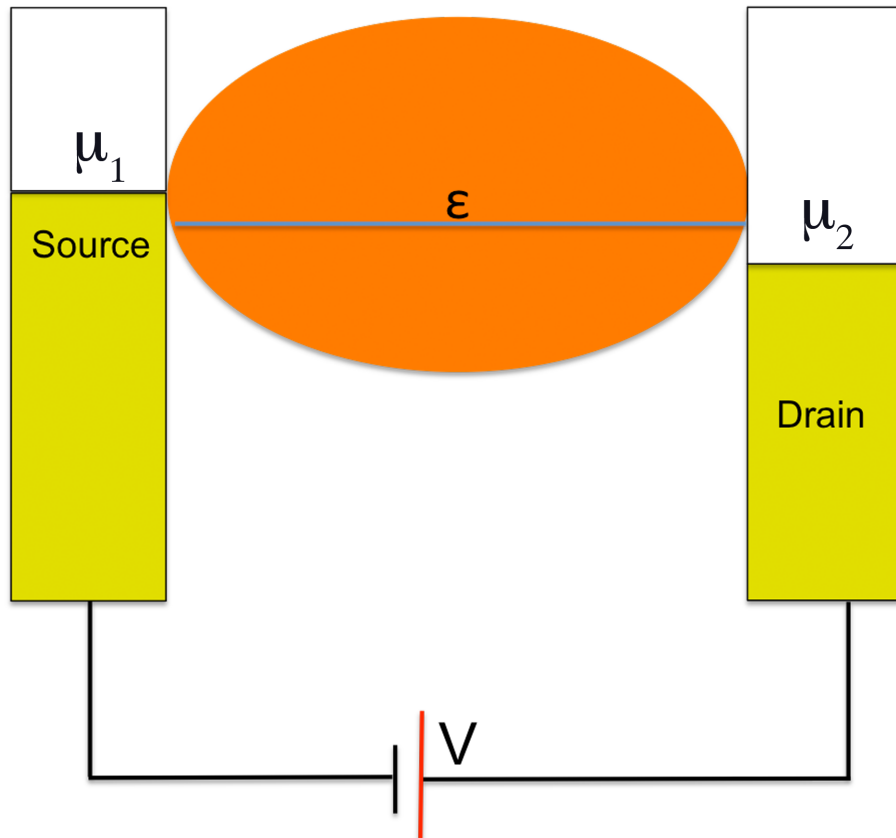


Figure 2.4: A schematic representation of mechanism of electron flow through a one-level channel in molecular scale devices. Adapted from the book “Electronic Transport in Mesoscopic Systems” by Supriyo Datta¹⁰⁵.

Note that we assumed the Hamiltonian of the molecule without the electrodes as H_C , where as the Hamiltonian of the left- and right-electrode is represented as H_L and H_R , respectively.

The Schrödinger equation for the corresponding problem then renders to:

$$\begin{bmatrix} H_L & V_{LC} & 0 \\ V_{LC}^\dagger & H_C & V_{CR}^\dagger \\ 0 & V_{CR} & H_R \end{bmatrix} \begin{bmatrix} |\phi_L\rangle \\ |\phi_C\rangle \\ |\phi_R\rangle \end{bmatrix} = E \begin{bmatrix} |\phi_L\rangle \\ |\phi_C\rangle \\ |\phi_R\rangle \end{bmatrix} \quad (2.36)$$

where $\begin{bmatrix} |\phi_L\rangle \\ |\phi_C\rangle \\ |\phi_R\rangle \end{bmatrix}$ are the single-particle wavefunctions associated with the three regions.

The matrix multiplication in Eq. 2.36 leads to three equations such as:

$$(E - H_L)|\phi_L\rangle = V_{LC}|\phi_C\rangle \quad (2.37)$$

$$V_{LC}^\dagger|\phi_L\rangle + H_C|\phi_C\rangle + V_{CR}^\dagger|\phi_R\rangle = E|\phi_C\rangle \quad (2.38)$$

$$V_{CR}|\phi_C\rangle + H_R|\phi_R\rangle = E|\phi_R\rangle. \quad (2.39)$$

Keeping the semi-infiniteness of the leads, a substitution of $E \rightarrow E \pm i\xi = z$ in Eq. 2.37

leads us to

$$|\phi_L\rangle = G_L(z)V_{LC}|\phi_C\rangle \quad (2.40)$$

with the Green's function of the left leads as :

$$G_L(z) = \frac{1}{z - H_L} \quad . \quad (2.41)$$

Similarly, the wavefunction for the right lead can be represented as:

$$|\phi_R\rangle = G_R(z)V_{CR}|\phi_C\rangle \quad . \quad (2.42)$$

Replacing Eq. 2.41 and 2.42 in Eq. 2.37 through 2.39, we get

$$[E - H_C - V_{LC}^\dagger G_L(z)V_{LC} - V_{CR}^\dagger G_R(z)V_{CR}]|\phi_C\rangle = 0. \quad (2.43)$$

Defining the self energies of the left and right electrode as $\Sigma_L(z) = V_{LC}^\dagger G_L(z)V_{LC}$ and $\Sigma_R(z) = V_{CR}^\dagger G_R(z)V_{CR}$, the Eq. 2.43 can be written as:

$$[E - H_C - \Sigma_L(z) - \Sigma_R(z)]|\phi_C\rangle = 0. \quad (2.43)$$

The single particle Green's function involved in Eq. 2.43 is the key factor in the development of transport in molecular scale electronics and it is defined as:

$$G(z) = \frac{1}{E - H_C - \Sigma_L(z) - \Sigma_R(z)}. \quad (2.44)$$

Considering that $z = E \pm i\xi$ in the expression of self-energies, we can write the self-energies as:

$$\sum_L^+(E) = \sum_L(E + i\xi) \quad (2.45)$$

$$\sum_L^-(E) = \sum_L(E - i\xi). \quad (2.46)$$

The Eq. 2.45 and 2.46 stands for the retarded and advanced self-energies, respectively.

Similarly, $\sum_R(z)$ may be expressed in terms of advanced and retarded forms. Therefore, we can define the broadening matrices as:

$$\Gamma_{L,R} = i \left[\sum_{L,R}^+(E) - \sum_{L,R}^-(E) \right] = -2Im \sum_{L,R}^+(E) \quad (2.47)$$

and the total broadening matrix as ¹⁰⁷:

$$\Gamma = \Gamma_L(E) + \Gamma_R(E) = i \left[\frac{G^+(E) - G^-(E)}{G^+(E)G^-(E)} \right]. \quad (2.48)$$

2.6.2. Landauer Formalism

The fundamental connection between the scattering theory of electrons and quantum conductance was proposed by Landauer in a conceptual framework. The backbone of the Landauer formula is based on the idea: ‘conductance is transmission¹⁰⁶’. In order to derive the Landauer formula, let us consider Fig. 2.4, once again, where we show a molecule sandwiched between two electrodes in the biased condition. As an effect of externally applied field, the Fermi energy shifts up for the left electrode and lowers down

for the right electrode. Assuming the battery connected to the leads maintains the non-equilibrium condition where the leads are kept in two different electrochemical potentials, we can write two corresponding Fermi functions:

$$f_1(E) = f_0(E - \mu_1) = \frac{1}{e^{\frac{E - \mu_1}{k_B T}} + 1} \quad (2.49)$$

$$f_2(E) = f_0(E - \mu_2) = \frac{1}{e^{\frac{E - \mu_2}{k_B T}} + 1} \quad (2.50)$$

which result in a driving force $-qV = \mu_1 - \mu_2$ for the electrons. Since the battery holds the contacts at different potentials, the source $[f_1(E)]$ will keep on pumping the electrons in the system and the drain $[f_2(E)]$ will keep on pulling them out, which essentially results in the current in the circuit. Therefore, the inflow (I_1) and outflow (I_2) of electrons via a single conduction channel may be represented as:

$$I_1 = T_{12}(E)[f_1(E) - f_2(E)] \quad (2.51)$$

$$I_2 = T_{21}(E)[f_2(E) - f_1(E)]. \quad (2.52)$$

Hence, the net current in the circuit (corresponding to all the available conduction channels) would be:

$$I = \frac{q}{h} \int_{-\infty}^{\infty} dE T(E) [f_1(E) - f_2(E)] \quad (2.53)$$

where

$$T(E) = \text{Trace}[\Gamma_L G^- \Gamma_R G^+] \quad (2.54)$$

$T(E)$ is called the transmission function, which physically represents the difference between two opposite fluxes of electrons, one from source to drain and one from drain to source. It may be envisaged from Eq. 2.49, 2.50 and 2.53 that at $\mu_1 = \mu_2$, there will be no current flowing in the circuit. However, a small bias changes the electrochemical potentials of the leads (μ_1, μ_2) and the transmission function. Therefore, current in the circuit at small bias may be written as ¹⁰⁶:

$$\begin{aligned} I \approx \frac{q}{h} & \left[\int_{-\infty}^{\infty} dE \delta T(E) [f_0(E - \mu_1) - f_0(E - \mu_2)] \right. \\ & \left. + \int_{-\infty}^{\infty} dE T(E) \delta [f_0(E - \mu_1) - f_0(E - \mu_2)] \right]. \end{aligned} \quad (2.55)$$

Since the first term in Eq. 2.55 vanishes, therefore it may be rewritten as:

$$I \approx \frac{q^2 V}{h} \int_{-\infty}^{+\infty} dE T(E) \left(-\frac{\partial f_0(E)}{\partial E} \right) \Big|_{E=\mu}. \quad (2.56)$$

This is essentially the Landauer formula with quantum conductance $G = \left(\frac{q^2}{h}\right) T_0$, which is proportional to the transmission function (T_0) as we mentioned earlier, with T_0 defined as:

$$T_0 = \int_{-\infty}^{+\infty} dE T(E) F_T(E - \mu). \quad (2.57)$$

The term F_t is called thermal broadening. The transmission function reaches its maximum value when the modes of one lead transmit perfectly to the other lead. This indicates that the number (M_{lead}) of modes available in the leads limits the value of the transmission function. However, if the number of modes in the molecule is M_{molecule} and $M_{\text{molecule}} < M_{\text{lead}}$, then the value of transmission function is proportional to $M_{\text{molecule}}^{106}$.

2.6.3. Büttiker Equation

Although the Landauer formula provides physical explanation to the conduction in the molecular-scale devices, however, interpretation of experimental results on conductance was not straight-forward up until the formalism proposed by Büttiker^{105,106}. The conductivity of the small-scale molecular devices is measured using four-probe

structure, which was not incorporated in Landauer formalism. According to Büttiker, the Landauer formula for two terminal devices can be extended to multiple terminals by writing the current at the i^{th} terminal as:

$$I_i = \left(\frac{q}{h}\right) \sum_k T_{ik} (\mu_i - \mu_k) \quad (2.58)$$

where T_{ik} is the average transmission function between k - to i -terminal. Therefore, assuming the terminal-2 is grounded, the current in four-probe architecture can be easily written as:

$$\begin{bmatrix} I_1 \\ I_3 \\ I_4 \end{bmatrix} = \frac{q}{h} \begin{bmatrix} T_{12} + T_{13} + T_{14} & -T_{13} & -T_{14} \\ -T_{31} & T_{31} + T_{32} + T_{34} & -T_{34} \\ -T_{41} & -T_{43} & T_{41} + T_{42} + T_{43} \end{bmatrix} \begin{bmatrix} \mu_1 \\ \mu_3 \\ \mu_4 \end{bmatrix}. \quad (2.59)$$

Landauer-Büttiker (LB) formalism is widely popular in quantum transport and has been used to provide explanations to the experimentally observed conductance in molecular devices. It is well understood that the LB-formalism works best in the coherent transport, however, it has also been reported that LB-formalism may be applied in incoherent transport if the vertical flow of electrons between the inter-energy levels is negligible. We shall use LB-formalism in Chapter 5 to investigate the gate-field effect in a three-terminal molecular device.

2.6.4. Non-Equilibrium Green's Function

The most critical approximation within the LB-approach is the inclusion of electron-electron interaction at the mean-field level, which is not valid specifically at the nano-junctions where large current densities are quite common¹⁰⁷. The non-equilibrium Green's function (NEGF) formalism takes this aspect into account by solving the time dependent Schrödinger equation for an interacting many-body system and then calculating the time dependent current. This is done by solving equations of motion for time-independent single particle Green's functions with all the remaining approximations made in deriving the LB-formalism.

$$I = \frac{e}{\pi\hbar} \int dE [f_L(E) - f_R(E)] T_{LR}(E) \quad (2.60)$$

where the transmission function $T_{LR}(E)$ is defined as:

$$T_{LR}(E) = 2 \text{Trace}[\Gamma_{LR}(E) G^+(E) \text{Im}[\Sigma^+(E)] G^-(E)]. \quad (2.61)$$

Where $G^+(E)$ and $G^-(E)$ stands for single-particle Green's functions retarded and advanced, respectively. The NEGF-approach explains some of the important features of quantum transport observed in experiments such as *Coulomb Blockade*, which could not be explained via LB-formalis; however, there are a number of aspects in quantum transport, which are yet to be answered and therefore, remain as “*open problem*”¹⁰⁷.

In Chapter 6, we shall use NEGF-approach employed in the popular code SMEAGOL⁹⁷ to investigate the transport properties of nano-bioconjugates that we shall discuss in Chapter 3.

CHAPTER 3

Theoretical Study of Physisorption of Nucleobases on Boron Nitride Nanotubes: A New Class of Hybrid Nano-Bio Materials*

3.1. Introduction

The nano-revolution continues to dominate the recent research-interest immediately after the discovery of their existence in 1991²⁵ due to the peculiar properties with compared to their bulk-counter parts as a result of dimensional confinement. Owing to the technological progresses along with the numerous efforts from both the theoretical and experimental communities, the nanostructured materials are now being used in mechanical, electronic, magnetic, optical and opto-electrical devices. Very recently, unification of nanomaterials with biological macromolecules has been reported to be appealing and attracted a great deal of research interests^{28,108,109}.

*Partially reproduced from the article “*Theoretical Study Of Physisorption Of Nucleobases On Boron Nitride Nanotubes: A New Class Of Hybrid Nano-biomaterials*”, with permission from S. Mukhopadhyay, S. Gowtham, R. H. Scheicher, R. Pandey, S. P. Karna; *Nanotechnology*, **21**, 165703 (2010) Copyrights ©2010 IOPScience. [doi:10.1088/0957-4484/21/16/165703](https://doi.org/10.1088/0957-4484/21/16/165703)

For example, molecular adsorption on inert-surfaces such as graphene offers an excellent model for tracking single molecules and intermolecular interaction via sophisticated surface analysis technique ⁸. Moreover, manipulating single molecules by scanning tunneling microscopy techniques is found to address the role of hydrogen bonds between the nucleobases in DNA-replication explaining the origin of life¹¹⁰. It is a general conviction that the self-assembly of biological macromolecules (*e.g.* DNA/RNA) on the template surface, such as graphene, has to do with the emergence of life under prebiotic conditions ⁸. As far as the theoretical investigations are concerned, interaction of the DNA/RNA with the nanomaterials is limited to the classical approaches as it is computationally prohibitively expensive for quantum mechanical approaches.

The nucleic acid bases, on the other hand, being the key components of the genetic macromolecules - deoxyribonucleic acid (DNA) and ribonucleic acid (RNA) - play a central role in all biological systems and thus have been a focus of intense research activities over the past five decades. A number of substrates, ranging from graphene ^{3,8} to Cu (110) ^{111,112}, have been used as templates for the molecular adsorption of these nucleobases in order to obtain the microscopic insights into these interactions and the key factors there of. The interaction was reported to vary from Coulombic (Cu (110)) to van der Waals (graphene) type with different amount of charge transfer involved in the interaction depending on the nature of the substrate. Recently, there has been a keen interest in understanding the interaction between nucleobases and carbon nanotubes ^{1-9,11,113} due to the potential application of the unique signature of the latter in probing the structural and conformational changes ^{10,11} of the former, and hence leading to new

detection mechanism ¹² and medical diagnostic tools. Note that, all these substrates are homo-nucleus in nature and therefore, do not offer any understanding about the variation in the interaction in the presence of a substrate being heterogeneous in nature.

Boron nitride nanotubes (BNNTs) have been the focus of several experimental and theoretical studies ^{24,31,114} due to their potential applications in high-speed electronics. BNNTs are a typical member of III-V semiconductors with morphology similar to that of carbon nanotubes (CNTs) but with their own distinct properties. A tubular structure of BN can be formed by rolling up a sheet of hexagonal rings, with boron and nitrogen in equal proportions possessing peculiar electrical ¹¹⁵, optical ¹¹⁶ and thermal ¹¹⁷ properties, which drastically differ from those of CNTs. It has been a challenge, so far, to synthesize CNTs of a particular kind where as BNNTs are semiconducting irrespective of their chirality or structural helicity²⁴. Additionally, the uniformity in the dispersion of BNNTs in the solution makes them more attractive over CNTs for biomedical applications ⁵¹.

Very recently, a thiol-modified DNA was used to obtain high concentration BNNT aqueous solutions assuming the interaction between DNA and multi-walled BNNT to be strong ¹¹⁸. Analysis of the transmission electron microscopy measurements showed that the thiol-modified DNA wraps around the tubular surface of BN. Thus, BNNTs have emerged themselves as an innovative tool for nanomedicine ¹¹⁹. In spite of the promising and impacting applications of CNTs in the field of nano-biotechnology, the poor dispersivity and widely varying issues with their biocompatibility as a function of their structural parameters prohibits them from being a safe and suitable candidate in biomedical applications ¹²⁰. The natural affinity of BNNTs to the cell membrane has been

confirmed by fluorescence microscopy analysis, more importantly without any apparent toxicity⁴⁶, which instigates the applications of BNNTs in drug delivery and cell therapy¹²⁰.

The tubular surface of BN consists of dissimilar atoms and, thus, its interaction with the nucleobases is expected to differ from that found in the case of either graphene or CNTs. The main objectives of this chapter is focused on providing the microscopic details about the self-organization of the nucleobases onto the tubular surface of BN and thereby identify the factors playing a role on the differences in the interaction for different base molecules. Wherever possible, we shall compare our results on bio-conjugated BNNTs with previously reported results in bio-conjugated CNTs⁴.

3.2. Simulation Model and Computational Details

We consider a high curvature (5, 0) single-walled BNNT of diameter of 0.416 nm, which has been predicted to be stable by theoretical calculations¹¹⁸. All calculations were performed by employing the plane wave pseudopotential approach within the local density approximation (LDA)¹²¹ of density functional theory (DFT)^{84,122}. The Vienna *ab-initio* Simulation Package (VASP)^{92,93} was used with the energy cut off of 850 eV and 0.03 eV/Å for its gradient. The periodically repeated BNNT units were separated by 15 Å of vacuum to avoid interaction between them. The (1x1x3) Monkhorst Pack grid¹²³ was used for *k*-point sampling of the Brillouin zone. The average B-N bond length in the

optimized configuration of the pristine BNNT is 1.44 Å, consistent with previously reported DFT calculations³⁵.

In the calculations of the energy surface describing the interaction of the nucleobases with BNNT, the nucleobases were allowed to approach the tubular surface in the direction perpendicular to the axis of the tube. In order to simulate an electronic environment resembling more closely the situation in DNA and RNA, the N atom of the base molecules linked to the sugar ring in nucleic acid was terminated with a methyl group. There is an additional benefit of introducing the small magnitude of steric hindrance due to the attached methyl group. It will help us to imitate a more probable situation in which a nucleobase in a strand would interact with the surface of the BNNT rather than an isolated nucleobase interacting with BNNT.

For simulations based on force fields^{2,7}, it is certainly possible to include all constituents of DNA, including the sugar-phosphate backbone. In the present first-principles study however, simulation of the nucleobases attached to the backbone (i.e. sugar + phosphate group) is computationally extremely expensive. The optimized configurations of the nucleobases-BNNT conjugate systems were obtained following a similar scheme as employed in the previous study of BNNT-CNT complex [12].

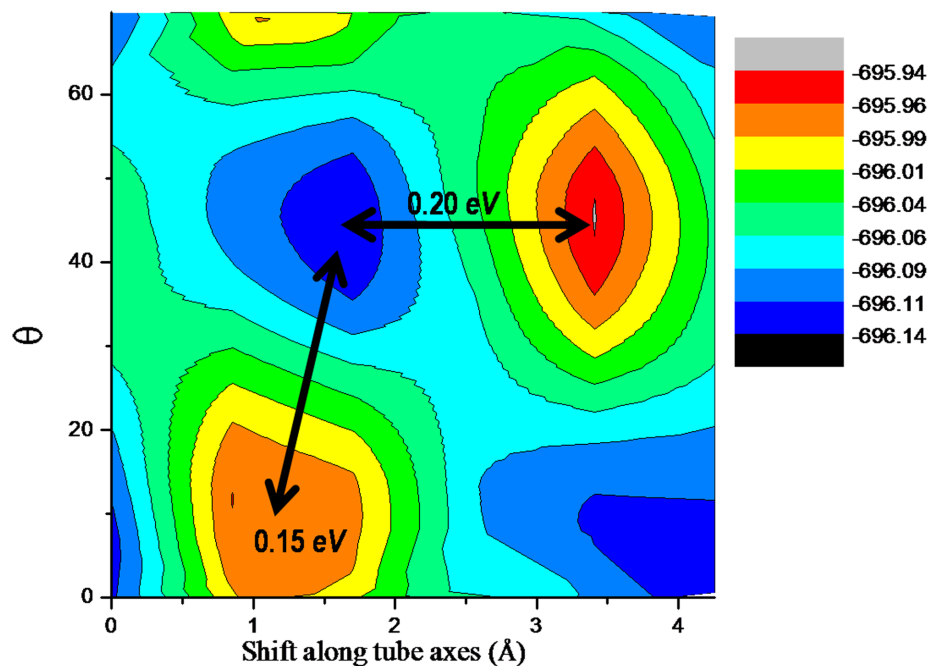


Figure 3.1. Potential energy surface plot (eV) for guanine scanning the surface of the BNNT. The energy barrier between the two adjacent local minima is 0.15 eV.

It consists of (i) an initial force relaxation calculation step to determine the preferred orientation and optimum height of the planar base molecule relative to the surface of the BNNT (ii) calculations of the potential energy surface [Fig. 3.1] for nucleobase-BNNT interaction by translating the relaxed base molecules parallel to the BNNT surface covering a surface area 4.26 Å in height, 70° in width, and containing a mesh of 230 scan points. The separation between base molecule and the surface of the BNNT was held fixed at the optimum height determined in step (i). (iii) a 360° rotation of the base molecules in steps of 5° to probe the energy dependence on the orientation of the base

molecules with respect to the underlying BNNT surface; and (iv) a full optimization of the conjugate system in which all atoms were free to relax.

Certainly, in a potential energy surface scan, some lateral restriction against sliding must be applied. However, it is true that, in principle, reorientation through rotations should be considered. This was not done here, for the following two reasons: first, regarding rotations around any axis that lies in the plane of the nucleobase (comparable to “roll” and “pitch” for airplanes), the preferred orientation of the nucleobase plane relative to the tube surface is parallel in order to maximize the attractive van der Waals (vdW) interaction while minimizing the repulsive interaction from overlapping electron clouds. Second, regarding rotations around the axis that goes perpendicular through the plane of the nucleobase (comparable to “yaw” for airplanes), at least for the larger purine base molecules, the preferred orientation is such that their longer dimension is aligned with the tube axis (as seen in the equilibrium geometries shown in Fig. 3.2) again in order to maximize the attractive interaction with the tube surface.

It should be pointed out that LDA due to a lack of the description of dispersive forces is, in principle, not the most optimal choice for calculating interaction energies of systems governed by the vdW forces. However, more sophisticated methods, such as many-body perturbation theory, which are more suitable for describing long-range forces, become prohibitively expensive for complex systems as considered here. Earlier studies^{124,125} have shown that, unlike the generalized gradient approximation (GGA)¹²⁶ for which the binding for vdW bound systems does not exist, the LDA approximation does

indeed provide reasonably good description of the dispersive interactions. Also a recent study ⁸ on the adsorption of adenine on graphite suggests that the potential energy surface obtained by using LDA and GGA with a modified version of the London dispersion formula for vdW interactions is effectively indistinguishable. Additionally, the LDA equilibrium distance between adenine and graphene obtained by LDA is found to be equal to that obtained using the GGA + vdW level of theory. This gives us confidence in the results obtained in the present study to be reasonably accurate in describing the nucleobase-BNNT interaction.

3.3. Results and Discussions

The calculated base-BNNT binding energy, E_b , the equilibrium base-BNNT distance, and the band gap of the corresponding base-BNNT complex are listed in Table 3.1. The optimized configurations of the nucleobase-BNNT conjugates are shown in Fig. 3.2. It should be noted that the base molecule was allowed to approach the tubular surface along the axes perpendicular to that of the tube while obtaining the potential energy surface. In addition to that as mentioned in the methodology section, we have scanned the surface of the tube [step (ii)] shown in Fig. 3.1.

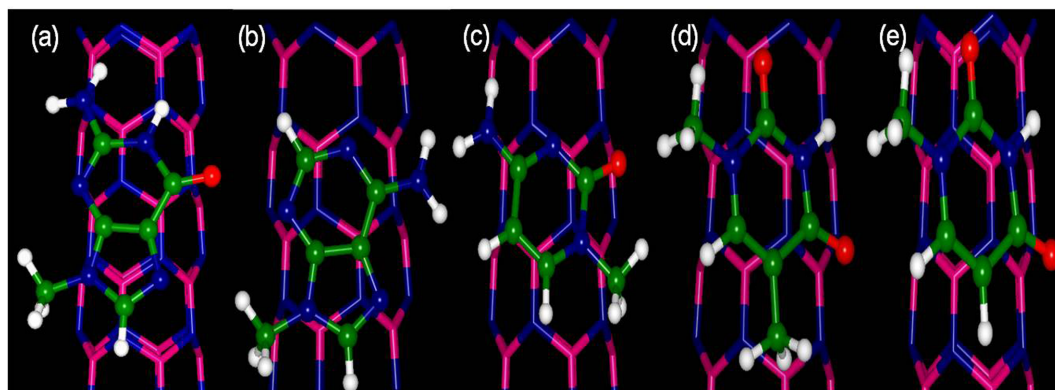


Figure 3.2: Equilibrium geometry of nucleobases adsorbed on the surface of the BNNT: (a) guanine, (b) adenine, (c) cytosine, (d) thymine and (e) uracil.

Then we have rotated the base molecule to check if any particular orientation of the base molecule was preferred [optimization step (iii)] and at the end the whole system was optimized relaxing BNNT and the nucleobases [optimization step (iv)]. The equilibrium configurations shown in Fig. 3.2 were the energetically most favorable ones.

None of the nucleobases show a perfect Bernal's AB stacking. This feature matches with what was found in the interaction of the nucleobases and SWCNT. There is, however, a slight difference in the stacking of the nucleobases between BNNT and SWCNT, because BNNT possess a hetero-nucleic surface unlike SWCNT. The partially negatively charged oxygen atom in guanine can interact electrostatically with the polar network of this heteronucleic BNNT surface, specifically in an attractive manner with the partial positive charges on boron, and repulsively with the partial negative charges on nitrogen.

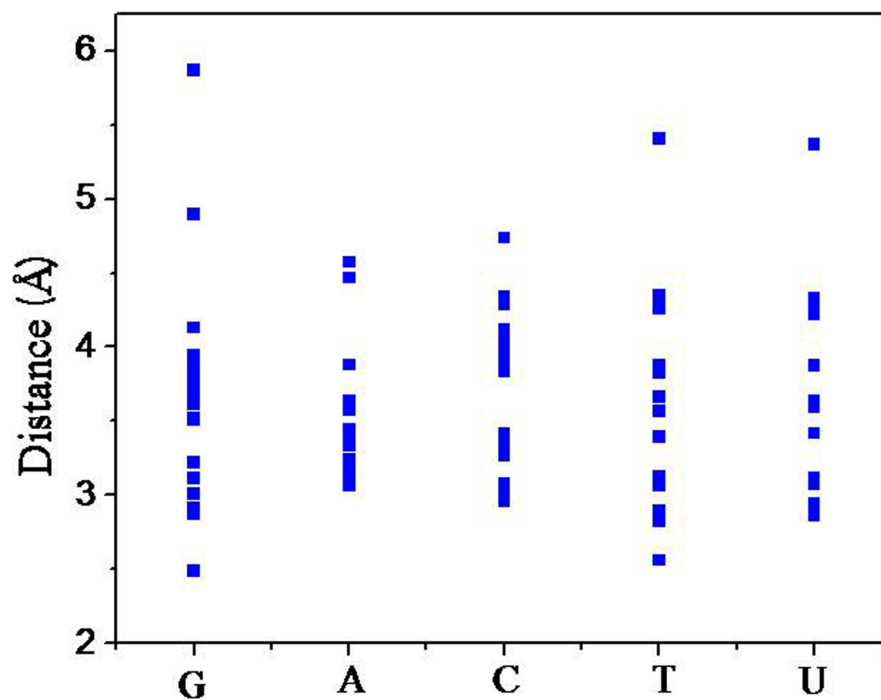


Figure 3.3: The distance between the nucleobase atoms and the tubular surface atoms in the equilibrium configurations of BNNT conjugates.

This could help to explain our theoretical observation that G+BNNT differs in several ways from A+BNNT as in the latter combination, adenine lacks the oxygen atom. Thus, the deviation in the stacking arrangement, the higher binding energy (see Table 3.1), and the slight tilting angle could all be consequences of that interaction between the oxygen atom of guanine and the polar network of the BNNT.

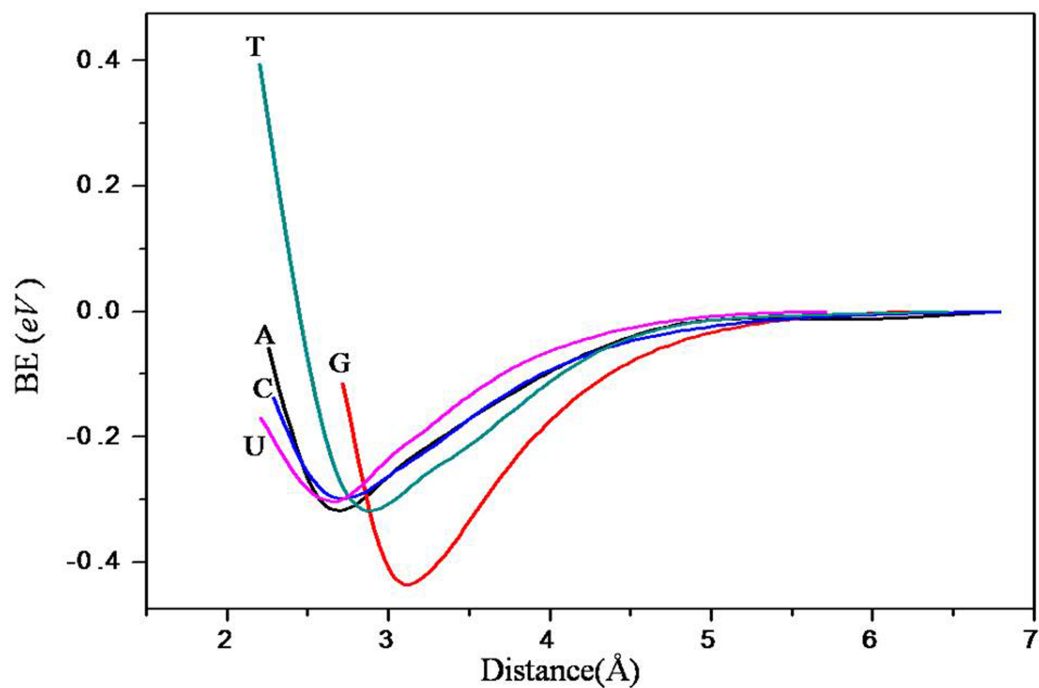


Figure 3.4: The potential energy variation of the nucleobases interacting with the BNNT as a function of the distance. The distance represents the separation between the center of the mass of the tubular surface and that of the base. A, G, C, T and U are represented by black, red, blue, green and pink lines, respectively. The zero of the energy is aligned to the non-interacting regime of the surface.

The nearest-neighbor distance ($R_{\text{base-BNNT}}$) of the individual atoms of the nucleobases from the tubular surface atoms is plotted in Fig. 3.3, which is found to depend on the nucleobases. We note that $R_{\text{base-BNNT}}$ is comparable to the average distance of organic molecules including amino functional groups and 2, 4, 6-trinitrotoluene physisorbed on BNNTs^{35,127}.

Fig. 3.4 shows the energy surface representing the interaction of nucleobases with BNNT. Here, the distance is taken to be the separation from the center of mass of the

tubular configuration to the center of mass of the nucleobases. The asymptotic limit of the energy surface is used to calculate the binding energy (E_b) of the system (Table 3.1) in which the base molecule is moved away from BNNT along the direction perpendicular to the tubular axis. The binding energy data is presented in Table 3.1.

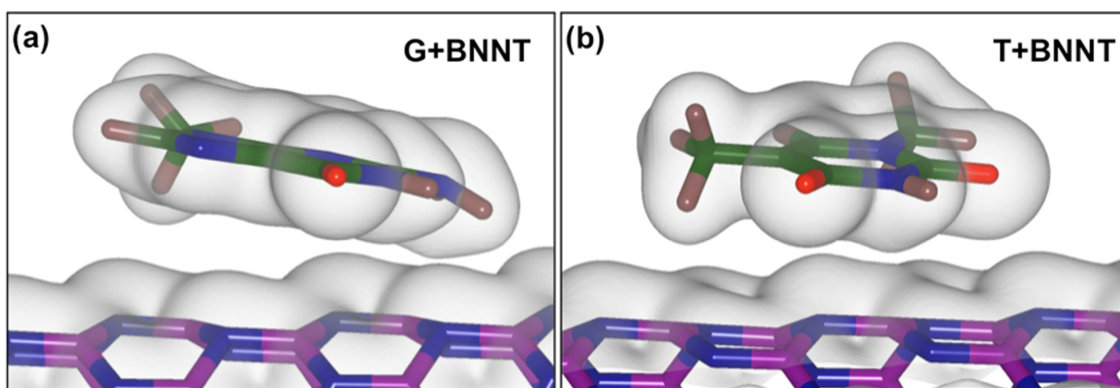


Figure 3.5: Total charge density of (a) guanine- (b) thymine- conjugated BNNTs. The iso-surface levels were set at 0.08 e/ bohr^3

The magnitude of the calculated binding energy exhibit the following order: $G > A \approx C \approx T \approx U$. It is worth noting that the binding energy of the nucleobases interacting with a high curvature CNT⁴ followed the order of $G > A > T > C \approx U$. Since E_b associated with CNTs was found to be correlated with the polarizability of individual bases, it was suggested that the interaction of nucleobases with CNTs was governed by dispersive forces like vdW, which varies with the polarizability of the interacting entity. The calculated polarizability values of G, A, C, T, U are 131.2, 123.7, 111.4, 108.5 and 97.6

$e^2 a_0^2 E_h^{-1}$, respectively, at the Hartree-Fock level of theory together with the second order Møller–Plesset corrections⁴.

Fig. 3.5 shows the total charge density plot of the representative conjugate system of G physisorbed on BNNT. The Bader charge analysis does not show a noticeable charge transfer in the conjugate system relative to the pristine BNNT and individual nucleobases; change in the total charge of the nucleobases being quite small ($< 10^{-2} e$). This is in contrast to the cases of covalent functionalized BNNTs^{49,127,128} where a significant charge transfer of the order of $0.36 e$ from the organic molecule such as NH_3 and amino functional groups to BNNT was reported. Our results are consistent with the case of 2, 4, 6-trinitrotoluene physisorbed on BNNTs reporting a very small charge transfer in the system³⁵.

In order to further understand the underlying interaction between the nucleobases and BNNT, we also calculated the polarizability of a BN sheet, which comes out to be $265.7 e^2 a_0^2 E_h^{-1}$ at the LDA level of theory. The polarizability of a BN sheet is therefore significantly smaller than $402.2 e^2 a_0^2 E_h^{-1}$ calculated for graphene at the same level of theory. This suggests that the tubular surface of a BNNT can be expected to be less polarizable than that of a CNT, which, in turn, would lead to relatively weaker vdW interactions between BNNT and nucleobases.

Table 3.1: Binding energy (E_b), band gap, and nearest-neighbor distance ($R_{\text{base-BNNT}}$) of nucleobase conjugated BNNT. The calculated LDA band gap of the pristine (5, 0) BNNT is 2.2 eV.

<i>System</i>	<i>E_b (eV)</i>	<i>R_{base-BNNT} (Å)</i>	Band gap (eV)
G+BNNT	0.42	2.49	1.0
A+BNNT	0.32	3.06	1.7
C+BNNT	0.31	2.96	1.8
T+BNNT	0.29	2.55	2.0
U+BNNT	0.29	2.86	2.1

This is reflected in the calculated binding energy values of physisorbed nucleobases on BNNT, which are lower in magnitude as compared to those associated with CNTs. For example, the calculated binding energy of G+BNNT conjugate is 0.4 eV while the corresponding value for the G+CNT conjugate is 0.5 eV.

From a comparison of the present results with those from a previous study indicates that the binding energy of nucleobases with (7, 7) BNNT is significantly higher than that with CNTs¹²⁸. This LDA study using numerical atomic orbitals reported a binding energy of about 1 eV for the G+BNNT conjugate system. This clearly suggests that the lower surface curvature of the (7, 7) BNNT (with a diameter of 9.60 Å) leads to a

stronger interaction with the nucleobases than a large surface curvature for the (5, 0) BNNT (with a diameter of 4.16 Å) considered in the present study. A similar trend in the effect of the surface curvature on the binding energy between nucleobase and carbon nanostructures, graphene³ and CNT⁴ was noted in previous studies¹²⁸. The semiconducting nature of BNNT with a band gap of about 2.2 eV can be seen in the calculated density of states shown in Fig. 3.6. This is in agreement with the recent LDA calculations on the pristine (4, 0) BNNTs reporting a direct band gap of about 2.0 eV¹²⁹.

□

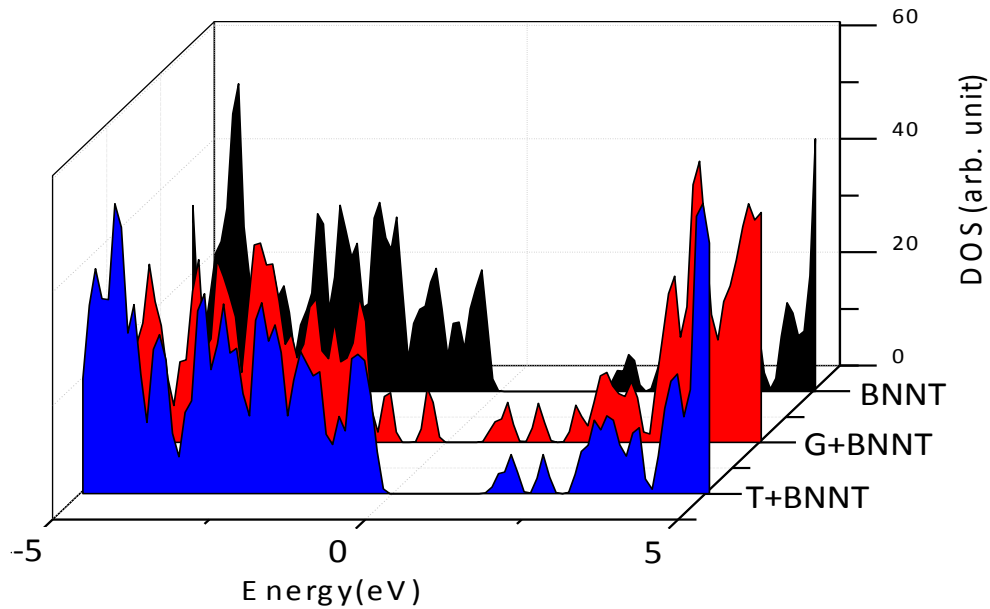


Figure 3.6: Density of states of a pristine BNNT, guanine- and thymine- conjugated BNNTs. The zero of the energy is aligned to the top of the valence band.

Both the top of the valence edge and bottom of the conduction edge of BNNT are associated with the N p-orbitals. The asymmetry in the DOS appears to be due to the difference in coupling strength between the π -orbitals of BNNT and the base molecule in the valence band compared to the conduction band. In the former case, contributions from the nucleobases dominate while contributions from the BNNT dominate in the latter case. The appearance of the mid gap states (Fig. 3.6) in the conjugated BNNT represents a mixing of electronic states of the nucleobases and BNNT separated at about 2.5 Å. It may be noted that the covalent interaction at the separation of 2.5 Å will be very weak¹³⁰.

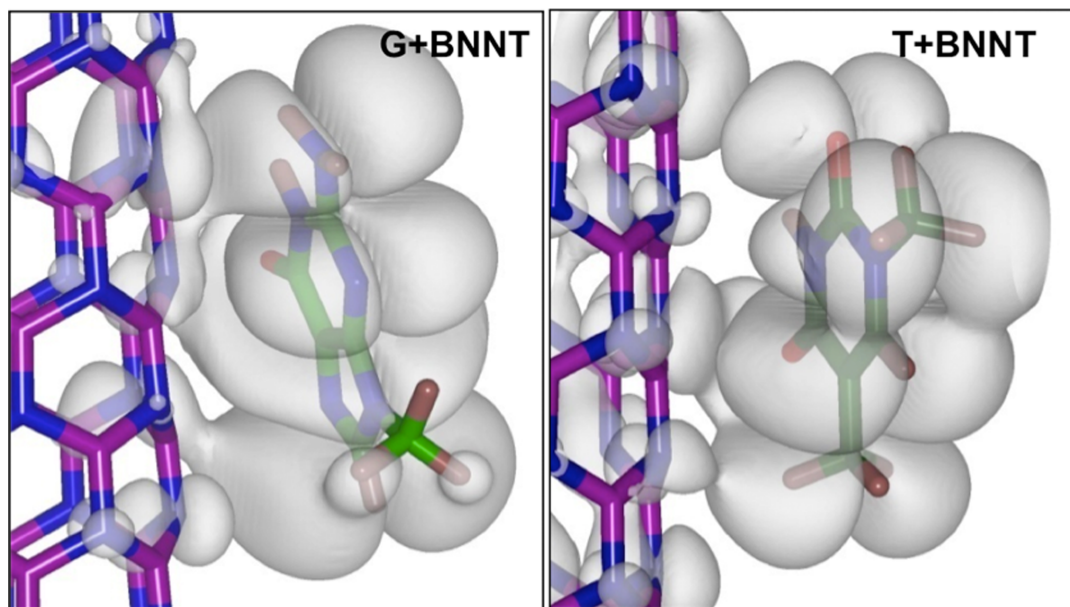


Figure 3.7: Partial charge density of the valence band of (left) guanine – and (right) thymine- conjugated BNNTs. The iso-surface levels were set at $0.0002 \text{ e}^-/\text{bohr}^3$.

The covalent nature of the interaction can be envisaged clearly in Fig. 3.7, where we plotted the partial charge density of the valence band for both the guanine- and thymine-conjugated BNNT. Higher degree of hybridization of electronic states from the guanine and BNNT explains the relatively higher dominance of the covalent forces in guanine conjugated BNNT compared to that in thymine conjugated BNNT. The minuteness of the iso-surface value indicates to the slenderness of the covalent forces present in these bio-conjugates. On the other hand a very small charge transfer from BNNT to oxygen of guanine may indicate the presence of a relatively weaker electrostatic interaction between BNNT and guanine. The vdW forces, however, essentially dominate the interaction between BNNTs and nucleobases.

3.4. Summary

In summary, we have investigated the interaction of the nucleobases on a high curvature, zigzag (5,0) BNNT by first-principles DFT method. Our calculations show that, except G, the base molecules (A, C, T, U) of DNA and RNA exhibit almost similar interaction strengths when physisorbed on BNNT. It is also observed that the binding energy of the base molecules not only depends upon their individual polarizability but also marginally depends on the degrees of mixing of electronic states with the tubular surface of BNNT. The strong binding of the BNNT with G compared to the other nucleobases suggests that this interaction can be used in sensing and also for distinguishing this base molecule from other nucleic acid bases.

CHAPTER 4

Sensitivity of Boron Nitride Nanotubes toward Biomolecules of Different Polarities*

4.1. Introduction

In recent years, the bioconjugated nanostructured materials including nanotubes^{13,14,41,43,131}, nanowires¹⁵, fullerenes¹⁶ and nanoparticles^{17,18} have emerged as new class of materials for biosensing and medical diagnostics applications. For example, the DNA-decorated carbon nanotubes were shown to be effective for chemical sensing of various odors¹⁹. On the other hand, probing of conformational changes in DNA *in vivo* triggered by a change in the surrounding ionic concentration showed a great possibility for new detection mechanism¹². Conversely, the structure-specific binding property of biomolecules has been used to sort carbon nanotubes of different kinds⁹. Despite such

*Reprinted with permission from S. Mukhopadhyay, R. H. Scheicher, R. Pandey, S. P. Karna; "Sensitivity Of Boron Nitride Nanotubes Toward Biomolecules Of Different Polarities"*J. Phys. Chem. Lett*, **2**, 2442 (2011). Copyright © 2011 American Chemical Society.

applications, a fundamental knowledge of the interactions of biomolecules with inorganic nanomaterials is quite limited. In order to fully capitalize on the novel properties of nano-bio conjugates, a detailed understanding of the nature, physical and chemical mechanisms, structure, and spatial distribution of the conjugating molecules and nanomaterials is critically important.

Recently, a number of first principles quantum chemical studies have focused on determining the site-specificity/selectivity of the biomolecular reactions with nanostructured materials. In case of nucleobases of DNA and RNA, it has been shown that the N-site is the preferred site for forming complex with metallic¹³² and semiconducting quantum dots³⁹. A considerable charge transfer occurs from nucleobases to metallic cluster, suggesting the dominance of electrostatic interaction in metal conjugates, while covalent interactions dominate in semiconducting conjugates. On the other hand, interactions of tubular configurations of carbon and boron nitride with nucleobases of DNA and RNA have been shown to mainly result from van der Waals (vdW) interactions, whose strength depends on individual polarizability of nucleobases^{4,42}.

As proteins play one of the most important roles in biology, it is expected that a similar understanding of their interactions with nanomaterials, as for DNA, would provide critical fundamental knowledge on their interactions and possibly guide utilization nanotechnology in proteomics. Toward that, recently a number of studies have focused on carbon-based nanostructures^{12,128,133-138} addressing the challenges to interface proteins with nanomaterials¹³⁹.

Boron nitride nanotubes (BNNTs) which possess similar morphology as carbon nanotubes (CNTs), but distinct properties of their own, appear to be potential candidates for bio-medical applications due to their uniformity and stability in dispersion in solution⁵¹. Unlike CNTs, whose electronic structure and properties vary widely based upon tube helicity, concentric layers, etc, the BNNTs are semiconducting regardless of their diameter and chirality²⁴. BNNTs are also found to be nontoxic to health and environment due to their chemical inertness and structural stability and, therefore, more suitable for medical applications such as drug delivery^{45,140}.

Toward that, we have performed first-principles quantum chemical calculations on the conjugation and electronic structure nature of amino acids, the building blocks of proteins, and BNNT. In principle, a complete understanding of physics and chemistry of the interaction between the amino acid and BNNT should include an investigation of all twenty amino acid molecules interacting with BNNTs. However, it would have been prohibitively computationally expensive especially with the level of accuracy we employed to obtain the optimized configurations of the bio-conjugates involving all amino acids. Instead, we considered three representative molecules belonging to three possible categories such as, aspartic acid (Asp): a dicarboxylic amino acid with a *negative charge*, arginine (Arg): a 3-carbon aliphatic chain with a *positively charged* guanidino group and tryptophan (Trp): a *non-polar* aromatic amino acid consisting of an indole functional group with an amine (Fig. 4.1). We expect that the interaction of BNNTs with these representative amino acid molecules will be similar to the other amino acid molecules falling under the same category depending on their polarity, qualitatively.

This choice of polar and non-polar amino acids is expected to reflect the common chemical properties of more complex protein macromolecules. It is important to note that the simulation model considered the amino acid molecules at their respective isoelectric points; the pH at which the amino acid molecules (Arg: 11.15, Asp: 2.77, Trp: 5.89) are neutral.

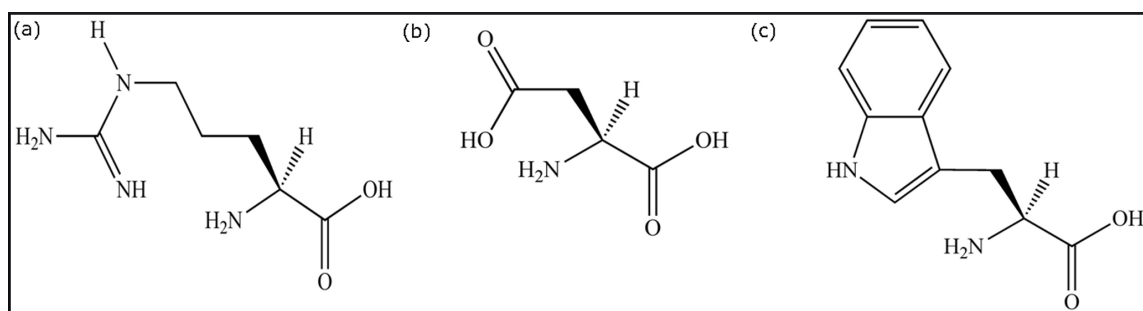


Figure 4.1. Chemical formulas of the studied amino acid molecules:(a) Arg [$C_6H_{14}N_4O_2$], (b) Asp [$C_4H_7NO_4$] and (c) Trp [$C_{11}H_{12}N_2O_2$].

Therefore, the main focus of this chapter would be on understanding how the polarity of the individual amino acid affects its interaction with BNNT. We shall compare the results from the polarity dependent interaction of BNNT and amino acid molecules with what was found for the non-polar nucleobases, discussed in Chapter 3.

4.2. Simulation Model and Computational Details

In the calculations, a plane-wave pseudopotential approach within the local density approximation (LDA) of density functional theory was employed using the Vienna *ab initio* Simulation Package (VASP). A $1 \times 1 \times 3$ Monkhorst-Pack grid¹²³ was used for k -points sampling of the Brillouin zone with an energy cutoff of 850 eV. The cutoff criterion for the force gradient was set as 0.03 eV Å⁻¹. The supercell considered for electronic structure calculations consisted of a (5,0) single-walled BNNT¹¹⁸ with a diameter of 4.16 Å. Since the amino acid molecules were set to approach the BNNT along the x-axis (perpendicular to the tube axis of the BNNT which is parallel to the z-axis) with different orientations, a large vacuum distance (~ 32 Å) was given in the x-direction to avoid the unphysical interaction of the repeating units, whereas a separation of 15 Å was given along the y-axis. The system is periodic in the z-axis (i.e. along the tube axis) to simulate an infinitely long BNNT. The average B–N bond length in the optimized configuration of the pristine BNNT is 1.44 Å, in agreement with previous first-principles DFT calculations³⁵.

Although, the LDA-DFT level of theory may not be the optimal choice for calculating interaction energies of weakly bound systems represented by vdW interactions, recent theoretical studies⁸ considering adsorption of adenine on graphite have shown that topology of the potential energy surface obtained by this method remains effectively indistinguishable from the one obtained using more sophisticated

generalized gradient approximation (GGA)¹²⁶ together with a modified version of the London dispersion formula for vdW interactions. Also, there are some cases where LDA has been shown to yield a better description of the weakly bound systems compared to the GGA, which fails to predict binding in otherwise vdW-bound systems.^{124,125} As a viable remedy toward the present investigation of biomolecules of different polarities where their interactions with BNNT might deviate from vdW forces, we used the LDA-DFT level of theory and followed the asymptotic approach to calculate the binding energy of a bioconjugated complex. It is expected that a possible cancellation of errors might qualitatively retain the relative trend and thereby, the basic underlying physics and chemistry governing the interaction of amino acid molecules with BNNT should be unaltered. However, it is noteworthy that since the LDA-DFT underestimates the band gap of the systems, discussions on the band gap of all the systems considered in this study are, therefore, qualitative.

We begin with individually optimized configurations of BNNT and the amino acid molecules and perform the following steps to obtain the equilibrium configuration of the bioconjugated system; **(i) *Selective dynamics***: An initial force relaxation calculation step to determine the preferred orientation and optimum height of the amino acid molecules relative to the tubular surface. **(ii) *Grid scan***: The energy surface is obtained by translating the relaxed amino acid molecules parallel to the BNNT surface covering a surface area 4.26 Å in height, 70° in angular range and containing a mesh of 230 scan points [Fig. 4.2]. The separation between the molecule and the tubular surface was held fixed at the optimum height determined in step (i). **(iii) *Rotation***: Considering the non-

planar structures of the amino acid molecules, we have investigated a number of different orientations how the molecules might possibly prefer to approach the side wall of BNNT.

(iv) Full optimization: A full optimization of the conjugated system starting from the lowest energy configuration obtained in the previous steps. In this step both the BNNT and amino acid molecule were free to relax. It is worth noting that our research group has successfully applied a similar optimization procedure on carbon and boron nitride nanostructures interacting with nucleobases of DNA and RNA^{4,42}.

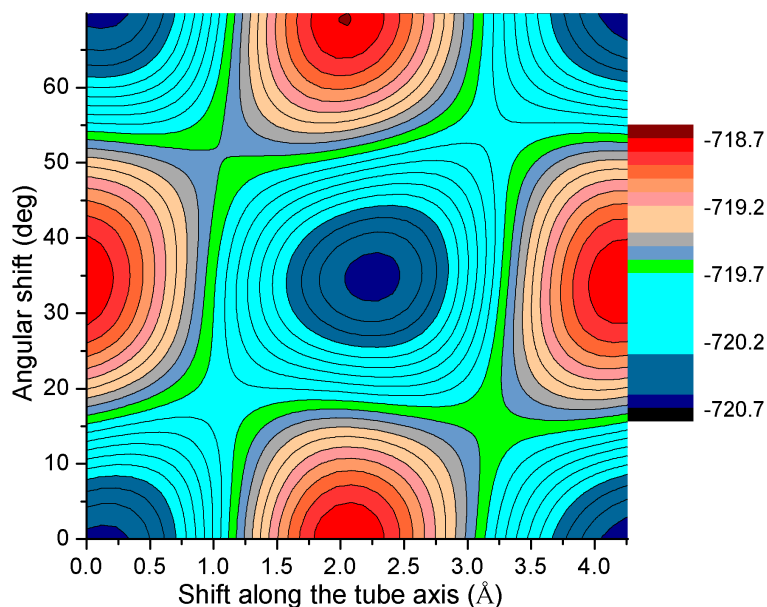


Figure 4.2. The calculated potential energy surface of the arginine scanning tubular surface of BNNT. The energy barrier between two adjacent local minima is 1.5 eV.

4.3. Results and Discussions

In the energy surface scan plot obtained in the optimization step (ii) shown in Fig. 4.2, a striking difference between the interaction of BNNT with the amino acid molecules and that with the nucleobases of DNA and RNA⁴² is revealed. For Arg-BNNT, the energy barrier between two adjacent minima is predicted to be significantly higher than what was reported for guanine-BNNT⁴². The molecular interaction of the Arg-conjugated BNNT therefore appears to be stronger than those in the nucleobase-conjugated BNNT. Fig. 4.3 shows the equilibrium configurations of Asp-BNNT, Arg-BNNT and Trp-BNNT complexes. It is interesting to note that Trp, the charge neutral amino acid molecule, gets adsorbed on BNNT with its five and six membered rings almost parallel to the surface of the tube.

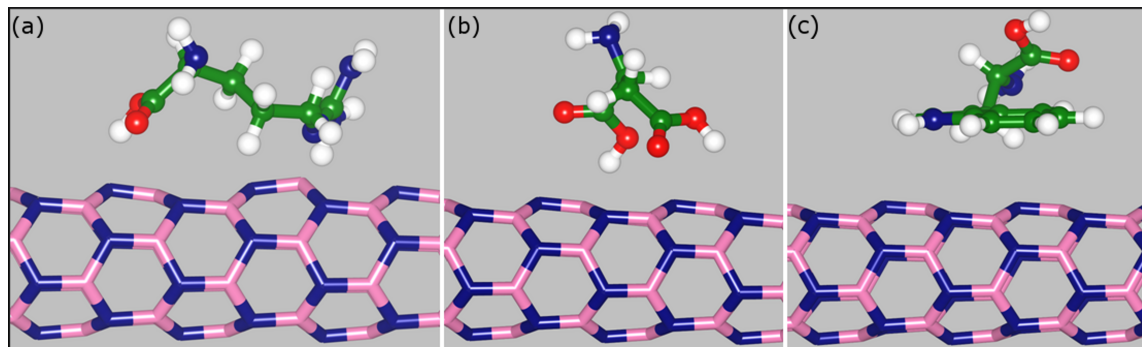


Figure 4.3. Equilibrium geometries of (a) Arg, (b) Asp and (c) Trp on the surface of BNNTs. Boron and nitrogen atoms are represented with pink and blue, respectively, whereas green, red and white colors stand for carbon, oxygen and hydrogen atoms, respectively.

But it does not follow a perfect Bernal's AB stacking as reported in earlier calculations for the neutral DNA/RNA nucleobases on the surface of BNNT⁴².

The interatomic separation of the individual atoms of the amino acid molecules from the atoms of the tubular surface in the equilibrium configuration is plotted in Fig. 4.4. The minimum $R_{\text{amino-BNNT}}$ is 1.6 Å, 2.01 Å and 2.87 Å for Arg, Asp and Trp, respectively. The minimum $R_{\text{Trp-BNNT}}$ is comparable to the separation calculated for neutral nucleobases (2.77 Å)⁴² and organic molecules (2.96 Å)³⁵ physisorbed on BNNTs. The minimum $R_{\text{Arg-BNNT}}$ is comparable to the intermediate distance between BNNT and chemisorbed amino functional groups NH_2CH_3 , $\text{NH}_2\text{CH}_2\text{OCH}_3$ and $\text{NH}_2\text{CH}_2\text{COOH}$ (1.74, 1.76 and 1.77 Å, respectively)¹²⁷. On the other hand, the minimum $R_{\text{Asp-BNNT}}$ is nearly the same as that calculated for NH_2COOH and BNNT (2.32 Å)¹²⁷. It therefore appears that the structural parameters of the ground state configurations depend strongly on the nature of the side-groups when adsorbed on the BNNTs, though the amino-functional group is present in all cases¹²⁷.

The predicted difference for $R_{\text{amino-BNNT}}$ of the Arg-BNNT, Asp-BNNT complexes, in a way, provides a guidance to differentiate the nature of the interaction regimes in the bioconjugates considered¹³⁰. For example, the minimum $R_{\text{Trp-BNNT}}$ of 2.87 Å is similar to the characteristic distance for vdW-bound systems¹⁴¹ where π -electrons associated with the [indole](#) functional group of Trp facilitate noncovalent interactions with the tubular surface of boron nitride.

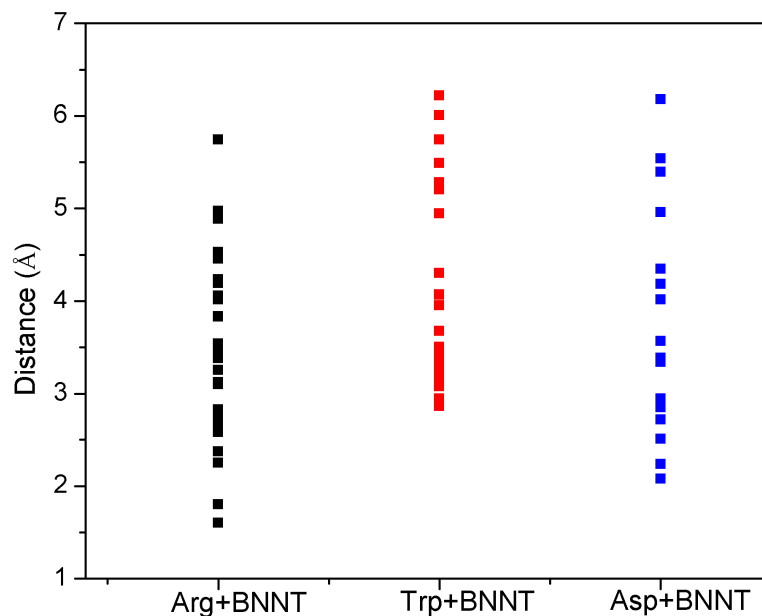


Figure 4.4: The distance between the atoms of the amino acid molecules and the tubular surface atoms in the equilibrium configurations of BNNT conjugates.

The binding energy of the amino acid conjugated BNNT was calculated using the asymptotic limit, moving the amino acid molecule away from the surface along the direction perpendicular to the tubular axis of the BNNT to the point beyond which the interaction between amino acid and BNNT becomes negligible (Fig. 4.5). The calculated binding energy is 3.53, 0.94 and 0.36 eV for Arg-BNNT, Asp-BNNT and Trp-BNNT, respectively (Table 4.1). The interaction strength therefore depends upon the chemical nature of the side-groups within the molecules themselves; the polar Arg and Asp molecules have a higher binding energy than the non-polar aromatic Trp.

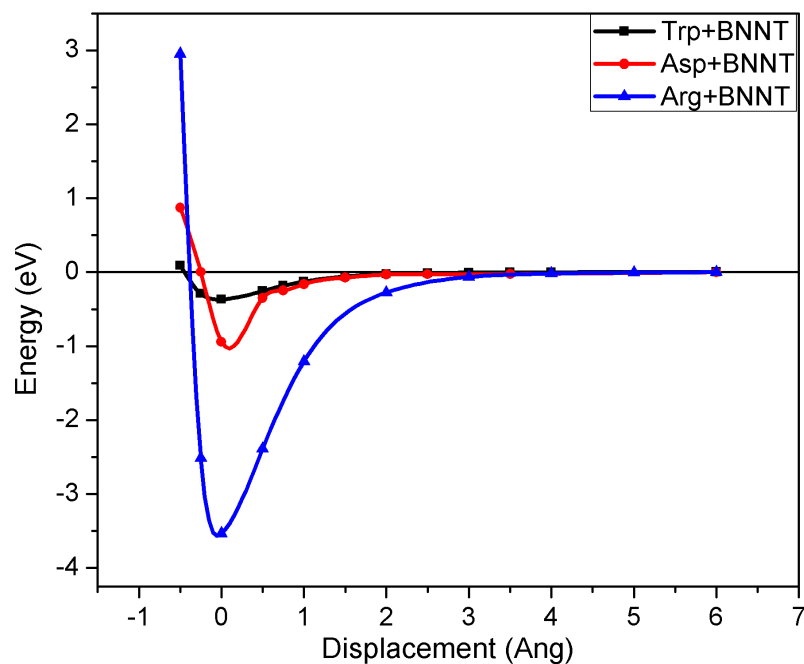


Figure 4.5: The potential energy variation of the amino acid molecules interacting with the BNNT as a function of the distance. Zero of the energy is aligned to the non-interacting regime of the surface. Zero of displacement represents the equilibrium configuration of the conjugated system.

It is worth noting that the same hierarchy of the order of the binding energy was obtained for a metallic (5, 5) CNT¹³³, though the range is much smaller than that of conjugated BNNT complex. The binding energies of the conjugated CNT complexes are reported to be 0.46, 0.19 and 0.16 *eV* for Arg-CNT, Asp-CNT and Trp-CNT, respectively.

Previously, (7,7) BNNTs were also anticipated to bind with one of the amino acid molecules (Alanine) rather strongly as compared to (7, 7) CNTs¹²⁸.

Table 4.1. Nearest-neighbor distance ($R_{\text{amino-BNNT}}$), binding energy, and band gap of amino acid conjugated BNNT.

System	$R_{\text{amino-BNNT}}$ (Å)	Binding energy (eV)	Band gap (eV)
Arg-BNNT	1.6	3.53	2.2
Asp-BNNT	2.1	0.94	2.1
Trp-BNNT	2.9	0.36	1.6

The semiconducting BNNTs are, therefore, predicted to be more sensitive towards amino acid molecules, having higher distinction ability relative to that of CNTs. Furthermore, the presence of polar bonds and intrinsic dipole moment indicates the possibility of using BNNTs as a more efficient protein immobilizer compared to CNTs.

Here we find an important relevance of this study on the protein chemistry. Previously, the proteins were reported to get physisorbed on the CNTs¹⁴ by weak dispersive forces where as BNNTs were found to immobilize the proteins through the electrostatic interactions between BNNT and the bound amino groups⁴⁹ because of the intrinsic polar-bonds present in BNNTs. Interestingly, the amino acid molecules

considered in this study exhibit similar preference as far as the binding to the CNTs/BNNTs are concerned. It is therefore conclusive enough to claim that the individual amino acid molecules retain their interaction properties even when interacting with CNTs/BNNTs as a part of a protein. The stronger binding of the proteins with the BNNTs may often be seen as a potential source of toxicity; however, BNNTs are known to be nontoxic^{45,140} so far. On the other hand the enhanced protein stability by BNNTs may, consequently, be utilized toward the enzyme degradation and increasing the activity via immobilization at the surface of the tube¹⁴².

In order to understand the effect of the adsorption of the molecules on the electronic properties of pristine BNNT, total density of the states (DOS) was calculated. No significant change in the characteristic features of the DOS was seen for Asp- and Arg-conjugated BNNT relative to that of the pristine BNNT. It resembles the “harmless modification” observed in chemisorbed amino-functional conjugates on BNNT¹²⁷. The LDA-DFT value of the band gap of the pristine (5,0) BNNT is 2.2 eV, whereas, the experimental value of the band gap of BNNT is about 5.5 eV¹¹⁶. This discrepancy can be explained in terms of the inherent limitation of LDA in describing the exchange-correlation energy. The band gap (E_g) in a semiconductor is the difference between the ionization potential and electron affinity. Therefore, E_g is the Kohn-Sham eigenvalue band gap of a N-electronic system (ϵ_g) plus a possible discontinuity (Δ) in the exchange-correlation potential arising due to; (a) the addition of an electron with density $\rho_c(\mathbf{r})$ in the conduction band, (b) the removal of an electron with density $\rho_v(\mathbf{r})$ from the valence band, and (c) the change in the external potential associated with the density changes

from $\rho_{N-1}(\mathbf{r}) + \rho_v(\mathbf{r})$ to $\rho_{N-1}(\mathbf{r}) + \rho_c(\mathbf{r})$.⁷⁹ The change in the density due to addition (removal) of an electron to (from) a N-electronic system varies inversely proportional to the total volume and vanishes for a periodic system such as an infinitely long BNNT in this study. Therefore, the contributions from both in (a) and (b) towards the discontinuity may be ignored here due to smallness. However, the last term mentioned in (c) cannot be ignored, in principle. The exchange-correlation energy within the LDA is local and regular, by definition and therefore, results in a vanishing Δ . As a consequence, the band gap calculated within LDA for semiconductors is underestimated by 40%⁷⁹.

For Trp-BNNT, the band gap is, however, drastically reduced to 1.6 eV indicating a significant change due to its non-covalent functionalization with Trp. The top of the valence band is associated with the N-2p orbitals of BNNT in both polar complexes. This is in contrast to the case of Trp-BNNT where reduction of the band gap is predicted due to appearance of an additional peak near the Fermi level. Interestingly, the projected density of states shown in Fig. 4.6 attributes this peak (forming the top of the valence band) with the Trp-p orbitals, though the nature of the bottom of the conduction band remains the same as that of the pristine BNNT. This is an ‘indirect’ confirmation of the weak vdW interaction describing Trp-BNNT conjugated system.

The valence bands of Trp and BNNT appear to be ‘unaltered’ unlike the cases of Asp and Arg conjugated systems where the top of the valence band consists of hybrid states from Asp or Arg along with the BNNT. A similar trend was reported in recent literature where band gap modification was predicted for neutral nucleobase molecules

when physisorbed onto BNNTs with vdW-interaction⁴² and no reduction in the band gap of the BNNT was noted when the interaction is ionic¹²⁷.

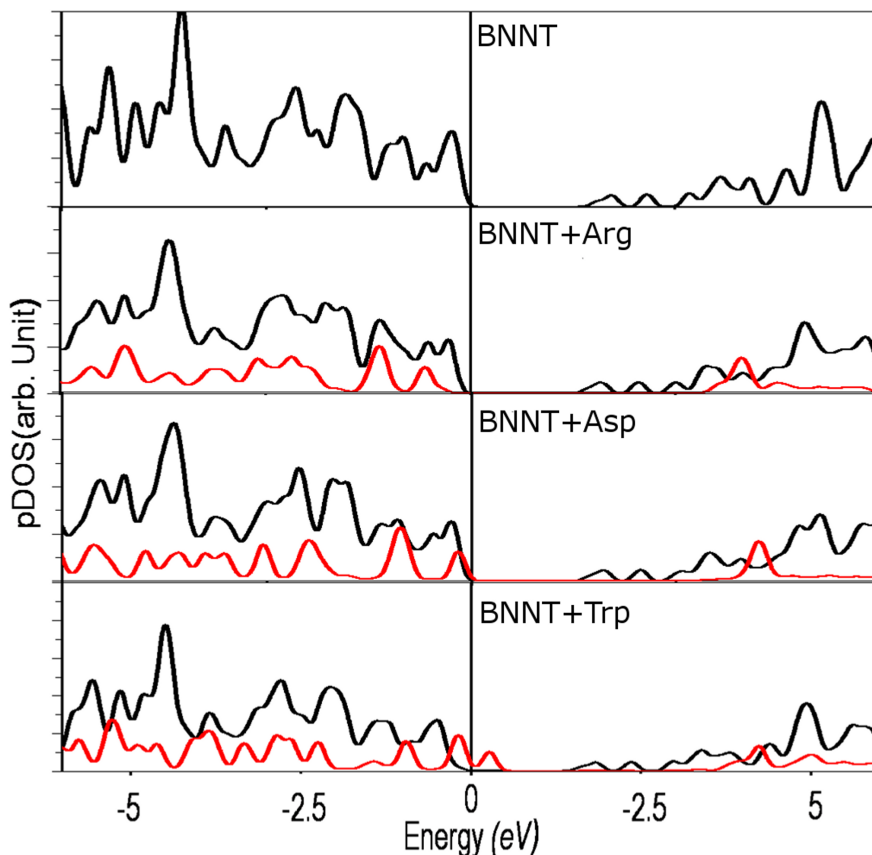


Figure 4.6. Projected density of states of pristine BNNT and amino acid conjugated BNNT. The black lines represent contributions from BNNT atoms and the red lines refer to contribution from atoms of the amino acid molecules.

It is worth mentioning here that Trp is also known as a protein fluorophore due to the fact that the fluorescence of a protein is governed by the Trp-residue. Its optical transitions, absorption at 280 nm and fluorescence at 348 nm, are associated with electronic transitions of the indole functional group (Fig. 4.1). A quenching of the Trp

fluorescence in the Trp-BNNT complex is therefore predicted, similar to the case predicted for Trp-ZnO complex¹⁴³.

A Bader charge analysis was performed to obtain the atomic charges of the ground state configurations of bioconjugates. Negligible charge transfer was found for Trp-BNNT while the polar complexes showed the charge transfer, e.g. in Arg-conjugated BNNT, a charge of 0.15e was transferred from B of BNNT to N of Arg at a distance of 1.6 Å. Since $R_{\text{Arg-BNNT}}$ is smaller than $R_{\text{Asp-BNNT}}$ (Fig. 4.4), the large difference in the binding energies (Table 4.1) of Arg-BNNT and Asp-BNNT complexes can be understood in terms of electrostatic interactions, as the Coulomb potential varies inversely proportionally with the distance between the interacting entities. The results of the Bader charge analysis are further reaffirmed by Fig. 4.7 showing a relatively large overlap of the electron clouds of Arg and BNNT compared to the cases of Asp-BNNT and Trp-BNNT. The strong attachment of the amino acid molecules onto the BNNTs by means of charge transfer mechanism were observed to be the key factor for the isolation of individual BNNTs via peptide wrapping¹⁴⁴ in recent experiments. The strong binding of Arg, and possibly the other positively charged amino acid molecules, onto the BNNTs with a significant charge transfer is perhaps the origin of the experimentally observed natural affinity of a protein toward BNNTs⁴⁹. This enables the BNNTs to immobilize the proteins directly, without the usage of any additional coupling reagent⁴⁹.

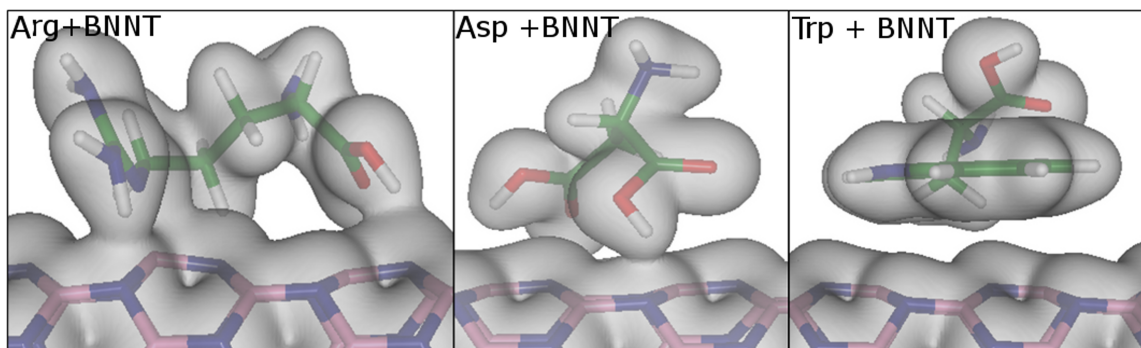


Figure 4.7: Total charge density of amino acid conjugated BNNT. The isosurface levels were set at $0.02 e^-/\text{bohr}^3$ for all the cases.

The covalent functionalization of multiwalled BNNTs was achieved¹⁴⁵ using organic functional groups, naphthoyl chloride ($\text{C}_{10}\text{H}_7\text{COCl}$), butyryl chloride ($\text{CH}_3(\text{CH}_2)_2\text{COCl}$), and stearoyl chloride ($\text{CH}_3(\text{CH}_2)_{16}\text{COCl}$). It was shown that these functional groups act as dopants in the BNNT introducing additional gap states due to charge transfer between the functional groups and BNNT¹⁴⁵. This is not the case for the amino acid-BNNT complexes considered. The polar amino acids, Asp and Arg do not introduce any additional states in the band gap of the pristine BNNT, though charge transfer occurs in the bioconjugated complex.

Combining the results of structural configuration, binding energy and analysis of atomic charges and electron density, we may therefore conclude that the non-polar Trp molecule gets physisorbed whereas the polar Arg and Asp molecules are bound to the tubular surface of BNNT by electrostatic interactions. A relatively large binding energy of the Arg-BNNT complex may suggest the possibility of Arg to be the amino acid that can facilitate a direct link to the tubular surface of BNNT.

4.4. Summary

In summary, we have investigated the interaction of a small diameter BNNT with three amino acid molecules of different polarities. For the neutral Trp molecule, the interaction is found to be mediated by vdW forces. For the polar Arg and Asp molecules, the interaction seems to be mainly governed by electrostatic forces. A large variation in the magnitude of binding energy in these bioconjugated complexes suggests a higher electronic sensitivity of semiconducting BNNTs relative to metallic CNTs for amino acids of different polarities leading to possible applications of BNNTs in protein immobilization. Additionally, the insights gained from this theoretical study are expected to assist in the future development of BNNTs with targeted chemoselectivity via suitable chemical functionalization. Calculations are currently in progress with oligopeptides consisting of a few connected amino acids to understand the role of neighboring amino acids in determining the nature of interaction for the conjugated BNNT.

CHAPTER 5

Controlling the performance of a three-terminal molecular transistor: Conformational versus Conventional gating*

5.1. Introduction

In Chapter 3 and 4, we saw how the molecules of different polarities affect the electronic properties of the BNNT. As we proposed at the beginning of this dissertation, our goal is to exploit these information and design a sensing device based on BNNT. The remaining task is to generate electronic signals in these hybrid systems and compare them with that from the pristine BNNTs. We anticipate the current-voltage characteristics in these hybrid systems would be different than that of the pristine BNNTs depending on the nature of interaction involved in the self-assemblies of these bio-molecules onto BNNTs. However, the transport properties at this length-scale (nanometer) do not only depend

*Reprinted with permission from S. Mukhopadhyay, R. Pandey, S. P. Karna; “Controlling The Performance Of A Three-Terminal Molecular Transistor: Conformational Versus Conventional Gating” *J. Phys. Chem. C*, **116**, 4840 (2012). Copyright © 2012 ACS.

upon the system of interest (bioconjugated BNNT, in this case). They depend greatly upon the nature of contacts at the electrode-molecule interfaces, the conduction channels available and so forth.

Before we go into the transport properties in a complex system such as bio-conjugated BNNT sandwiched in between the gold electrodes, it is probably much easier to understand the mesoscopic transport phenomenon in a molecular structure with simplified electrode-architecture. This Chapter is therefore devoted to understand the microscopic details and impacting factors in transport properties in a 3-terminal molecular transistor. Molecular-scale electronics has been a subject of intense experimental^{52,53,76,146-149} and theoretical studies^{54,55,61,150-157} in the past decade aiming to use organic, inorganic (nano-structured materials), and biological molecules as active elements of electronic devices. In the case of organic molecules, several pioneering experiments to measure current (I)-Voltage (V) characteristics of single molecular structures in two-terminal (wire) configurations have been reported. In keeping with experiments, extensive theoretical investigations have been performed to explain observed experimental results as well as to develop detailed fundamental understanding of the underlying physics and chemistry. An ambitious, but technically challenging goal in the molecular scale electronics is to realize three-terminal devices^{54, 68,70,72,73,75,158,159}, where the current through a molecular architecture under bias can be modulated by a second gate field, analogous to the current in inorganic field-effect transistors (FETs). Theoretical studies by He *et al.*¹⁵² have shown that such an FET can be realized in a donor-acceptor (D-A)-junction (J)-A-D architecture by applying a second field across a

third arm of triphenyl ring connected to the junction. The switching effect is noted to result from the modulation of the wavefunction and energies of molecular orbitals (MOs) as well as the dipole moment of the molecule as a function of the applied gate field. Ghosh *et al.*⁵⁴ and Perrine *et al.*¹⁵⁵ have investigated the effects of a gate-field in several simpler organic structures under bias. Experimental observation of electric field gating in a single organic molecule has been reported in a number of recent articles^{70,76,147}.

Electric-field gating of organic molecular current under bias is a natural extension of the current microelectronics FETs, however, it is not as desirable as in microelectronics due to the technical challenges associated with the assembly of organic molecular systems in appropriate orientation and the requirements of applying a second external field, which potentially would induce additional changes to the electronic and geometric structure of the molecule. Also, it does not fully utilize the versatility of the structure-electronic property relationships of organic molecules. For example, organic molecular architectures, offer the possibilities of chemical/structural gating in which the change in the structure due to molecular rotation, conformational change, or coupling of vibrational modes with electronic modes can modulate tunneling current across the molecule under biased condition. In fact, chemical gating, in general, is a dominant phenomenon in a wide range of naturally occurring biological process, such as, bacterial photosynthetic reaction centers¹⁶⁰⁻¹⁶², protein reactions^{163,164} and KcsA potassium channel¹⁶⁵. The chemical gating also plays a key role in the mechanism for the enzyme specificity¹⁶⁶. Even though it is obvious that ‘conformational gating’ is very common in nature, it has not received full attention for molecular electronics.

In a typical donor-bridge-acceptor architecture the electron transfer (ET) is shown to critically depend upon the conformational change (e.g. torsion angle) given to its molecular-moieties¹⁶⁷. Theoretical studies on organic molecular wires^{54,57} also suggest strong current modulation due to conformational changes. A recent experiment by Venkatraman *et al.*¹⁶⁸ has also shown the dependence of electronic conductance on the molecular conformation.

In this Chapter, we show by first-principles quantum mechanical calculations that chemical gating due to change in conformation in the unbiased (third) branch of a three-armed organic structure, similar to the one used by He *et al.*,¹⁵² can lead to an order of magnitude current switching across the conducting arms under biased condition. Application of a second field to the conformational-gated high-conducting (ON) state of the molecule appears to switch OFF and again ON (with reduced magnitude of current) by a phase factor, $\phi=\pi/2$. In contrast, application of second field across the third arm of the molecular architecture under biased condition exhibits usual voltage gating effect accompanied with a decrease in threshold voltage (V_{ds}) with increasing gate bias. We compare the effects of chemical and voltage gating and show the dependence of voltage gating on the geometry (conformation) of the third branch in the three-terminal architecture.

5.2. Simulation Model and Computational Details

As shown in Fig. 5.1, the three-terminal molecular architecture considered in this study consists of two diode units namely ABD and DBA in which the donor (D) and acceptor (A) moieties are derived from 1,3-diaminobenzene and 1,2,4,5-tetracyanobenzene, respectively. The π -conjugated phenyl ring was used as the bridge (IC_1) between the diode structures. The bridging phenyl ring is also covalently bonded to the π -conjugated triphenyl moieties (IC_2 and IC_3), referred to here as the “gate (G)” arm, in analogy to the microelectronic FETs. The model architecture is likely to translate the internal conducting states with respect to the pseudo-Fermi level as described in a previous study¹⁶⁹ on a model biphenyl molecular transistor. In this study, the conformational changes of the system are considered by rotating IC_2 relative to IC_1 in the clockwise (i.e. outward rotation) and the anti-clockwise (i.e. inward rotation) direction by 30° . As noticed from Fig. 5.1, the system is symmetric along the source (S)-drain (D) direction (with a zero dipole component), while asymmetric in the gate direction (with a large dipole component). Atomic gold wire is taken to be source and drain electrodes. In order to eliminate the interfacial effects introduced by thiol groups, we used the $C\equiv CH$ group as contacts at source and drain.

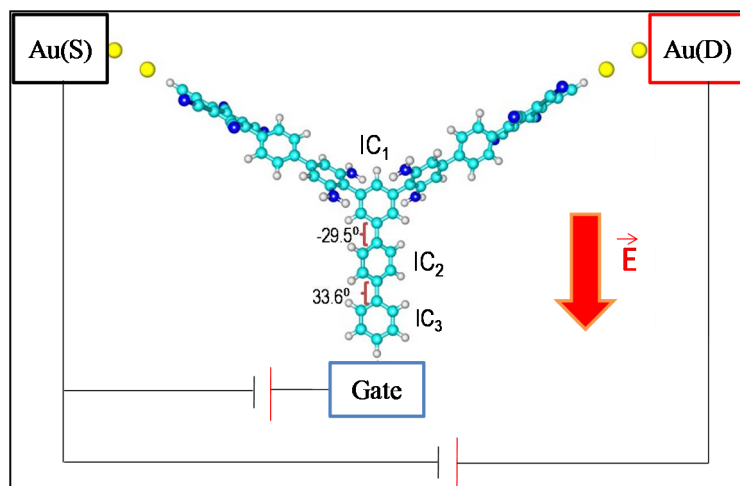


Figure 5.1: Schematic diagram of the setup of a unimolecular transistor-like device ABD-IC-DBA. C, N, H and Au atoms are depicted by green, blue, white and yellow spheres, respectively. A positive bias is applied at the source (S) and a gate field \vec{E} is applied in the direction as shown.

We are aware of the errors that might arise due to the simplicity in designing the electrodes and contacts. To validate our approach to model the contact and electrodes and justify the relevance of our theoretical approximations in real experiments, we have compared our results with the experimental study on ODT-based molecular transistor⁷⁶. Interestingly, our calculated results were found to be in great agreement with those reported in the experiments. The positive gate field is defined with respect to the direction of the dipole moment of the molecule as shown in Fig. 5.1.

The electron transport calculations were carried out in two steps: **(A)** In the first step, electronic-structure calculations were performed on the extended molecular complex consisting of Au-molecule-Au, instead of ‘an isolated molecule’, in the framework of the density functional theory (DFT) with B3LYP functional form^{87,90} and

the LanL2DZ basis set (please see section **2.4.1** for a detailed description) as implemented in GAUSSIAN03¹⁷⁰. It is worth noting that the calculated results obtained at the B3LYP-DFT level of theory is not likely to match the accuracy of the results obtained using GW approximation¹⁰⁴, though recent investigations on Au-benzene-Au have treated only the molecule with GW approximation while considering the electronic structure of the contact gold in the DFT level of theory¹⁰⁴. Since our focus is on predicting qualitative features of electronic transport of the extended molecular complex, we believe that treating both contact and the molecule at the DFT level of theory^{171,172} is a viable alternative.

The extended molecular complex is the core scattering region of the molecular transport system, composed of the molecule and atomic-scale gold contacts in the form of atomic wire coupled to the source and drain electrodes. (B) In the second step, the I_d - V_{ds} characteristics of the molecular complex were calculated using Green's function based Landauer-Büttiker formalism^{105,173,174} in the framework of the DFT. In this approach, the tunneling current (I_d) as a function of the applied bias (V_{ds}) in such a device can be expressed as:

$$I_d = \frac{2e}{h} \int_{-\infty}^{\infty} T(E, E_g) [f(E - \mu_1) - f(E - \mu_2)] dE \quad (5.1)$$

Where μ_1 and μ_2 are the electrochemical potentials in the source and drain electrodes under an external bias V_{ds} , $f(E)$ is the Fermi-Dirac distribution function. For instance, a

positive bias lowers the electrochemical potential at the drain by eV which may be expressed as:

$$\mu_1 - \mu_2 = eV \quad (5.2)$$

and gives rise to different Fermi–Dirac distribution functions at the source and the drain

$$f(E - \mu_1) = \frac{1}{e^{\frac{E - \mu_1}{k_B T} + 1}} \quad (5.3)$$

$$f(E - \mu_2) = \frac{1}{e^{\frac{E - \mu_2}{k_B T} + 1}}$$

which is the driving force for generating the source–drain current, I_d .

The transmission function is a measure of the strength of electron transmission through the various allowed channels, which in the present case are the participating one-electron molecular levels coupled to the metallic reservoirs (emitter/source and collector/drain). It is assumed here, that the molecule is in contact with metals at two ends, referred to as the left and right electrodes.

$T(E, E_g)$ is the electron transmission function at a gate potential of V_g which was obtained from the Green's function approach^{105,175}.

$$T(E, E_g) = \text{Tr} \left[\Gamma_L^{V_g}(E, V) G^{V_g}(E, V) \Gamma_R^{V_g}(E, V) G^{V_g^\dagger}(E, V) \right] \quad (5.4)$$

$$G(E, E_g) = [E \times I - H_{NT}(E, E_g) - \sum_L(E, E_g) - \sum_R(E, E_g)]^{-1} \quad (5.5)$$

Where

$H_{NT}(E, E_g)$ is the orthogonalized non-equilibrium Kohn–Sham (KS) Hamiltonian matrix of the active region of the device in the presence of the gate field obtained by an appropriate partitioning of $H^T(E, E_g)$ ¹⁷² in Eqn. 5.6.

E = injection energy of the tunneling electron.

I = is the identity matrix.

$\Gamma_{L(R)}(E, E_g)$ = twice the imaginary part of the self-energy matrices $\sum_{L(R)}^{V_g}$ ^{175,176}

$$\sum_{L(R)}^{V_g} = C_{L(R)}^+ G_{L(R)}^{V_g} C_{L(R)}$$

The total Hamiltonian of the system in the presence of the external electric fields due to V_g is represented as:

$$H^T[E, E_g] = H^0 + H' + H'' \quad (5.6)$$

where H^0 is the Hamiltonian in the absence of external perturbations, and H' and H'' represent perturbations due to applied gate field and the geometric perturbation applied at the gate arm, respectively. Essentially, $H' = -\vec{\epsilon}_g \times \sum_i r_i$ where $\vec{\epsilon}_g$ are the applied gate field and r_i is the coordinate of the i^{th} electron whereas H'' incorporates the change in the electronic structure properties due the geometric perturbations at the gate arm.

To observe the effect of voltage gating, the geometrical configuration of the molecular complex obtained at the zero field was used for all the calculations assuming that the external electric field employed does not significantly modify the geometry of the architecture. The change in the total charge of the molecule is found to be negligible in the range of gate field considered because the molecular electrochemical potential remains confined in an energy range where the molecule has a very low density of states (DOS). The effect of the capacitance due to the charge redistribution under a non-zero gate field is taken into account via a self-consistent calculation. The Fock matrix F and overlap matrix S (corresponding to a non-orthogonal set of wave functions) from the Kohn–Sham solution of the extended molecule electronic structure calculation for each gate potential were used for electron transport calculations via Eq. 5.1-5.4. To calculate the “conformational gating” the IC₂ in Fig. 5.1 was further rotated by 30° and the I_d-V_{ds} were calculated according to the procedure described above.

5.3. Results and Discussions

We consider the conformational changes in the device system in terms of the relative orientation of the phenyl rings in the “gate” arm e.g. rotation of IC₂ with respect to IC₁ by 30°. Specifically, the configurations considered are: **(A)** “O”: The ground state configuration (“O”) where IC₂ is out of plane by $\sim -30^\circ$ (anti-clockwise) with respect to IC₁. **(B)** “A”: IC₂ is given an anti-clockwise rotation by 30° relative to the ground state configuration, “O” (i.e. IC₂ is -60° out of plane with respect to IC₁). **(C)** “B”: IC₂ is given a clockwise rotation by 30° relative to the ground state configuration, “O” making IC₂ and IC₁ almost planar in the architecture.

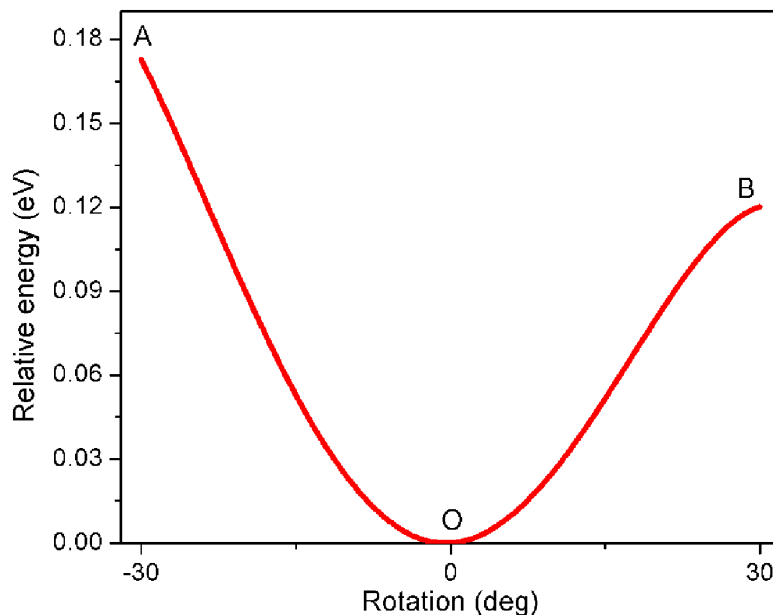


Figure 5.2: The effect of the conformational changes of the gate molecule on the total energy of the system. The zero of energy is aligned to the ground state energy of the system. ‘O’ corresponds to the ground state configuration and ‘A’ and ‘B’ represent the cases when IC₂ is rotated w. r. t. IC₁ by 30°, anti-clockwise and clockwise, respectively.

Fig. 5.2 shows the effect of conformational change on the total energy of the system showing that the anticlockwise rotation of IC_2 reduces the stability of the system slightly more than that of the clockwise rotation (energy barrier between state “A” and “O” is 0.18 eV and that of “O” and “B” is 0.13 eV). In the architecture described above [Fig. 5.1], the effect of an applied field between the S and D ends acts as a perturbation to polarize the charge distribution and mix one-electron energy levels of the system. The additional perturbation along the G arm likely induces additional change in the spatial distribution of the electron charge density and therefore the one-electron energy levels of the system. Specifically, we consider:

- (i) Conformational change in the gate molecule via rotation of IC_2 with respect to IC_1 [Fig. 5.1]
- (ii) Perturbation due to the electric field parallel to the gate arm, which is symmetric with respect to source and drain but asymmetric in the gate direction.

First we shall discuss the effect of the perturbations individually and then the combined effect of (i) and (ii).

5.3. A. Conformational gating

In Fig. 5.3, we show the effect of conformational changes in the gate molecule on the $I_d - V_{ds}$ characteristics. When no gate voltage is applied, the three-terminal device

should ideally behave like a two-terminal device. It may be seen from Fig. 5.3 that the response of the device to the applied bias voltage is insignificant for configurations ‘O’ and ‘B’ even when the bias is high ($V_{ds} = 2V$). The current, on the other hand, rises steeply for the configuration ‘A’ (i. e. IC_2 is out of plane relative to IC_1 approximately by 60°) with $V_{ds} > 1.6 V$.

To understand the calculated I_d - V_{ds} characteristics, we examined the transmission functions, shown in Fig. 5.4(a), for all configurations.

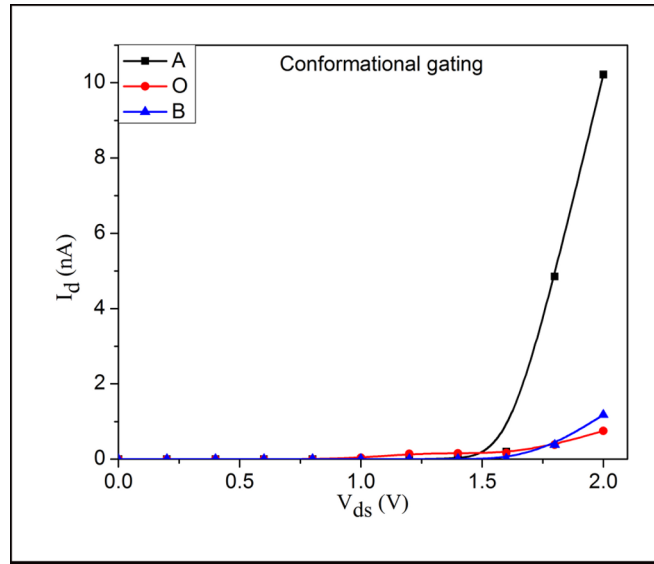


Figure 5.3: The effect of the conformational gating at the gate arm on the I_d - V_{ds} curves. The ‘O’ corresponds to the ground state and ‘A’ and ‘B’ corresponds to 30° anti-clockwise and clockwise rotation of IC_2 relative to the ground state configuration of the device, respectively.

Considering Fig. 5.4(a) we clearly note a direct correlation between the magnitude of the transmission function and the tunneling current in the device system. For example, the transmission function associated with configuration ‘A’ is much higher than that of the other two configurations, leading to a current an order of magnitude larger compared to those for other configurations. It is, therefore, evident that the conformational change in the unbiased branch of the molecule enhances the electron tunneling probability in the biased arms (conduction channel), in the present architecture. It is interesting to note that similar chemical gating effect that is conformational change in a branched arm of biological macromolecules, lead to significant changes in charge transfer across other ends of the molecule¹⁶⁰⁻¹⁶². The same phenomenon also plays a key role in the modulation of chemical-gated ion-channel current, where conformational changes in trans-membrane proteins opens or closes the ion-channel pores¹⁶⁵.

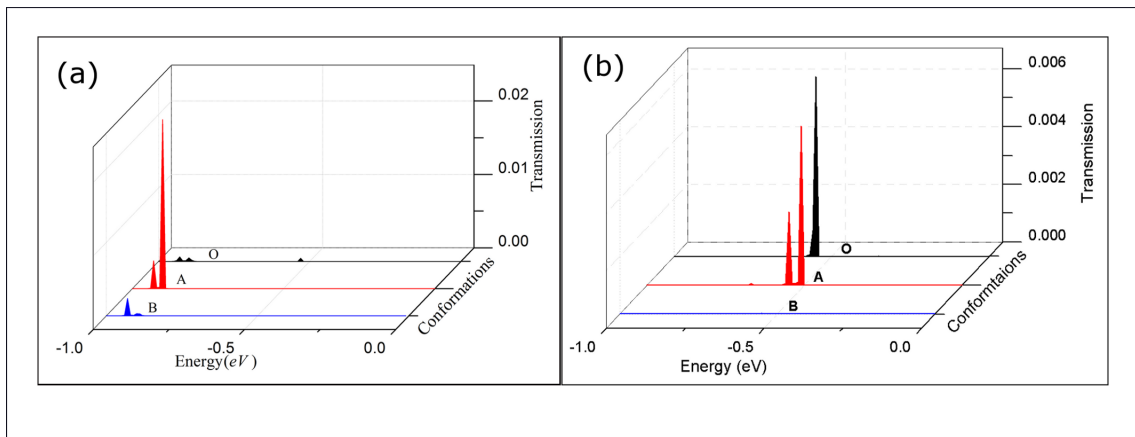


Figure 5.4: The effect of the conformational gating at the gate arm on the transmission functions responsible for the $I_d - V_{ds}$ curves for (a) $V_g = 0V$ and (b) $V_g = 3V$.

To further understand the origin of the higher current in “A”, we examined the effect of conformational gating on the molecular orbital (MO) energy levels of the complex architecture, shown in [Fig. 5.5(a)]. We notice that the conformational gating neither changes the highest occupied (HO)- – lowest unoccupied (LU) MO gap of the system nor the dipole moment associated with “A” and “B” significantly from that of the ground state (“O”). However, a considerable rearrangement of the molecular energy levels takes place in the MO energy levels in the regime further down (HOMO-4 and below) [Fig. 5.5(a)].

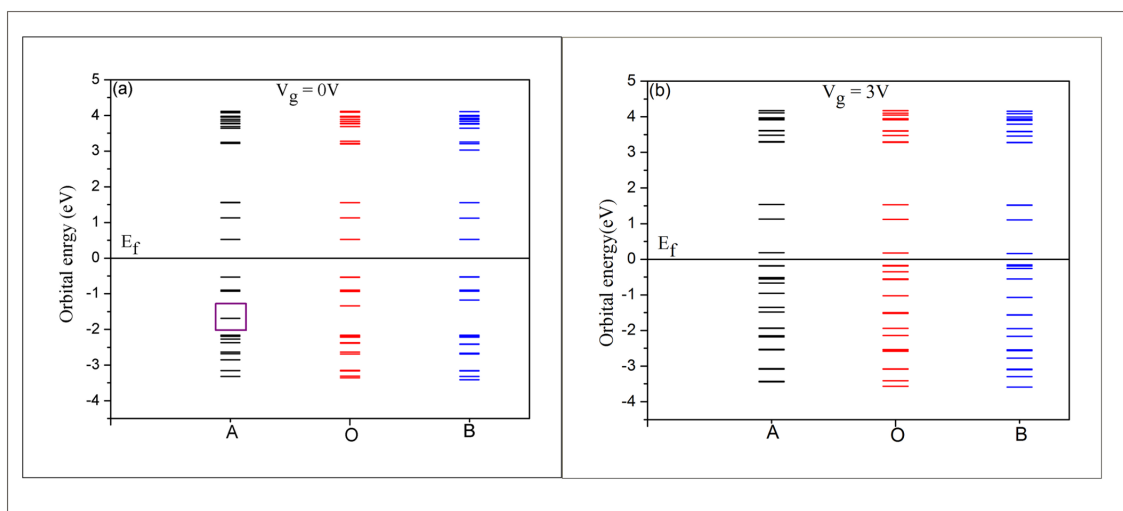


Figure 5.5: Evolution of molecular orbital under (a) conformational gating and (b) both the conformational and voltage gating. Zero of the energy represents the Fermi energy of the system. A square indicates the significant rearrangement.

Fig. 5.6a shows the nature of HOMO's in all the three cases. “O”, “A” and “B” where it appears that the conformational gating affects the current via localization/delocalization of the electronic wave function in the conducting channel. For example, the wave

function is relatively more localized towards the conducting channel for configuration “A” resulting into a higher transmission function as compared to that of “O” and “B”. In other words, the non-planar orientation of the π -electron moieties at the gate arm lifts the carriers up to the S-D channel from the G arm, leading to a high-conducting (ON) state for the system. Our results can be correlated with the role of conformational gating in the photosynthetic reaction center ¹⁶⁴ and enzyme specificity where the conformational gating in the enzyme simply turns the active site to the inert toward the substrate and vice versa ¹⁶⁶ via charge transfer mechanism.

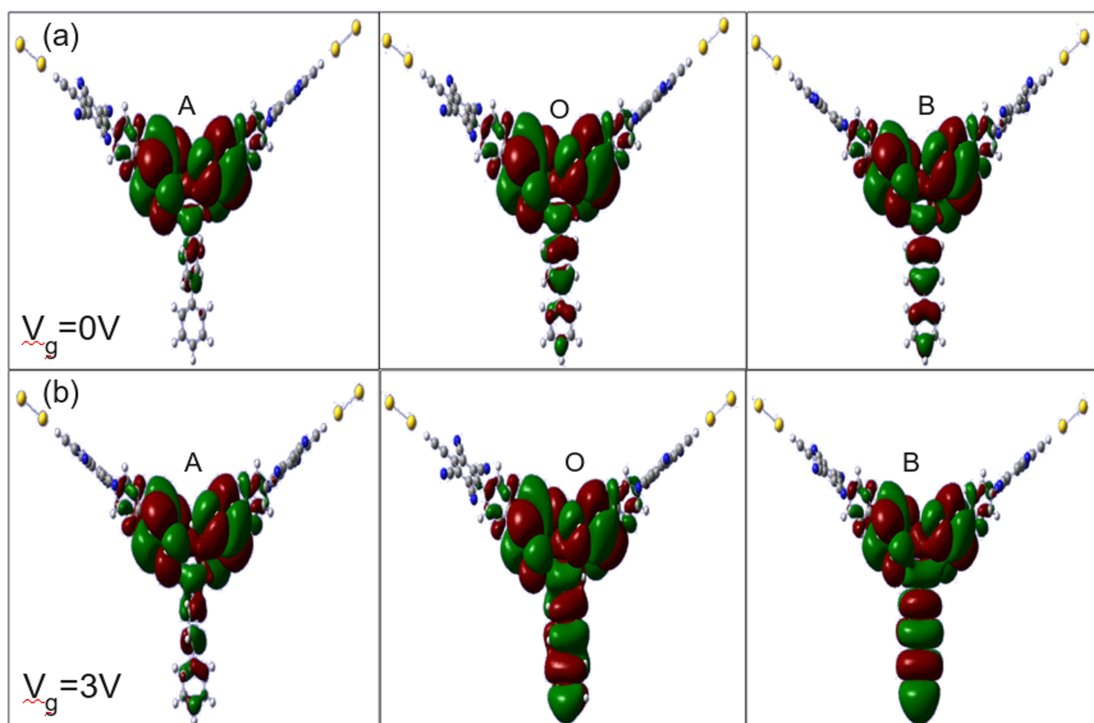


Figure 5.6: Evolution of HOMO for (a) conformational gating (i.e. “A”, “O” and “B” configurations) and (b) both conformational and voltage gating. An isovalue of $0.002 e/\text{bohr}^3$ ($1/10^{\text{th}}$ of the default) is used.

The current modulation ($\frac{I_{ON}}{I_{OFF}}$) by pure conformational gating ($V_g = 0$) is found to be approximately 14 at $V_{ds} = 2V$ [Fig. 5.3].

5.3. B. Voltage gating

For the voltage gating, the $I_d - V_{ds}$ characteristics were found to be independent of gate field in the low bias field regime, i.e. $V_{ds} < 1V$. However, with increase in V_{ds} , I_d increases dramatically [Fig. 5.7] due to the resonant tunneling as discussed previously

152,166

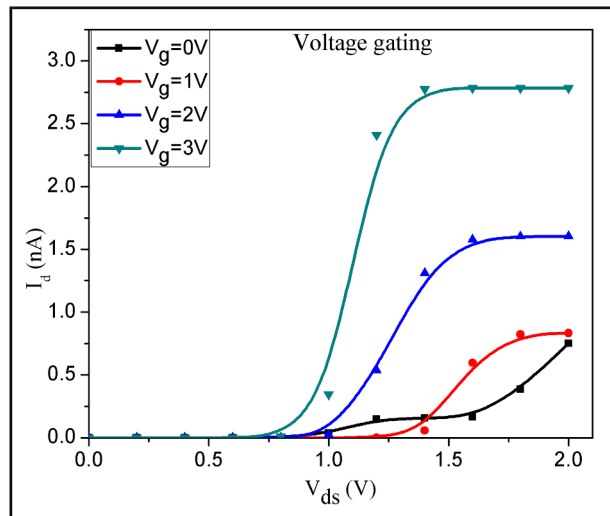


Figure 5.7: $I_d - V_{ds}$ curves for the ground state of the device under various applied gate voltages.

It has been previously noted that the intrinsic dipole moment and the induced polarization of the molecule due to the applied external perturbation play an important role on quantum transport in molecular systems.¹⁶⁷ Therefore, it is useful to examine the relationship of dipole moment, polarization and energy-level mixing with the switching behavior noted here. Although the system has a zero dipole moment along the S-D arm, the polarity along the G arm produces a permanent dipole moment, along the z -direction ensuring a strong electrostatic coupling between the gate arm and rest of the molecular architecture. Moreover, the dipole moment varies significantly and almost linearly with the external electric field. The positive field enhances the dipole moment and lowers the energy of the system. From the examination of the evolution of MO energy, He *et al.* explained that the gap between the MOs representing the donor (D) group and the acceptor (A) group narrows with a positive field (enhancement mode) and thus the current increases significantly.¹⁵² The current modulation reaches its maximum ($\frac{I_{ON}}{I_{OFF}}=160$) when $V_g = 3V$ at $V_{ds} \approx 1.4 V$.

5.3. C. Conformational and Voltage gating

When we consider the combined effects of the conformational changes and the gate field, the architecture shows a peculiar behavior in its I_d-V_{ds} characteristics. Application of the gate field in the conformational-gated “ON” state reduces the

magnitude of current. For $V_g = 1\text{V}$, the response of the device in configuration “B” to the bias voltage, $V_{ds} > 1$, dominates over the other configurations. On the other hand, the configurations “A” and “O” show a higher response current for $V_g = 2\text{V}$ and 3V at the lower bias voltage ($V_{ds} = \sim 0.5\text{ V}$) [Fig. 5.8(a-c)]. The current for “O”, however, seems to increase steadily with increase in V_g [Figure 5.8(a-c)]. It is clear that the effect of voltage gating in this three-terminal architecture critically depends upon the geometry and shows a peculiar behavior when the system is away from the equilibrium geometry.

To summarize the combined effects we looked into the so-called transfer curve (I_d vs. V_g) for $V_{ds} = 2\text{V}$ in Fig. 5.9. Here, I_d for “O” increases steadily with V_g as can be expected in the case of “voltage gating only” [Fig. 5.7]. For configurations “A” and “B”, I_d shows diminishing oscillatory behavior with increasing V_g . It may also be noted that the magnitude of I_d oscillates in the cases of ‘A’ and ‘B’ with a phase factor of $\pi/2$. Note that the conformational changes given to IC_2 in “A” and “B” are opposite in nature, i.e. anti-clockwise and clockwise rotations, respectively. As the voltage gating is turned on, the magnitude of transmission function [Fig. 5.4b] reduces significantly, and thus explains the lower current for $V_g \neq 0$.

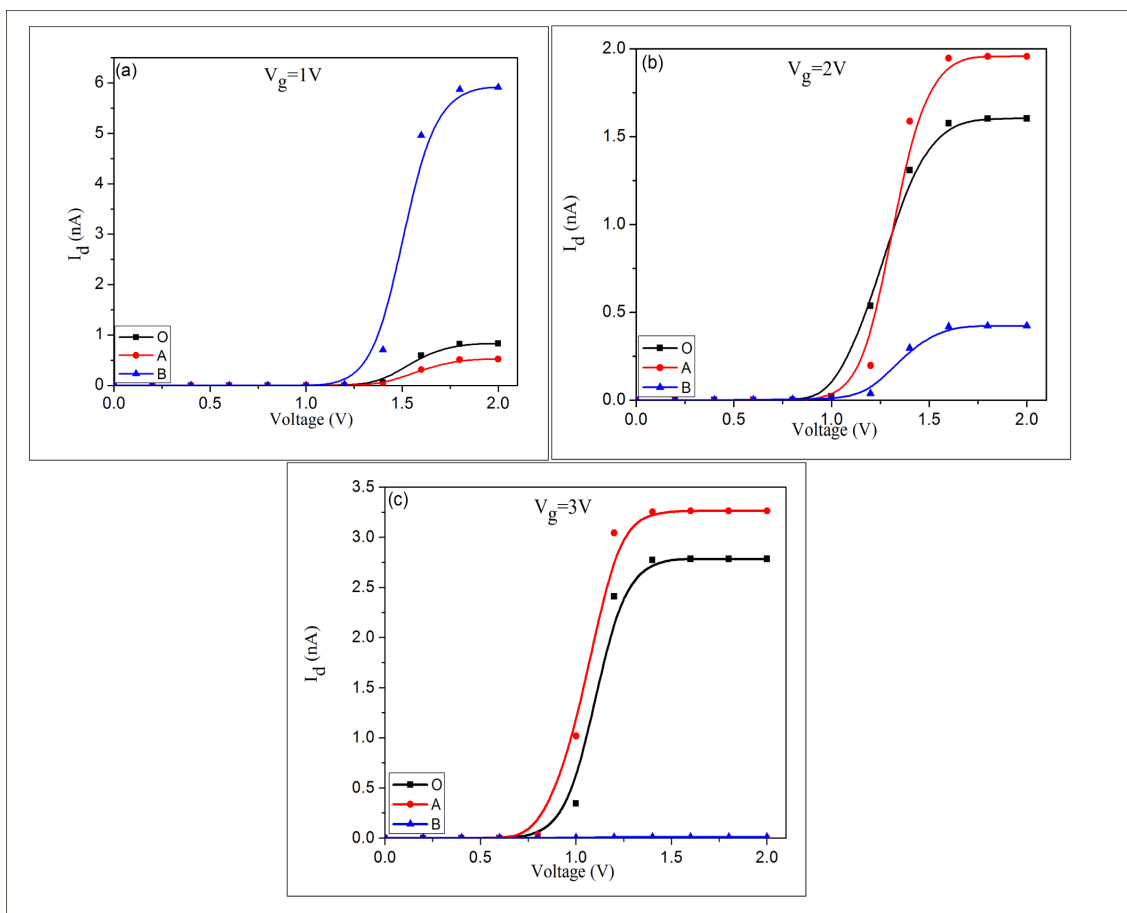


Figure 5.8: Effects of conformational and voltage gating; I_d - V_{ds} curves for all three conformations at: (a) $V_g = 1V$, (b) $V_g = 2V$, (c) $V_g = 3V$.

In spite of the reduction in the HOMO-LUMO gap [Fig. 5.5(b)] due to the applied V_g , the magnitude of I_d decreases for a non-zero value of V_g . It may be due to the fact that V_g shifts molecular orbitals relative to the case of $V_g = 0$ affecting the rearrangement found in Fig. 5.5(a). For example, the wave function is more localized in the conducting channel when $V_g = 0$ [Fig. 5.6a] for “A” relative to that when $V_g = 3V$ shown in Figure 6b. Obviously, higher degree of localization of the electronic wave function along the

conduction channel at $V_g = 3V$ found in configuration “A” [Fig. 5.6b] explains the higher transmission [Fig. 5.4b] and therefore, the higher current in Fig. 5.9.

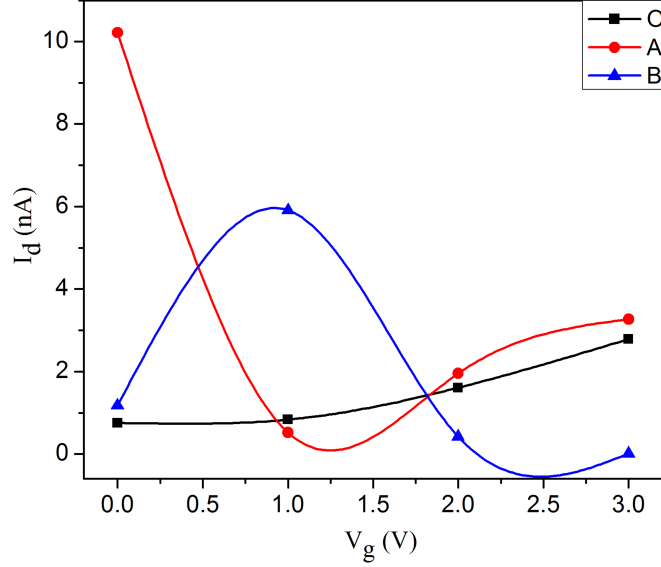


Figure 5.9: Transfer curve representing variation of I_d as a function of applied V_g at $V_{ds} = 2V$. The ground state of the device is “O”. The current corresponding to the configuration ‘A’ and ‘B’ varies with the applied V_g with a phase factor of $\pi/2$.

The maximum current modulations with respect to the ground state modulation $\left[\frac{I_{ON}}{I_{OFF}} \right]$

are 7.1, 1.2, 1.2 for $V_g = 1V, 2V, 3V$, respectively, in the presence of conformational and

voltage gating. Note that the $\frac{I_{ON}}{I_{OFF}}$ under the effect of exclusive conventional and

conformational gating was found to be 160^{152} and 14. Therefore, we may conclude that

the current modulation reaches its maximum value when either conventional or conformational gating is applied and diminishes under their conjugal effects.

Although our objective in this study is to look into the possibility to control the current in a molecular transistor by conformational change instead of the conventional gating, it is worth mentioning that it is possible to rotate IC₂ relative to the rest of the gate-arm architecture experimentally. We are aware of the potential difficulties to achieve the above mentioned conformational change via induced electric field effect^{177,178} which would possibly interfere with the gate-field and it would be difficult to distinguish their effects separately. In recent experiments, however, photo-induced conformational changes¹⁷⁹ and thereby realization of electronic switches^{58,180} in metal-molecule-metal junctions have been a viable practice. Since inclusion of a third electrode (for voltage gating) is likely to change the molecular geometry which the performance of the transistor critically depends on [Fig. 5.9], it might be more desirable to implement the photon-assisted conformational gating via UV-irradiation⁵⁸ in real experiments.

5.4. Summary

In summary, a non-planar orientation of IC₂ at the gate arm leads to a highly conductive “ON” state of three-terminal molecular architecture under biased conditions due to the charge transfer from the gate arm to the conduction arm (channel) of the molecule. This is similar to the conformational gating effect in biological processes such as photosynthetic reaction centers and enzyme specificity. The current modulation

reaches its maximum only under the exclusive effect of voltage or conformational gating and decreases when both of them are present. In presence of the voltage gating, the tunneling current corresponding to conformational gating in two different directions appears to exhibit oscillatory nature with a phase factor of $\pi/2$.

CHAPTER 6

Effect of Molecular Adsorption on the Transport Properties of Boron Nitride Nanotubes and Carbon Nanotubes: Applicability of BNNTs and CNTs as Biosensors

6.1. Introduction

Interaction between the carbon nanotube and deoxyribonucleic acid (DNA) has been a subject of interest for almost two decades^{5,181-188} ever since it was known that CNTs possess many interesting properties, which can be applied in various fields. For example, application of CNT-DNA conjugates as DNA transporters¹⁸⁹, biosensors¹⁹, field effect transistors¹⁹⁰ emerged itself as a new era. DNA has been used as an agent for CNT-dispersion and sorting in solution^{191,192}. These results instigated further investigations for a detailed understanding of the interaction of CNTs with inorganic and organic moieties.

There is also an increasing interest in the usage of CNTs for supporting and detecting DNA through electronic¹⁹³ and optical means^{5,12} and it was reported that single stranded (ss)-DNA of different lengths generally wrap around single-walled CNTs forming tight helices^{183,192}. Apart from multifarious applications, mentioned above, functionalized CNTs are reported to be potential candidates in biomedical applications.

To come up with the theoretical proposals, several experiments were designed to facilitate the DNA-CNTs conjugates as biosensors. Recently, an experiment¹⁹⁴ to design a DNA-decorated CNT-based FET reported that the interaction of DNA with the CNT does not change the response of the device to the applied bias, significantly, although the nucleobases were reported to bind to the CNTs with different binding strengths⁴. It was vaguely argued that it might be because of the scattering centers arising due to the surface defects arising from the interaction of the DNA with the CNT¹⁹⁴. Interestingly, an enhanced field effect was predicted for BNNT with organic molecules adsorbed on it⁸². It is therefore very important to understand how the nucleobases interact with the CNT and how does this interaction affect the transport through the BNNT/CNT-based electronic devices.

Biomedical applications of CNTs are, however, not very appealing because of their toxicity and non-uniformity in dispersion in the solution^{43,140}. Boron nitride nanotube, a non-carbon based nanotube with similar surface morphology, on the other hand, is reported to possess uniformity in dispersion in the solution and therefore readily applicable in biomedical applications without any apparent toxicity^{43,140}. Interestingly, the hetero-nuclei BNNTs are reported to bind with one of the nucleobases with a higher

binding strength and predicted to be useful as a biosensors⁴². It is therefore worth exploring the missing link between the interaction strength of these nucleobases with CNTs⁴ and BNNTs⁴² versus their effects on the transport properties of CNT- and BNNT-conjugated nano-bio complexes.

In this chapter we systematically investigate the effects of the adsorption of the DNA/RNA nucleobases (guanine, adenine, cytosine thymine, and uracil) on the electronic transport of CNTs and BNNTs. Our objective is to understand how the adsorption of the nucleobases affects the electrical transport properties of metallic (CNTs) and semiconducting (BNNTs) nanotube and thereby, their applicability as a biosensors.

6.2. Simulation Model and Computational Details

We consider a high curvature (5, 0) single-walled BNNTs and CNTs of diameter of 0.416 and 0.392 nm, respectively. The methods employed in this study can be divided into two parts. In the first part the composite systems (BNNT/CNT + nucleobases) were optimized by employing the plane wave pseudopotential approach within the local density approximation (LDA)¹²¹ of density functional theory (DFT)^{84,122}. The Vienna ab initio Simulation Package (VASP) was used^{92,93} with the energy cut off of 850 eV and 0.03 eV/Å for its gradient. The periodically repeated units were separated by 15 Å of vacuum to avoid interaction between them. The (1x1x3) Monkhorst Pack grid¹²³ was used for *k*-point sampling of the Brillouin zone. In order to simulate an electronic

environment resembling more closely the situation in DNA and RNA, the C atom of the base molecules linked to the sugar ring in nucleic acid was terminated with a methyl group. The additional benefit of introducing the small magnitude of steric hindrance due to the attached methyl group is to imitate a more probable situation in which a nucleobase in a strand would interact with the surface of the BNNT/CNT.

Because of the complexity of the systems, the optimization was performed in four steps as follows: (i) an initial force relaxation calculation step to determine the preferred orientation and optimum height of the planar base molecule relative to the surface of the tube (ii) calculations of the potential energy surface⁴² for nucleobase-tube interaction by translating the relaxed base molecules parallel to the tube surface covering a surface area 4.26 Å in height, 70⁰ in width, and containing a mesh of 230 scan points. The separation between base molecule and the surface of the BNNT was held fixed at the optimum height determined in step (i). (iii) a 360⁰ rotation of the base molecules in steps of 5⁰ to probe the energy dependence on the orientation of the base molecules with respect to the underlying BNNT surface; and (iv) a full optimization of the conjugate system in which all atoms were free to relax. In order to minimize the steric effect due the added methyl group, the base molecules were rotated, keeping the intermediate distance fixed. It should be pointed that LDA due to a lack of the description of dispersive forces is, in principle, not the most optimal choice for calculating interaction energies of systems governed by vdW forces. However, more sophisticated methods, such as many-body perturbation theory, which are more suitable for describing long-range forces, become prohibitively expensive for complex systems as considered here. Earlier studies^{124,125} have shown that,

unlike the generalized gradient approximation (GGA)¹²⁶ for which the binding for vdW bound systems does not exist, the LDA approximation does indeed provide reasonably good description of the dispersive interactions. Also a recent study⁸ on the adsorption of adenine on graphite suggests that the potential energy surface obtained by using LDA and GGA with a modified version of the London dispersion formula for vdW interactions is effectively indistinguishable. Moreover, the LDA equilibrium distance between adenine and graphene obtained is found to be equal to that obtained using GGA+vdW level of theory. This gives us confidence in the results obtained in the present study to be reasonably accurate in describing nucleobase-BNNT/CNT interaction. The details of the optimization method can be found elsewhere^{4,42}.

The bias-dependent electron transmission and current are calculated using the non-equilibrium Green's functional (NEGF) method based on the Keldysh formalism, as implemented in the SMEAGOL program^{96,97}. The current via the gold-connected bilayer GNRs can be obtained as:

$$I = \frac{e}{h} \int_{-\infty}^{\infty} T(E, V) [f(E - \mu_1) - f(E - \mu_2)] \quad (6.1)$$

where μ_1 and μ_2 are the electrochemical potentials in the two contacts under an external bias V , $f(E)$ is the Fermi-Dirac distribution function. The transmission function, $T(E, V)$ is an important intrinsic factor describing the quantum mechanical transmission probabilities for electrons. The semi-infinite effect of the left (right) electrode is taken

into account by introducing the self-energy Σ_L (Σ_R) in the effective Hamiltonian. A detailed description about the electronic transport can be found in Chapter 2.

The self-consistent LDA-DFT calculations on bulk gold with the k-space sampling of $2 \times 2 \times 100$ grid were used to obtain the values of self energies for transport calculations. The complex part of the integral leading to the charge density is computed using 300 energy points on the complex semicircle, 300 points along the line parallel to the real axis and 30 poles. The integral over real energies necessary at finite bias is evaluated over 1500 points. It is worth noting that the transmission depends on both the electron energy E and the applied external bias V .

6.3. Results and Discussions

In the optimized configuration, the equilibrium separation between BNNT/CNT and nucleobases falls under the range from 2.6-3.0 Å, which is in agreement with earlier calculation for bio-molecules adsorbed on BNNTs^{42,82} and CNTs⁴. It confirms the validity of our approach, used to obtain the hybridized configuration and also the level of accuracy employed in the calculations. The other geometric parameters and electronic properties in the nucleobase-conjugated BNNT/CNT systems are in excellent agreement with the earlier theoretical studies^{4,42}. We shall now focus on the effect of the adsorption of the nucleobases on the transport properties of the metallic CNT and semiconducting BNNT.

Fig. 6.1 shows the model structure we employed for the transport calculations where the central scattering region includes eight 5X5 Au-layers, grown in the [001] direction of the bulk Au-surface, on either side of the electrodes. While the BNNT/CNT and nucleobase hybrids are fully optimized in the absence of gold, the spacing between BNNT and gold is determined by single-point calculations. Interestingly, the optimum distance (in terms of energy) between B-terminated and N-terminated BNNT and gold surface is the same (1.8 Å). The distance between two gold surfaces is 23.5 Å, which corresponds to an electric field of 0.043 V/Å for the applied bias voltage ($V_{ds}=1$ V).

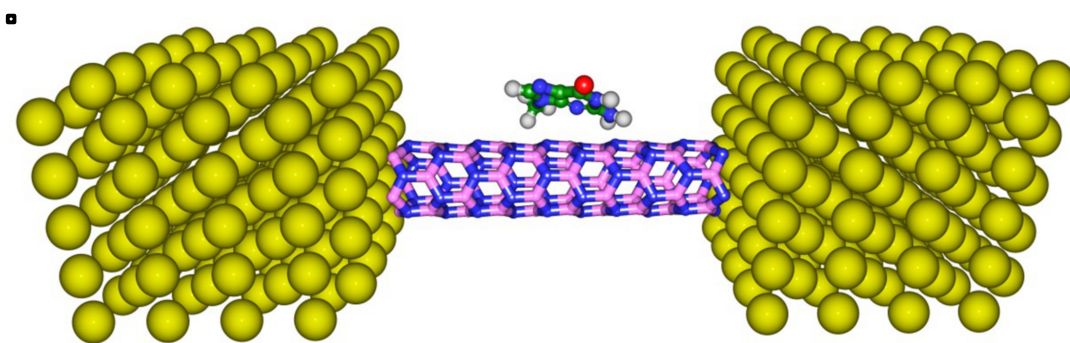


Figure 6.1. A schematic view of G+BNNT coupled with [001] gold electrodes. Symbols: Au in yellow, B in green, N in dark blue, H in light blue, C in grey and O in pink. The optimum distance between BNNT and gold as adopted as 1.8 Å in each side from single-point calculations. The average distance between Guanine and BNNT is about 3.5 Å.

The length of BNNTs/CNTs in this study is considered about 20 Å in order to minimize the undesired interaction between the nucleobases and the electrodes. Additionally, we modeled junction between the metallic electrodes and nanotube-hybrids

for all the cases symmetrically so that the contributions from the interfacial effects in the transport properties of these systems become inconsequential. This enables us to focus on the modulation in transport properties of the nanotubes only due to the hybridization with the nucleobases.

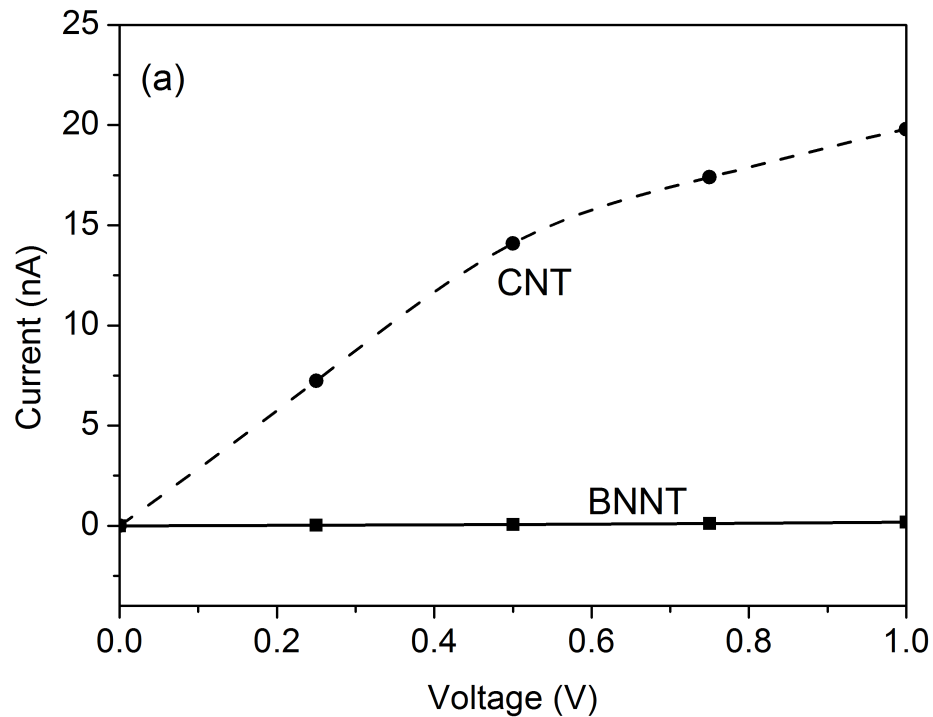


Figure 6.2. I-V characteristics of pristine BNNT and CNT in the small bias regime.

The calculated transmission functions are illustrated in Fig. 6.3 where CNT and BNNT are shown to exhibit their intrinsic transport properties; there exists a finite gap near Fermi energy for BNNT. The diameter of the tubes considered in this study might be

questionable here, but it was demonstrated before that small diameter CNTs do not follow the general dependencies on chirality as larger CNTs do, however, they will be metallic regardless of their chirality¹⁹⁵, and BNNTs are semiconducting in nature irrespective of their chirality²⁴. The subsequent finite transmission peaks [Fig. 6.3] near the Fermi energy of CNT-sandwiched between the electrodes explains its metal-like conductivity and steep rise in current as soon as the external bias voltage is turned on. On the other hand, due to the absence of any conduction channel for the pristine BNNT [Fig. 6.3] explains the low conductivity of BNNT. The conductance of bare BNNT at 1 Volt is only $2.34 \times 10^{-6} G_0$, G_0 being the conductance quantum corresponding to a fully opened conduction channel, suggesting that the transmission falls into the tunneling region.

The effects of molecular adsorption on the conductivity of these nanotubes are demonstrated in Fig. 6.4 with the corresponding transmission functions in Fig. 6.5. It is clear from Fig. 6.4(a) that the molecular adsorption does not affect the conductivity of the metallic CNTs significantly. Although, the binding energy of guanine with CNT is strongest among all the other nucleobases⁴, its effect on the conductivity of the CNT is insignificant. Guanine appears to introduce additional conduction channel [Fig. 6.4(a)] near the Fermi energy of the conjugated system, but contradictorily reduce the conductivity of the existing channels [height of the transmission peaks] of the pristine CNT. Since the current is calculated by summing up the contribution from all the transmission channels in the bias window, the current in the guanine conjugated CNT does not undergo a significant change compared with the pristine CNT.

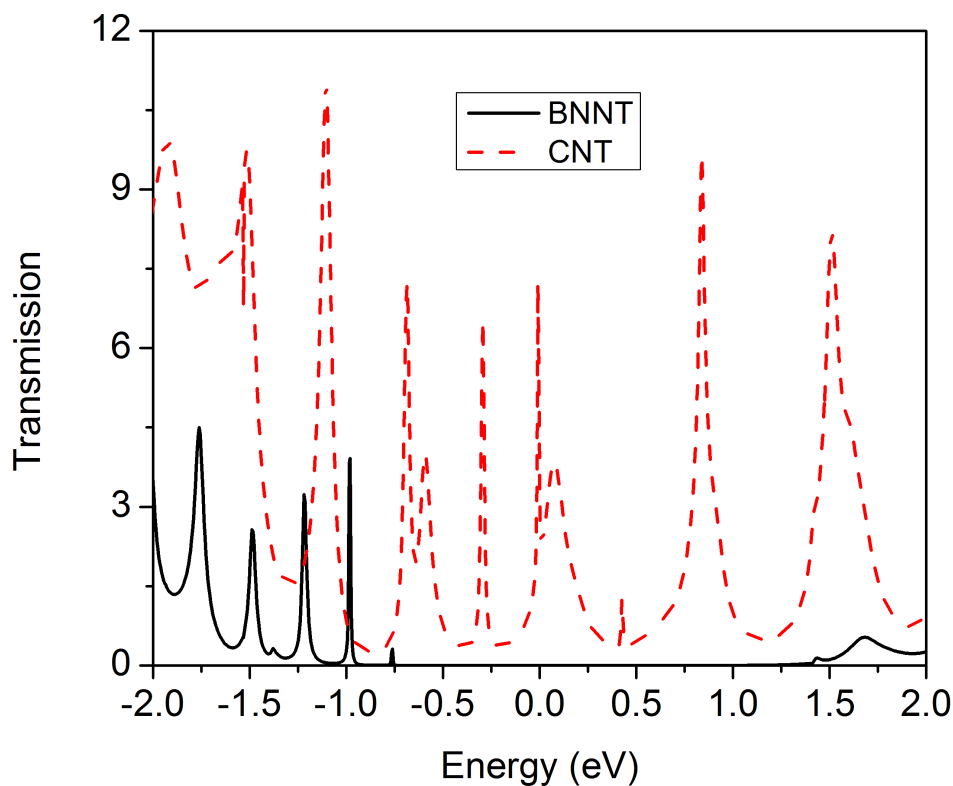


Figure 6.3. Characteristic transmission function of pristine BNNT and CNT at zero external bias explaining the I-V characteristics in Figure 6.2.

In contrast with the CNT, guanine appears to induce a notable enhancement in the current compared with pristine BNNT, while other base-BNNT hybrids render currents, similar to or smaller than that of pristine BNNT. In the bias range explored in this study, the normalized currents in BNNT-conjugated systems follow the following hierarchy: $G > 1 > C > A \sim U > T$, where the normalized currents are defined as the ratio of current of each kind of hybrid systems to that of pristine BNNT. The conductivity of the BNNT

gets enhanced by about 44% in its conjugated configuration with guanine. A comparison of the underlying transmission functions of BNNT and nucleobase at zero bias is given in Fig. 6.5(b) leading to the current in Fig. 6.4(b). It appears that when the external bias is not applied, guanine offers a new conduction channel near the Fermi energy of the conjugated systems in addition to the characteristic peaks of the BNNT unlike the other nucleobases, which fail to enhance the conductivity of BNNTs. It is worth noting here that the distinct adsorption feature of guanine –conjugated BNNT was reported in a previous theoretical study²¹ where a higher degree of hybridization of the electronic wave function of guanine and BNNT was argued to be responsible for a higher binding energy and a dramatically decreased energy gap compared with other hybrids.

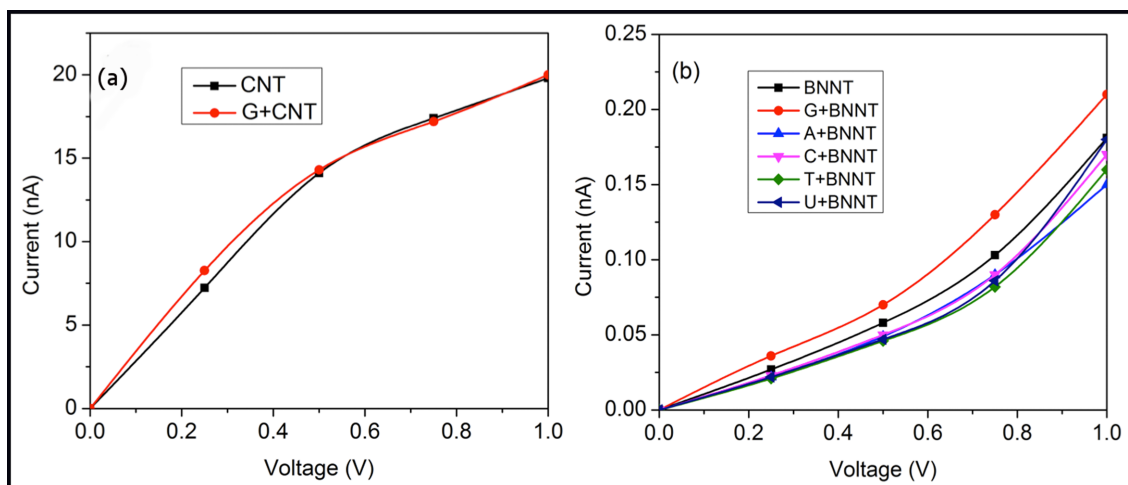


Figure 6.4. Effect of molecular adsorption on the transport properties of CNT and BNNT: I-V characteristics of (a) CNT and (b) BNNT with the nucleobases adsorbed on it. Note: I-V characteristics for other CNT-conjugates [CNT+ A/C/T/U] are not shown here as they superimpose with that of CNT.

As far as the comparison between the effects of the molecular adsorption of nucleobases on transport properties are concerned, it might be concluded that BNNTs are more sensitive to the attachment of molecules compared to CNTs. For example, the strength of attachment of guanine with CNT and BNNT was both predicted to be 0.1 eV higher than that of the other nucleobases but the conductivity of BNNTs was noted to be enhanced by 44% while no significant variation is seen for CNT.

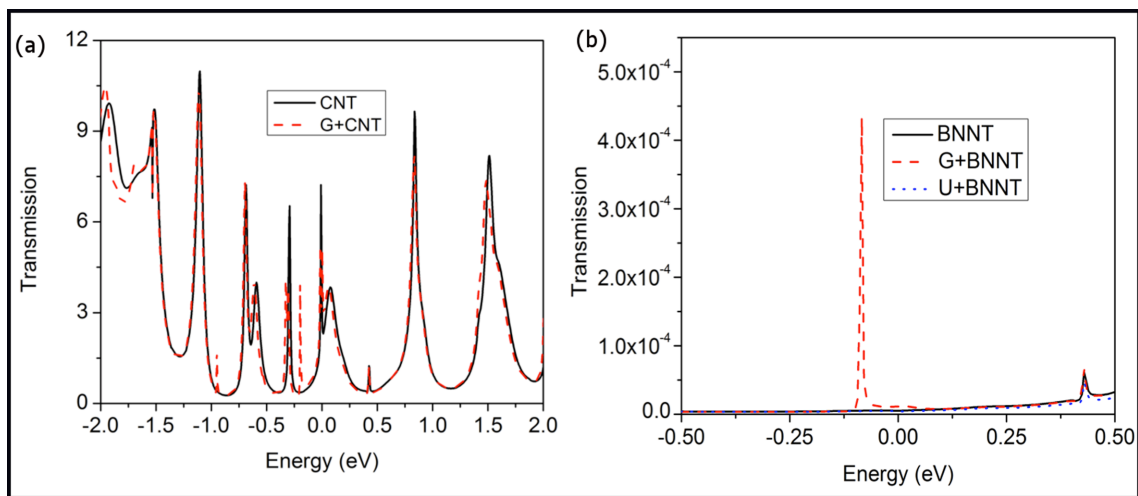


Figure 6.5. Effect of molecular adsorption on the transmission functions corresponding the I-V characteristics in Figure 6.4: (a) Transmission function of CNT and CNT+G and (b) Transmission function of BNNT, BNNT+G and BNNT+U at zero external bias.

This is consistent with the previous theoretical calculation⁸² where weak attachment of trinitrotoluene, benzaldehyde and benzoic acid was found to affect the

current in their conjugated systems with BNNT. It might be because of the high background current from the metallic CNT, which makes the small variation in the current due to the molecular adsorption apparently difficult to detect unlike the semiconducting BNNTs where the background current is very small ($I_{\text{CNT}} / I_{\text{BNNT}} > 10^2$). Adsorption of molecules [such as molecules of different polarities³⁸] on BNNTs with a much wider variation in binding strengths might be anticipated to have more conspicuous effect on the transport properties and therefore would offer a better sensing possibility by BNNTs.

6. 4. Summary

To summarize, the I-V characteristics of nucleobase conjugated (5, 0) BNNT and (5, 0) CNT sandwiched between gold electrodes are studied using LDA-DFT combined with non-equilibrium Green's function technique. The calculated results show one to one relation between the strength of binding of the molecules adsorbed on BNNTs and their effect on the transport properties of BNNTs. Contrastingly; the transport properties of CNTs remain unaffected in the presence of the investigated adsorbed molecules. One of the nucleobases, guanine, which was reported to bind both with BNNTs and CNTs with the highest binding strength, leads to a current 44% higher than that of pristine BNNT while does not affect the current of the pristine CNT. The one-sidedness of the nucleobases to the transport properties of CNTs and BNNTs is explained in terms of opening of new conduction channels in the bias window and their contribution to the total current. We find the large background current from the metallic CNT [$I_{\text{CNT}}/I_{\text{BNNT}} > 10^2$]

makes it indifferent to the small contribution due to the molecular adsorption. This indicates to the fact that BNNTs are more suitable candidates for their applications in bio-detection/bio-sensing compared to metallic CNTs.

CHAPTER 7

Summary and Future Perspectives

7.1. Summary

It might not be an easy task to convince oneself that BNNTs are better than CNTs, at this point of time, as far as their applicability in biomedical applications is concerned. This is because BNNTs and their usages in different avenues, has been overruled by CNTs. But it is not difficult to anticipate that a new era is about to come when BNNTs and related technologies will be at the frontier of the scientific community. In this dissertation, we have explored some aspects of the bioconjugation of BNNTs via first-principles based calculations based on density functional theory. Following is the list of major information that we gained from this work and is expected to provide some guidance to the experimental efforts:

1. We found that adsorption of DNA/RNA nucleobases: adenine (A), guanine (G), cytosine (C), thymine (T) and uracil (U) on the outer wall of a high curvature semiconducting single-walled BNNTs is dominated by van der Waals forces. The binding energy shows the order: $G > A \approx C \approx T \approx U$, implying that the interaction strength of the high curvature BNNT with the nucleobases, is nearly the same, G being an exception. The charge transfer involved in the process of adsorption of nucleobases was found to be insignificant.

2. A higher binding energy for the G–BNNT conjugate appears to result from hybridization of the molecular orbitals of G and the BNNT and therefore, the modulation of band gap of BNNT was found to be maximum for G-conjugated BNNT compared to the other nucleobases. However, all the nucleobases appeared to introduce new mid gap states and thereby band gap modulation of BNNT. The energy gap predicted for the G–BNNT conjugate relative to that of the pristine BNNT might be useful in the application of this class of biofunctional materials to the design of next-generation sensing devices.

3. We explored the sensitivity of BNNT towards amino acids of different polarities based on the three representative amino acids, namely, tryptophan (Trp), a nonpolar aromatic amino acid, and aspartic acid (Asp) and arginine (Arg), both polar amino acids are considered for their interactions with BNNT. We noted that polar molecules, Asp and Arg, exhibit relatively stronger binding with the tubular surface of BNNT. The process of adsorption was accompanied by significant amount of charge transfer and therefore, mediated by Coulombic forces. The strong binding between the polar amino acid molecules and BNNT indicates the potential application of BNNTs in protein-

stabilization. The band gap of the tube remained unaltered in the chemisorption of the polar molecules.

4. Trp being non-polar in nature exhibited weak binding onto the surface of BNNT, similar to the nucleobase molecules, with no significant charge transfer associated in the interaction. Band gap modulation of BNNT was found in Trp-conjugated BNNT as we predicted for the charge neutral nucleobases.

5. The predicted higher sensitivity of BNNTs compared to carbon nanotubes (CNTs) toward amino acid polarity suggests BNNTs to be a better substrate for protein immobilization than CNTs. On the other hand, the enhanced protein stability by BNNTs may, consequently, be utilized toward the enzyme degradation and to increase the activity via immobilization at the surface of the tube.

6. In the ground state of a three terminal molecular transistor, a typical example of quantum transport at mesoscopic length scale, with a non-planar gate-arm, we tunnel current (I_d) as a function of external bias (V_{ds}) across the two D–A substituted arms to exhibit insulator-semiconductor behavior. However, a significant increase, by more than an order of magnitude, and a distinct variation in the current are predicted in its operational mode ($V_{ds} > 1.5$ V) when additional conformational changes at the gate-arm is introduced. Surprisingly, neither the HOMO–LUMO gap nor the dipole moment of the system undergoes significant changes due to pure conformational gating unlike in a “voltage” gating. Instead, the observed conformational gating affects the current via localization/delocalization of the electronic wave function in the conduction channel.

7. Furthermore, the tunneling current corresponding to conformational gating in two different directions appears to exhibit oscillatory nature with a phase factor of $\pi/2$ in the presence of the gate field. The current modulation was found to reach its maximum only under the exclusive effect of voltage or conformational gating and diminishes when both of them are present.

8. When the transport properties of the nucleobase-conjugated BNNT was calculated, we found a notable enhancement in the current for guanine conjugated BNNT where as for the other nucleobases the conductivity of the tube remained unaltered. The mid-gap states introduced during the course of adsorption of guanine onto BNNT, was found to play an important role in the enhance conductivity of the G-BNNT hybrid system.

9. Contrastingly, the transport properties of metallic CNTs remain unaffected in the presence of the adsorbed nucleobases. The large background current from the metallic CNT [$I_{\text{CNT}}/I_{\text{BNNT}} > 10^2$] makes it indifferent to the small contribution due to the molecular adsorption. This indicates that BNNTs are more suitable candidates for their applications in bio-detection/bio-sensing compared to metallic CNTs.

This thesis work is expected to provide minute details regarding bioconjugation of nanomaterials towards biodetection and instigate experimental efforts to explore the possibility of using BNNTs over CNTs for biosensing applications. Throughout in this dissertation, we have used quantum mechanical approaches with an acceptable level of accuracy. However, one should note the limitations and approximation we made to tackle specific problem of interest. Therefore, numerical estimation of the possible error bar is expected to vary for different approaches and is yet to be established, quantitatively.

7.2. Future Perspectives

In order to investigate and understand a system with a large number of locally interacting, identical constituents on a far bigger scale than the size of the constituents, it is a viable practice to use few effective degrees of freedom to describe the system's behavior with a few phenomenological parameters. Recent trends to describe larger biological systems with the solvent effect thus include classical molecular dynamics (MD) with well-tested parameterizations. It is true that the classical approaches employed in the commonly used MD-codes, such as NAMD, LAMMPS, etc. describes the larger biological systems with reasonably good accuracy, quantum mechanical approaches, on the other hand, define the conjugated systems with nanomaterials with satisfactory accuracy. However, the popular MD-codes do not include parameters for most of the inorganic elements especially those in nanostructure environments and therefore, do not offer the flexibility to explore the whole range of available nanomaterials. Furthermore, quantum approaches are prohibitively expensive for the larger biological systems.

Bridging these two approaches for a fast and better prediction of systems with numerous degrees of freedom and scope for relaxation demands exploitation of the speed of the commonly available MD-codes, such as, NAMD, LAMMPS, GROMACS, etc. with appropriate parameterizations to obtain the “global minima” of the nanobiocomposites and then exploit the accuracy of the quantum chemical calculations (VASP, GAUSSIAN) to investigate their properties. This is expected to answer several

questions, such as: (I) how the interaction features of the nanomaterials with the biological systems vary at a far larger scale, beyond the scope of quantum mechanical approaches, (II) whether the interaction properties in the ideal gas phase calculations survive in the presence of solvents, (III) how important it is to consider chemical environment due to the backbone and the neighboring molecules in the nano-bio interaction and whether they have something to do with bio-toxicity, (IV) after what extent of size of the biological matter does their response become invariant to the nanomaterials, and so forth.

The above-mentioned approach, its development (parameterization) and applications to interface nanomaterials with biological systems require critical understanding of site- and shape-dependent nano-bio interaction, high performance computing facility and experimental verification.

Meanwhile, we initiated the study focused on the sequence dependent interaction of a fragment of single stranded DNA with BNNT. The objective of this study is to understand how the interaction of the isolated nucleobases with BNNT varies in the chemical environment of the other nucleobases and the polar backbone [Fig. 7.1].

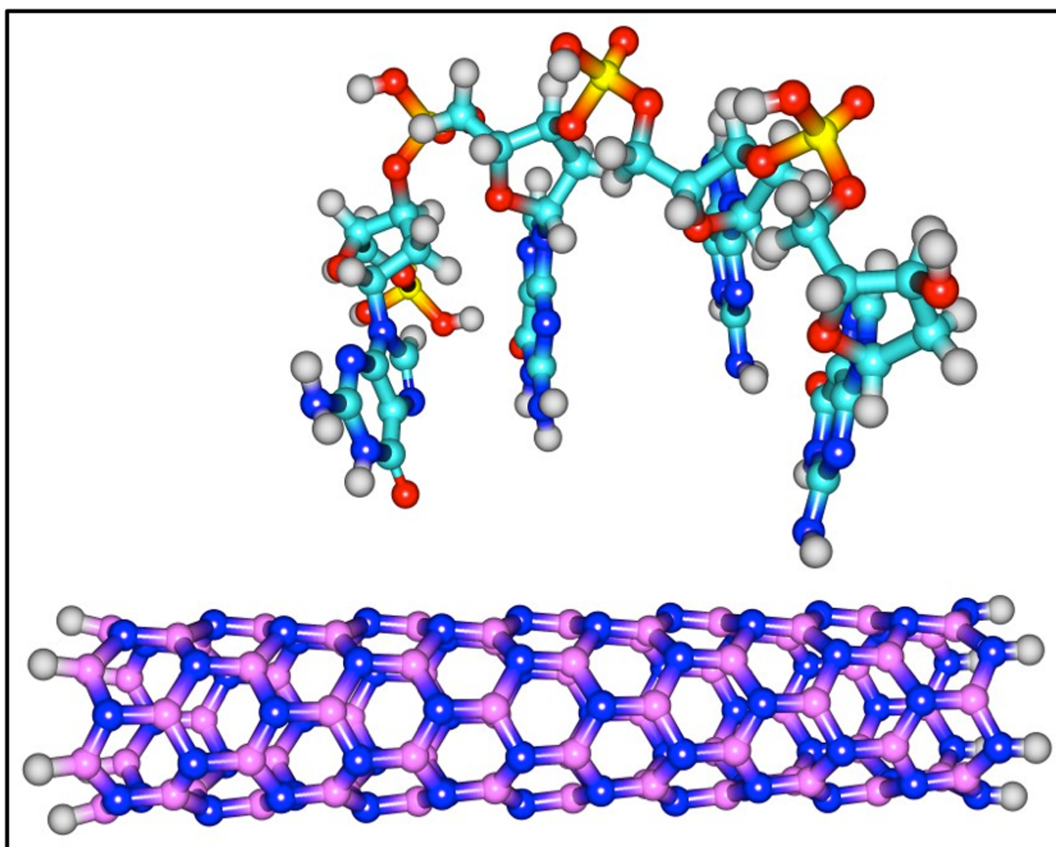


Figure 7.1: The self-assembly of a fragment of ss-DNA on the top of a BNNT.

Since the number of the atoms involved in the DNA-conjugated BNNT is large, we employed the semi-empirical (AM1¹⁹⁶⁻¹⁹⁹) approaches to optimize the structure using GAUSSIAN 09. We have also tested the appropriateness of this approach by reproducing the adsorption length ($R_{\text{BNNT-DNA}}$) from quantum mechanical calculations solving the Kohn–Sham equations based on the density functional theory (DFT) with the gradient-corrected B3LYP functional form⁸⁶ and Lee, Yang, and Parr correlation functional⁹⁰. We used Los Alamos National Laboratory (LANL2DZ)⁹¹ as basis set.

In order to understand the role of sequence in DNA in deciding the interaction strength, we simulated both the heterogeneous DNA with all the nucleobases present with a proper sequence as reported before and also homogeneous one by substituting the nucleobases by any one of them. For example, a homogeneous DNA-fragment will be composed of either four guanine or cytosine. Additionally, the properties of the composite systems are being calculated with and without the presence of water in order to understand the effect of solvents in these kinds of interaction. From the preliminary results we anticipate notable variation in the strength of interaction with which the DNA binds to the tube, depending upon the sequence and chemical environment (solvent).

References

- (1) Das, A.; Sood, A. K.; Maiti, P. K.; Das, M.; Varadarajan, R.; Rao, C. N. R. *Chemical Physics Letters* **2008**, 453, 266.
- (2) Enyashin, A. N.; Gemming, S.; Seifert, G. *Nanotechnology* **2007**, 18.
- (3) Gowtham, S.; Scheicher, R. H.; Ahuja, R.; Pandey, R.; Karna, S. P. *Physical Review B* **2007**, 76, 033401
- (4) Gowtham, S.; Scheicher, R. H.; Pandey, R.; Karna, S. P.; Ahuja, R. *Nanotechnology* **2008**, 19, 125701
- (5) Jeng, E. S.; Moll, A. E.; Roy, A. C.; Gastala, J. B.; Strano, M. S. *Nano Letters* **2006**, 6, 371.
- (6) Johnson, R. R.; Johnson, A. T. C.; Klein, M. L. *Nano Letters* **2008**, 8, 69.
- (7) Meng, S.; Maragakis, P.; Papaloukas, C.; Kaxiras, E. *Nano Letters* **2007**, 7, 45.
- (8) Ortmann, F.; Schmidt, W. G.; Bechstedt, F. *Physical Review Letters* **2005**, 95, 186101/1.
- (9) Tu, X. M.; Manohar, S.; Jagota, A.; Zheng, M. *Nature* **2009**, 460, 250.
- (10) Rajendran, A.; Magesh, C. J.; Perumal, P. T. *Bba-Gen Subjects* **2008**, 1780, 282.
- (11) Vaidyanathan, V. G.; Nair, B. U. *J Inorg Biochem* **2003**, 95, 334.

- (12) Heller, D. A.; Jeng, E. S.; Yeung, T. K.; Martinez, B. M.; Moll, A. E.; Gastala, J. B.; Strano, M. S. *Science* **2006**, *311*, 508.
- (13) Chen, R. J.; Bangsaruntip, S.; Drouvalakis, K. A.; Kam, N. W. S.; Shim, M.; Li, Y. M.; Kim, W.; Utz, P. J.; Dai, H. J. *Proceedings of the National Academy of Sciences of the United States of America* **2003**, *100*, 4984.
- (14) Kang, Y.; Liu, Y. C.; Wang, Q.; Shen, J. W.; Wu, T.; Guan, W. J. *Biomaterials* **2009**, *30*, 2807.
- (15) Cui, Y.; Wei, Q. Q.; Park, H. K.; Lieber, C. M. *Science* **2001**, *293*, 1289.
- (16) Benyamini, H.; Shulman-Peleg, A.; Wolfson, H. J.; Belgorodsky, B.; Fadeev, L.; Gozin, M. *Bioconjugate Chemistry* **2006**, *17*, 378.
- (17) Hong, R.; Fischer, N. O.; Verma, A.; Goodman, C. M.; Emrick, T.; Rotello, V. M. *Journal of the American Chemical Society* **2004**, *126*, 739.
- (18) You, C. C.; Agasti, S. S.; De, M.; Knapp, M. J.; Rotello, V. M. *Journal of the American Chemical Society* **2006**, *128*, 14612.
- (19) Staii, C.; Johnson, A. T. *Nano Letters* **2005**, *5*, 1774.
- (20) Delmotte, A.; Tate, E. W.; Yaliraki, S. N.; Barahona, M. *Phys Biol* **2011**, *8*.
- (21) Krishnamoorthy, N.; Yacoub, M. H.; Yaliraki, S. N. *Biomaterials* **2011**, *32*, 7275.

- (22) Delvenne, J. C.; Yaliraki, S. N.; Barahona, M. *Proceedings of the National Academy of Sciences of the United States of America* **2010**, *107*, 12755.
- (23) Grima, R.; Yaliraki, S. N.; Barahona, M. *Journal of Physical Chemistry B* **2010**, *114*, 5380.
- (24) Chopra, N. G.; Luyken, R. J.; Cherrey, K.; Crespi, V. H.; Cohen, M. L.; Louie, S. G.; Zettl, A. *Science* **1995**, *269*, 966.
- (25) Iijima, S. *Nature* **1991**, *354*, 56.
- (26) Luo, Z. T.; Lu, Y.; Johnson, A. T. C. *Abstracts of Papers of the American Chemical Society* **2011**, *241*.
- (27) Yin, H. S.; Zhou, Y. L.; Zhang, H. X.; Meng, X. M.; Ai, S. Y. *Biosens Bioelectron* **2012**, *33*, 247.
- (28) Balasubramanian, K.; Burghard, M. *Anal Bioanal Chem* **2006**, *385*, 452.
- (29) Kang, J. W.; Hwang, H. J. *Journal of Physics-Condensed Matter* **2004**, *16*, 3901.
- (30) Li, Y. F.; Yu, H. Q.; Li, H.; Zhang, K.; An, C. G.; Liew, K. M.; Liu, X. F. *Journal of Physical Chemistry C* **2010**, *114*, 11421.
- (31) Rubio, A.; Corkill, J. L.; Cohen, M. L. *Physical Review B* **1994**, *49*, 5081.
- (32) An, L.; Fu, Q. A.; Lu, C. G.; Liu, J. *Journal of the American Chemical Society* **2004**, *126*, 10520.

- (33) Jarillo-Herrero, P.; Sapmaz, S.; Dekker, C.; Kouwenhoven, L. P.; van der Zant, H. S. J. *Nature* **2004**, *429*, 389.
- (34) Tans, S. J.; Verschueren, A. R. M.; Dekker, C. *Nature* **1998**, *393*, 49.
- (35) Akdim, B.; Kim, S. N.; Naik, R. R.; Maruyama, B.; Pender, M. J.; Pachter, R. *Nanotechnology* **2009**, *20*, 355705 (8 pp.).
- (36) Zhi, C. Y.; Bando, Y.; Tang, C. C.; Honda, S.; Sato, K.; Kuwahara, H.; Golberg, D. *Angew Chem Int Edit* **2005**, *44*, 7932.
- (37) Lei, J. P.; Ju, H. X. *Chem Soc Rev* **2012**, *41*, 2122.
- (38) Mukhopadhyay, S.; Scheicher, R. H.; Pandey, R.; Karna, S. P. *J Phys Chem Lett* **2011**, *2*, 2442.
- (39) Shewale, V.; Joshi, P.; Mukhopadhyay, S.; Deshpande, P.; Pandey, R.; Hussain, S.; Karna, S. P. *J Phys. chem. C* **2011**, *115*, 10426.
- (40) Mirzaei, M.; Arshadi, S.; Abedini, S.; Yousefi, M.; Meskinfam, M. *Solid State Sci* **2012**, *14*, 689.
- (41) Wong, S. S.; Joselevich, E.; Woolley, A. T.; Cheung, C. L.; Lieber, C. M. *Nature* **1998**, *394*, 52.
- (42) Mukhopadhyay, S.; Gowtham, S.; Scheicher, R. H.; Pandey, R.; Karna, S. P. *Nanotechnology* **2010**, *21*, 165703.

- (43) Chen, R. J.; Zhang, Y. G.; Wang, D. W.; Dai, H. J. *Journal of the American Chemical Society* **2001**, *123*, 3838.
- (44) Gao, Z. H.; Zhi, C. Y.; Bando, Y.; Golberg, D.; Serizawa, T. *Acs Appl Mater Inter* **2011**, *3*, 627.
- (45) Chen, X.; Wu, P.; Rousseas, M.; Okawa, D.; Gartner, Z.; Zettl, A.; Bertozzi, C. R. *Journal of the American Chemical Society* **2009**, *131*, 890.
- (46) Ciofani, G.; Raffa, V.; Menciassi, A.; Cuschieri, A. *Biotechnol Bioeng* **2008**, *101*, 850.
- (47) Ciofani, G.; Raffa, V.; Menciassi, A.; Dario, P. *Journal of Nanoscience and Nanotechnology* **2008**, *8*, 6223.
- (48) Ciofani, G.; Ricotti, L.; Danti, S.; Moscato, S.; Nesti, C.; D'Alessandro, D.; Dinucci, D.; Chiellini, F.; Pietrabissa, A.; Petrini, M.; Menciassi, A. *Int J Nanomed* **2010**, *5*, 285.
- (49) Zhi, C.; Bando, Y.; Tang, C.; Golberg, D. *Journal of the American Chemical Society* **2005**, *127*, 17144.
- (50) Ikuno, T.; Sainsbury, T.; Okawa, D.; Frehet, J. M. J.; Zettl, A. *Solid State Communications* **2007**, *142*, 643.
- (51) Yu, J.; Chen, Y.; Cheng, B. M. *Solid State Communications* **2009**, *149*, 763.

- (52) Kagan, C. R.; Afzali, A.; Martel, R.; Gignac, L. M.; Solomon, P. M.; Schrott, A. G.; Ek, B. *Nano Letters* **2003**, *3*, 119.
- (53) Keane, Z. K.; Ciszek, J. W.; Tour, J. M.; Natelson, D. *Nano Letters* **2006**, *6*, 1518.
- (54) Ghosh, A. W.; Rakshit, T.; Datta, S. *Nano Letters* **2004**, *4*, 565.
- (55) Hod, O.; Baer, R.; Rabani, E. *Journal of the American Chemical Society* **2005**, *127*, 1648.
- (56) Aviram, A.; Ratner, M. A. *Chemical Physics Letters* **1974**, *29*, 277.
- (57) Pati, R.; Karna, S. P. *Physical Review B* **2004**, *69*, 155419.
- (58) Mativetsky, J. M.; Pace, G.; Elbing, M.; Rampi, M. A.; Mayor, M.; Samori, P. *Journal of the American Chemical Society* **2008**, *130*, 9192.
- (59) Diez-Perez, I.; Hihath, J.; Lee, Y.; Yu, L. P.; Adamska, L.; Kozhushner, M. A.; Oleynik, I. I.; Tao, N. J. *Nat Chem* **2009**, *1*, 635.
- (60) Cornaglia, P. S.; Grempel, D. R.; Ness, H. *Physical Review B* **2005**, *71*.
- (61) Di Ventra, M.; Pantelides, S. T.; Lang, N. D. *Applied Physics Letters* **2000**, *76*, 3448.
- (62) He, H.; Pandey, R.; Karna, S. P. *Nanotechnology* **2008**, *19*.
- (63) Mukhopadhyay, S.; Pandey, R.; Karna, S. P. *Journal of Physical Chemistry C* **2012**, *116*, 4840.

- (64) Park, H.; Park, J.; Lim, A. K. L.; Anderson, E. H.; Alivisatos, A. P.; McEuen, P. L. *Nature* **2000**, *407*, 57.
- (65) Green, J. E.; Choi, J. W.; Boukai, A.; Bunimovich, Y.; Johnston-Halperin, E.; DeIonno, E.; Luo, Y.; Sheriff, B. A.; Xu, K.; Shin, Y. S.; Tseng, H. R.; Stoddart, J. F.; Heath, J. R. *Nature* **2007**, *445*, 414.
- (66) Nitzan, A.; Ratner, M. A. *Science* **2003**, *300*, 1384.
- (67) Metzger, R. M.; Chen, B.; Hopfner, U.; Lakshmikantham, M. V.; Vuillaume, D.; Kawai, T.; Wu, X. L.; Tachibana, H.; Hughes, T. V.; Sakurai, H.; Baldwin, J. W.; Hosch, C.; Cava, M. P.; Brehmer, L.; Ashwell, G. J. *Journal of the American Chemical Society* **1997**, *119*, 10455.
- (68) Reed, M. A.; Zhou, C.; Muller, C. J.; Burgin, T. P.; Tour, J. M. *Science* **1997**, *278*, 252.
- (69) Frank, S.; Poncharal, P.; Wang, Z. L.; de Heer, W. A. *Science* **1998**, *280*, 1744.
- (70) Kubatkin, S.; Danilov, A.; Hjort, M.; Cornil, J.; Bredas, J. L.; Stuhr-Hansen, N.; Hedegard, P.; Bjornholm, T. *Nature* **2003**, *425*, 698.
- (71) Song, H.; Reed, M. A.; Lee, T. *Advanced Materials* **2011**, *23*, 1583.
- (72) Liang, W. J.; Shores, M. P.; Bockrath, M.; Long, J. R.; Park, H. *Nature* **2002**, *417*, 725.

- (73) Park, J.; Pasupathy, A. N.; Goldsmith, J. I.; Chang, C.; Yaish, Y.; Petta, J. R.; Rinkoski, M.; Sethna, J. P.; Abruna, H. D.; McEuen, P. L.; Ralph, D. C. *Nature* **2002**, *417*, 722.
- (74) Parida, P.; Lakshmi, S.; Pati, S. K. *Journal of Physics-Condensed Matter* **2009**, *21*.
- (75) Andrews, D. Q.; Solomon, G. C.; Van Duyne, R. P.; Ratner, M. A. *Journal of the American Chemical Society* **2008**, *130*, 17309.
- (76) Song, H.; Kim, Y.; Jang, Y. H.; Jeong, H.; Reed, M. A.; Lee, T. *Nature* **2009**, *462*, 1039.
- (77) Szabo, A.; Ostlund, S. N. *Modern Quantum Chemistry: Introduction to Advanced Electronic Structure Theory* First edition ed.; Macmillan Publishing Co., Inc., 1982.
- (78) Born, M.; Oppenheimer, R. *Annalen der Physik* **1927**, *389*, 457.
- (79) Kohanoff, J. *Electronic Structure Calculations for Solids and Molecules: Theory and Computational Methods*; First edition ed.; Cambridge University Press, 2006.
- (80) Merzbacher, E. *Quantum Mechanics*; John Wiley & Sons Inc.: New York, 1998.
- (81) Martin, M. R. *Electronic Structure*; Second edition ed.; Cambridge University Press, 2005.
- (82) Thomas, L. H. *Proc. Cambridge Philos. Soc.* *23*, 542 **1927**, *23*, 542.

- (83) Hohenberg, P.; Kohn, W. *Phys. Rev. B* **1964**, *76*, 6062.
- (84) W. Kohn; Sham, L. J. *Phys. Rev.* **1965**, *140*, 5.
- (85) Parr, G. R.; Weitao, Y. *Density-Functional Theory of Atoms and Molecules* Oxford University Press, 1994.
- (86) Becke, A. D. *Journal of Chemical Physics* **1993**, *98*, 1372.
- (87) Becke, A. D. *Journal of Chemical Physics* **1993**, *98*, 5648.
- (88) Perdew, J. P.; Burke, K.; Ernzerhof, M. *Physical Review Letters* **1996**, *77*, 3865.
- (89) Becke, A. D. *Phys Rev A* **1988**, *38*, 3098.
- (90) Lee, C. T.; Yang, W. T.; Parr, R. G. *Physical Review B* **1988**, *37*, 785.
- (91) Hay, P. J.; Wadt, W. R. *Journal of Chemical Physics* **1985**, *82*, 270.
- (92) Kresse, G.; Furthmuller, J. *Computational Materials Science* **1996**, *6*, 15.
- (93) Kresse, G.; Joubert, D. *Physical Review B* **1999**, *59*, 1758.
- (94) Junquera, J.; Paz, O.; Sanchez-Portal, D.; Artacho, E. *Physical Review B* **2001**, *64*.
- (95) Soler, J. M.; Artacho, E.; Gale, J. D.; Garcia, A.; Junquera, J.; Ordejon, P.; Sanchez-Portal, D. *Journal of Physics-Condensed Matter* **2002**, *14*, 2745.

- (96) Rocha, A. R.; Garcia-Suarez, V. M.; Bailey, S.; Lambert, C.; Ferrer, J.; Sanvito, S. *Physical Review B* **2006**, *73*.
- (97) Rocha, A. R.; Garcia-Suarez, V. M.; Bailey, S. W.; Lambert, C. J.; Ferrer, J.; Sanvito, S. *Nature Materials* **2005**, *4*, 335.
- (98) Hamann, D. R. *Physical Review B* **1989**, *40*, 2980.
- (99) Schluter, M.; Bachelet, G. B.; Baraff, G. A.; Hamann, D. R.; Greenside, H. *B Am Phys Soc* **1981**, *26*, 390.
- (100) Schluter, M.; Hamann, D. R.; Chiang, C. *B Am Phys Soc* **1980**, *25*, 394.
- (101) Hamann, D. R.; Schluter, M.; Chiang, C. *Physical Review Letters* **1979**, *43*, 1494.
- (102) Laasonen, K.; Car, R.; Lee, C.; Vanderbilt, D. *Physical Review B* **1991**, *43*, 6796.
- (103) Vanderbilt, D. *Physical Review B* **1990**, *41*, 7892.
- (104) Thygesen, K. S.; Rubio, A. *Physical Review B* **2008**, *77*, 115333.
- (105) Datta, S. *Electronic Transport Properties in Mesoscopic Systems*; Cambridge University Press, 1995.
- (106) Datta, S. *Quantum Transport: Atom to Transistor*; Forth Edition ed.; CAMBRIDGE UNIVERSITY PRESS, 2009.
- (107) Ventra, D. M. *Electrical Transport in Nanoscale Systems*; First Edition ed.; CAMBRIDGE UNIVERSITY PRESS, 2008.

- (108) Cui, X. L.; Liu, G. D.; Lin, Y. H. *J Biomed Nanotechnol* **2005**, *1*, 320.
- (109) Kumar, M. A.; Jung, S.; Ji, T. *Sensors-Basel* **2011**, *11*, 5087.
- (110) Sowerby, S. J.; Cohn, C. A.; Heckl, W. M.; Holm, N. G. *Proceedings of the National Academy of Sciences of the United States of America* **2001**, *98*, 820.
- (111) Chen, Q.; Frankel, D. J.; Richardson, N. V. *Langmuir* **2002**, *18*, 3219.
- (112) Preuss, M.; Schmidt, W. G.; Bechstedt, F. *Physical Review Letters* **2005**, *94*.
- (113) Johnson, R. R.; Kohlmeyer, A.; Johnson, A. T. C.; Klein, M. L. *Nano Letters* **2009**, *9*, 537.
- (114) Riikonen, S.; Foster, A. S.; Krasheninnikov, A. V.; Nieminen, R. M. *Physical Review B* **2009**, *80*.
- (115) Pati, R.; Panigrahi, P.; Pal, P. P.; Akdim, B.; Pachter, R. *Chemical Physics Letters* **2009**, *482*, 312.
- (116) Lauret, J. S.; Arenal, R.; Ducastelle, F.; Loiseau, A.; Cau, M.; Attal-Tretout, B.; Rosencher, E.; Goux-Capes, L. *Physical Review Letters* **2005**, *94*, 037405.
- (117) Xiao, Y.; Yan, X. H.; Xiang, J.; Mao, Y. L.; Zhang, Y.; Cao, J. X.; Ding, J. W. *Applied Physics Letters* **2004**, *84*, 4626.
- (118) Xiang, H. J.; Yang, J. L.; Hou, J. G.; Zhu, Q. S. *Physical Review B* **2003**, *68*, 035427.

- (119) Ciofani, G.; Raffa, V.; Mencias, A.; Cuschieri, A. *Nano Today* **2009**, *4*, 8.
- (120) Sun, C. H.; Yu, H. X.; Xu, L. Q.; Ma, Q. A.; Qian, Y. T. *J Nanomater* **2010**.
- (121) Perdew, J. P.; Zunger, A. *Physical Review B* **1981**, *23*, 5048.
- (122) P. Hohenberg; Kohn, W. *Phys. Rev.* **1964**, *136*, B865.
- (123) Monkhorst, H. J.; Pack, J. D. *Physical Review B* **1976**, *13*, 5188.
- (124) Simeoni, M.; De Luca, C.; Picozzi, S.; Santucci, S.; Delley, B. *Journal of Chemical Physics* **2005**, *122*, 214710.
- (125) Tournus, F.; Latil, S.; Heggge, M. I.; Charlier, J. C. *Physical Review B* **2005**, *72*, 075431
- (126) Perdew, J. P.; Chevary, J. A.; Vosko, S. H.; Jackson, K. A.; Pederson, M. R.; Singh, D. J.; Fiolhais, C. *Physical Review B* **1992**, *46*, 6671.
- (127) Wu, X. J.; An, W.; Zeng, X. C. *Journal of the American Chemical Society* **2006**, *128*, 12001.
- (128) Zheng, J. X.; Song, W.; Wang, L.; Lu, J.; Luo, G. F.; Zhou, J.; Qin, R.; Li, H.; Gao, Z. X.; Lai, L.; Li, G. P.; Mei, W. N. *Journal of Nanoscience and Nanotechnology* **2009**, *9*, 6376.
- (129) Zhang, Z. H.; Guo, W. L.; Dai, Y. T. *Journal of Applied Physics* **2009**, *105*.

- (130) Grabowski, S. J.; Sokalski, W. A.; Dyguda, E.; Leszczynski, J. *Journal of Physical Chemistry B* **2006**, *110*, 6444.
- (131) Pantarotto, D.; Partidos, C. D.; Graff, R.; Hoebeke, J.; Briand, J. P.; Prato, M.; Bianco, A. *Journal of the American Chemical Society* **2003**, *125*, 6160.
- (132) Soto-Verdugo, V.; Metiu, H.; Gwinn, E. *Journal of Chemical Physics* **2010**, *132*, 195102.
- (133) Chang, C. M.; Jalbout, A. F. *Thin Solid Films* **2010**, *518*, 2070.
- (134) Cveticanin, J.; Joksic, G.; Leskovac, A.; Petrovic, S.; Sobot, A. V.; Neskovic, O. *Nanotechnology* **2010**, *21*, 015102.
- (135) Gan, L. B.; Zhou, D. J.; Luo, C. P.; Tan, H. S.; Huang, C. H.; Lu, M. J.; Pan, J. Q.; Wu, Y. *Journal of Organic Chemistry* **1996**, *61*, 1954.
- (136) Rajesh, C.; Majumder, C.; Mizuseki, H.; Kawazoe, Y. *Journal of Chemical Physics* **2009**, *130*, 124911.
- (137) Sun, W. M.; Bu, Y. X.; Wang, Y. X. *Journal of Physical Chemistry B* **2008**, *112*, 15442.
- (138) Vardanega, D.; Picaud, F. *Journal of Biotechnology* **2009**, *144*, 96.
- (139) Kane, R. S.; Stroock, A. D. *Biotechnology Progress* **2007**, *23*, 316.
- (140) Cohen, M. L.; Zettl, A. *Physics Today* **2010**, *63*, 34.

- (141) Watson, J. D.; Baker, T. A.; Bell, S. P.; Gann, A.; Levine, M.; Losick, R. *Molecular Biology of the Gene*; Fifth Edition ed.; Benjamin Cummings, 2004.
- (142) Lynch, I.; Dawson, K. A. *Nano Today* **2008**, *3*, 40.
- (143) Joshi, P.; Shewale, V.; Pandey, R.; Shanker, V.; Hussain, S.; Karna, S. P. *Physical Chemistry Chemical Physics* **2011**, *13*, 476.
- (144) Gao, Z. H.; Zhi, C. Y.; Bando, Y.; Golberg, D.; Serizawa, T. *Journal of the American Chemical Society* **2010**, *132*, 4976.
- (145) Zhi, C. Y.; Bando, Y.; Tang, C. C.; Golberg, D. *Physical Review B* **2006**, *74*, 153413.
- (146) Lee, J. O.; Lientschnig, G.; Wiertz, F.; Struijk, M.; Janssen, R. A. J.; Egberink, R.; Reinhoudt, D. N.; Hadley, P.; Dekker, C. *Nano Letters* **2003**, *3*, 113.
- (147) Xu, B. Q.; Xiao, X. Y.; Yang, X. M.; Zang, L.; Tao, N. J. *Journal of the American Chemical Society* **2005**, *127*, 2386.
- (148) Yu, L. H.; Keane, Z. K.; Cizek, J. W.; Cheng, L.; Stewart, M. P.; Tour, J. M.; Natelson, D. *Physical Review Letters* **2004**, *93*, 266802.
- (149) Yu, L. H.; Natelson, D. *Nano Letters* **2004**, *4*, 79.
- (150) Bratkovsky, A. M.; Kornilovitch, P. E. *Physical Review B (Condensed Matter and Materials Physics)* **2003**, *67*, 115307.

- (151) Choi, Y. C.; Kim, W. Y.; Park, K. S.; Tarakeshwar, P.; Kim, K. S.; Kim, T. S.; Lee, J. Y. *Journal of Chemical Physics* **2005**, *122*, 094706.
- (152) He, H.; Pandey, R.; Karna, S. P. *Nanotechnology* **2008**, *19*, 505203.
- (153) Ke, S. H.; Baranger, H. U.; Yang, W. T. *Physical Review B* **2005**, *71*, 113401.
- (154) Perrine, T. M.; Dunietz, B. D. *Physical Review B* **2007**, *75*, 195319.
- (155) Perrine, T. M.; Smith, R. G.; Marsh, C.; Dunietz, B. D. *J Chem Phys* **2008**, *128*, 154706.
- (156) Son, Y. W.; Ihm, J.; Cohen, M. L.; Louie, S. G.; Hyoun Joon, C. *Physical Review Letters* **2005**, *95*, 216602/1.
- (157) Yang, Z. Q.; Lang, N. D.; Di Ventra, M. *Applied Physics Letters* **2003**, *82*, 1938.
- (158) Galperin, M.; Ratner, M. A.; Nitzan, A.; Troisi, A. *Science* **2008**, *319*, 1056.
- (159) Joachim, C.; Gimzewski, J. K.; Aviram, A. *Nature* **2000**, *408*, 541.
- (160) Graige, M. S.; Feher, G.; Okamura, M. Y. *Proceedings of the National Academy of Sciences of the United States of America* **1998**, *95*, 11679.
- (161) Walden, S. E.; Wheeler, R. A. *Journal of Physical Chemistry B* **2002**, *106*, 3001.
- (162) Xu, Q.; Gunner, M. R. *Biochemistry* **2002**, *41*, 2694.
- (163) Balabin, I. A.; Onuchic, J. N. *Science* **2000**, *290*, 114.

- (164) Rabenstein, B.; Ullmann, G. M.; Knapp, E. W. *Biochemistry* **2000**, *39*, 10487.
- (165) Baker, K. A.; Tzitzilonis, C.; Kwiatkowski, W.; Choe, S.; Riek, R. *Nature Structural & Molecular Biology* **2007**, *14*, 1089.
- (166) Zhou, H. X.; Wlodek, S. T.; McCammon, J. A. *Proceedings of the National Academy of Sciences of the United States of America* **1998**, *95*, 9280.
- (167) Davis, W. B.; Ratner, M. A.; Wasielewski, M. R. *Journal of the American Chemical Society* **2001**, *123*, 7877.
- (168) Venkataraman, L.; Klare, J. E.; Nuckolls, C.; Hybertsen, M. S.; Steigerwald, M. L. *Nature* **2006**, *442*, 904.
- (169) Lang, N. D.; Solomon, P. M. *Nano Letters* **2005**, *5*, 921.
- (170) Frisch, M. J.; Trucks, G. W.; Schlegel, H. B.; Scuseria, G. E.; Robb, M. A.; Cheeseman, J. R.; Montgomery, J., J. A.; Vreven, T.; Kudin, K. N.; Burant, J. C. e. a.; 03 ed.; Gaussian, Inc: Pittsburg, 2003.
- (171) Barraza-Lopez, S.; Park, K.; Garcia-Suarez, V.; Ferrer, J. *Physical Review Letters* **2009**, *102*, 246801.
- (172) Pati, R.; McClain, M.; Bandyopadhyay, A. *Physical Review Letters* **2008**, *100*, 246801.
- (173) Buttiker, M. *Physical Review Letters* **1986**, *57*, 1761.

- (174) Landauer, R. *Journal of Physics-Condensed Matter* **1989**, *1*, 8099.
- (175) Tian, W. D.; Datta, S.; Hong, S. H.; Reifengerger, R.; Henderson, J. I.; Kubiak, C. P. *Journal of Chemical Physics* **1998**, *109*, 2874.
- (176) He, H. Y.; Pandey, R.; Karna, S. P. *Chemical Physics Letters* **2007**, *439*, 110.
- (177) Lastapis, M.; Martin, M.; Riedel, D.; Hellner, L.; Comtet, G.; Dujardin, G. *Science* **2005**, *308*, 1000.
- (178) Moresco, F.; Meyer, G.; Rieder, K. H.; Tang, H.; Gourdon, A.; Joachim, C. *Physical Review Letters* **2001**, *86*, 672.
- (179) Chang, C. W.; Lu, Y. C.; Wang, T. T.; Diao, E. W. G. *Journal of the American Chemical Society* **2004**, *126*, 10109.
- (180) Choi, B. Y.; Kahng, S. J.; Kim, S.; Kim, H.; Kim, H. W.; Song, Y. J.; Ihm, J.; Kuk, Y. *Physical Review Letters* **2006**, *96*, 156106.
- (181) Meng, S.; Wang, W. L.; Maragakis, P.; Kaxiras, E. *Nano Letters* **2007**, *7*, 2312.
- (182) Chen, C. L.; Yang, C. F.; Agarwal, V.; Kim, T.; Sonkusale, S.; Busnaina, A.; Chen, M.; Dokmeci, M. R. *Nanotechnology* **2010**, *21*.
- (183) Gigliotti, B.; Sakizzie, B.; Bethune, D. S.; Shelby, R. M.; Cha, J. N. *Nano Letters* **2006**, *6*, 159.

- (184) Heller, I.; Janssens, A. M.; Mannik, J.; Minot, E. D.; Lemay, S. G.; Dekker, C. *Nano Letters* **2008**, 8, 591.
- (185) Johnson, A. T. C.; Staii, C.; Chen, M.; Khamis, S.; Johnson, R.; Klein, M. L.; Gelperin, A. *Semiconductor Science and Technology* **2006**, 21, S17.
- (186) Johnson, A. T. C.; Staii, C.; Chen, M.; Khamis, S.; Johnson, R.; Klein, M. L.; Gelperin, A. *Physica Status Solidi B-Basic Solid State Physics* **2006**, 243, 3252.
- (187) Lu, Y. R.; Bangsaruntip, S.; Wang, X. R.; Zhang, L.; Nishi, Y.; Dai, H. J. *Journal of the American Chemical Society* **2006**, 128, 3518.
- (188) Martin, W.; Zhu, W. S.; Krilov, G. *Journal of Physical Chemistry B* **2008**, 112, 16076.
- (189) Gao, H. J.; Kong, Y. *Annual Review of Materials Research* **2004**, 34, 123.
- (190) Lu, J.; Nagase, S.; Zhang, X. W.; Wang, D.; Ni, M.; Maeda, Y.; Wakahara, T.; Nakahodo, T.; Tsuchiya, T.; Akasaka, T.; Gao, Z. X.; Yu, D. P.; Ye, H. Q.; Mei, W. N.; Zhou, Y. S. *Journal of the American Chemical Society* **2006**, 128, 5114.
- (191) Zheng, M.; Jagota, A.; Semke, E. D.; Diner, B. A.; McLean, R. S.; Lustig, S. R.; Richardson, R. E.; Tassi, N. G. *Nature Materials* **2003**, 2, 338.
- (192) Zheng, M.; Jagota, A.; Strano, M. S.; Santos, A. P.; Barone, P.; Chou, S. G.; Diner, B. A.; Dresselhaus, M. S.; McLean, R. S.; Onoa, G. B.; Samsonidze, G. G.; Semke, E. D.; Usrey, M.; Walls, D. J. *Science* **2003**, 302, 1545.

- (193) Star, A.; Tu, E.; Niemann, J.; Gabriel, J. C. P.; Joiner, C. S.; Valcke, C. *Proceedings of the National Academy of Sciences of the United States of America* **2006**, *103*, 921.
- (194) Hwang, J. S.; Kim, H. T.; Son, M. H.; Oh, J. H.; Hwang, S. W.; Ahn, D. *Physica E-Low-Dimensional Systems & Nanostructures* **2008**, *40*, 1115.
- (195) Liu, H. J.; Chan, C. T. *Physical Review B* **2002**, *66*.
- (196) Dewar, M. J. S. *Cc/Eng Tech Appl Sci* **1985**, *16*.
- (197) Dewar, M. J. S.; Mckee, M. L.; Rzepa, H. S. *Journal of the American Chemical Society* **1978**, *100*, 3607.
- (198) Dewar, M. J. S.; Zoebisch, E. G.; Healy, E. F.; Stewart, J. J. P. *Journal of the American Chemical Society* **1985**, *107*, 3902.
- (199) Dewar, M. J. S.; Zoebisch, E. G.; Healy, E. F.; Stewart, J. J. P. *Journal of the American Chemical Society* **1993**, *115*, 5348.

Appendix A

Computational Resources

All the calculations presented in this dissertation were carried out on our group machine RAMA, a 286 processor Beowulf Linux cluster. A typical time estimation of the calculations reported in this dissertation is illustrated in Table A.1.

Table A.1: A typical CPU-time required for the major optimization steps in Chapters 3 and 4.

Optimization Step	Number of Calculation	MP-kgrid	Number of Processors	CPU time (Hour)
Selective Dynamics	1	1x1x3	8	162
Grid Scan	220	1x1x3	1	23
Rotation Scan	72	1x1x3	1	22
Full Optimization	1	1x1x3	8	233

Appendix B

List of Related Publications

1. **Saikat Mukhopadhyay**, R. Pandey, S. P. Karna; “*Microscopic insight into orbital gating*” (To be submitted).
2. R. G. Amorim, X. Zhong, **Saikat Mukhopadhyay**, R. Pandey, S. P. Karna; “*Understanding the Properties of Semiconducting Nanomembranes: hexagonal BN, AlN, and GaN*” (Submitted).
3. X. Zhong, **Saikat Mukhopadhyay**, R. Pandey and S. P. Karna; “*Applicability of CNTs and BNNTs as Biosensor: Effect of Molecular Adsorption on the Transport Properties of Boron Nitride Nanotube and Carbon Nanotube*” (To be submitted).
4. **Saikat Mukhopadhyay**, R. L. Martin, R. Pandey and E. R. Batista; “*Consequences of Defects in Electronic Conduction of poly-p-phenylene-vinylene Oligomer*” (To be submitted).

5. **Saikat Mukhopadhyay**, R. Pandey, S. P. Karna; “*Controlling the performance of a three-terminal molecular transistor: Conformational vs. Conventional gating*” J. Phys. Chem. C **116**, 4840 (2012).
6. **Saikat Mukhopadhyay**, R. H. Scheicher, R. Pandey, S. P. Karna; “*Sensitivity of Boron Nitride Nanotubes toward molecules of different polarities: A new detection mechanism*” J. Phys. Chem. Lett. **2**, 2442 (2011).
7. V. Shewale, P. Joshi, **Saikat Mukhopadhyay**, M. Deshpande, R. Pandey, S. Hussain, S. P. Karna; “*First-Principles Study Of Nanoparticle-Biomolecular Interactions: Anchoring Of A (ZnO)₁₂ Cluster On Nucleobases*” J. Phys. Chem. C, **115**, 10426 (2011).
8. **Saikat Mukhopadhyay**, S. Gowtham, R. H. Scheicher, R. Pandey, S. P. Karna; “*Theoretical Study Of Physisorption Of Nucleobases On Boron Nitride Nanotubes: A New Class of Hybrid Nanomaterials*” Nanotechnology, **21**, 165703 (2010).
9. **Saikat Mukhopadhyay**, S. Gowtham, R. H. Scheicher, R. Pandey, S. P. Karna; “*New nano-bio hybrid-material unveiled*” LAB TALK (Highlighted articles), Apr 6 (2010).
10. **Saikat Mukhopadhyay**, S. Gowtham, R. Pandey, A. Costales; “*Theoretical Study Of Small Clusters Of Indium Oxide: InO, In₂O, InO₂, In₂O₂*” J. of Mol. Struct.: THEOCHEM, **948**, 31 (2010).
11. C. Ozdogan, **Saikat Mukhopadhyay**, W. Hayami, Z. B. Guvenc, R. Pandey, I. Boustani; “*The Unusually Stable B₁₀₀ Fullerene, Structural Transitions In Boron*

*Nanostructures, And A Comparative Study of α - And γ -Boron and Sheets” J. Phys. Chem. C, **114**, 4362 (2010).*

12. **Saikat Mukhopadhyay**, H. He, R. Pandey, Y. K. Yap, I. Boustani; “*Novel spherical boron clusters and structural transition from 2D quasi-planar structures to 3D double-rings*” J. Phys.: Conf. Ser. **176**, 012028 (2009).

Appendix C

Copyrights



To: permissions@iop.org,
Cc:
Bcc:
Subject: Copyright and permission needed
From: Saikat Mukhopadhyay <smukhopa@mtu.edu> - Sunday 17/06/2012 17:40

Hello,

I want to reproduce the following journal article for my Doctoral thesis:

✓ *Nanotechnology* , **21**, 165703[6pp] (2010)

I am the first author of the article.

I would really appreciate if you kindly grant me permission to do so.

Thanking you,

Sincerely,
Saikat Mukhopadhyay
Department of Physics
Michigan Technological University,
Houghton, MI 49931

PERMISSION TO REPRODUCE AS REQUESTED IS GIVEN PROVIDED THAT:

- ~~(a) the consent of the author(s) is obtained~~
- (b) the source of the material including author, title of article, title of journal, volume number, issue number (if relevant), page range (or first page if this is the only information available), date and publisher is acknowledged.
- (c) for material being published electronically, a link back to the original article should be provided (via DOI).

IOP Publishing Ltd
Temple Circus
Temple Way
BRISTOL
BS1 6BE



18/06/2012
Date

Rights & Permissions


Figure C.1: Copyright permission from IOPScience for using the content, partially or completely, published by S. Mukhopadhyay *et al.* The results and related discussion has been used in Chapter 3.

Appendix D

Copyrights



[Home](#) [Account Info](#) [Help](#)



Title: Sensitivity of Boron Nitride Nanotubes toward Biomolecules of Different Polarities
Author: Saikat Mukhopadhyay et al.
Publication: Journal of Physical Chemistry Letters
Publisher: American Chemical Society
Date: Oct 1, 2011
Copyright © 2011, American Chemical Society

Logged in as:
Saikat Mukhopadhyay
[LOGOUT](#)

PERMISSION/LICENSE IS GRANTED FOR YOUR ORDER AT NO CHARGE

This type of permission/license, instead of the standard Terms & Conditions, is sent to you because no fee is being charged for your order. Please note the following:

- Permission is granted for your request in both print and electronic formats, and translations.
- If figures and/or tables were requested, they may be adapted or used in part.
- Please print this page for your records and send a copy of it to your publisher/graduate school.
- Appropriate credit for the requested material should be given as follows: "Reprinted (adapted) with permission from (COMPLETE REFERENCE CITATION). Copyright (YEAR) American Chemical Society." Insert appropriate information in place of the capitalized words.
- One-time permission is granted only for the use specified in your request. No additional uses are granted (such as derivative works or other editions). For any other uses, please submit a new request.



[BACK](#) [CLOSE WINDOW](#)

Copyright © 2012 Copyright Clearance Center, Inc. All Rights Reserved. [Privacy statement](#).
Comments? We would like to hear from you. E-mail us at customercare@copyright.com


Figure D.1: Copyright permission from American Chemical Society (ACS) for using the content, partially or completely, published by S. Mukhopadhyay *et al.* The results and related discussion has been used in Chapter 4.

Appendix E

Copyrights



[Home](#)[Account Info](#)[Help](#)



Title: Controlling the Performance of a Three-Terminal Molecular Transistor: Conformational versus Conventional Gating
Author: Saikat Mukhopadhyay et al.
Publication: The Journal of Physical Chemistry C
Publisher: American Chemical Society
Date: Feb 1, 2012
Copyright © 2012, American Chemical Society

Logged in as:
Saikat Mukhopadhyay
Account #: 3000544241
[LOGOUT](#)

PERMISSION/LICENSE IS GRANTED FOR YOUR ORDER AT NO CHARGE

This type of permission/license, instead of the standard Terms & Conditions, is sent to you because no fee is being charged for your order. Please note the following:

- Permission is granted for your request in both print and electronic formats, and translations.
- If figures and/or tables were requested, they may be adapted or used in part.
- Please print this page for your records and send a copy of it to your publisher/graduate school.
- Appropriate credit for the requested material should be given as follows: "Reprinted (adapted) with permission from (COMPLETE REFERENCE CITATION). Copyright (YEAR) American Chemical Society." Insert appropriate information in place of the capitalized words.
- One-time permission is granted only for the use specified in your request. No additional uses are granted (such as derivative works or other editions). For any other uses, please submit a new request.

[BACK](#)[CLOSE WINDOW](#)

Copyright © 2012 [Copyright Clearance Center, Inc.](#) All Rights Reserved. [Privacy statement.](#)
Comments? We would like to hear from you. E-mail us at customer@copyright.com

Figure E.1: Copyright permission from American Chemical Society (ACS) for using the content, partially or completely, published by S. Mukhopadhyay *et al.* The results and related discussion has been used in Chapter 5.